

Rochester Institute of Technology

## RIT Digital Institutional Repository

---

Theses

---

2008

### Experimental investigation on the effects of surface roughness on microscale liquid flow

Tim Brackbill

Follow this and additional works at: <https://repository.rit.edu/theses>

---

#### Recommended Citation

Brackbill, Tim, "Experimental investigation on the effects of surface roughness on microscale liquid flow" (2008). Thesis. Rochester Institute of Technology. Accessed from

This Thesis is brought to you for free and open access by the RIT Libraries. For more information, please contact [repository@rit.edu](mailto:repository@rit.edu).

# **Experimental investigation on the effects of surface roughness on microscale liquid flow**

*by*

**Timothy Brackbill**

*A thesis submitted in  
partial fulfillment of the  
requirement for the*

*B.S./M.S.*

*in*

*Mechanical Engineering*

Approved by:

Dr. Satish G. Kandlikar

Thesis Advisor

Department of Mechanical Engineering

Dr. Steven Weinstein

Department of Mechanical Engineering

Dr. Jeffery Kozak

Department of Mechanical Engineering

Dr. Edward Hensel

Department of Mechanical Engineering

Department of Mechanical Engineering

Rochester Institute of Technology

May 1st 2008

## I. Abstract

Microfluidics has become of interest recently with shrinking device sizes. Roughness structures left from machining processes on the inside of tubes and channels that were once not a concern may now create relative roughness that exceeds 5%. Confusion still exists in the literature as to the extent of the effects of roughness on laminar flow. This work aims to experimentally examine the effects of different roughness structures on internal flows in high aspect ratio rectangular microchannels. A total of four test sections were fabricated to test samples with different patterned rough surfaces, and to also vary the two opposite surfaces forming the long faces of the channel. These test sections allowed the same roughness samples to be tested at varying relative roughnesses and allowed a systematic study on their effects on pressure drop. The first test section looked at sawtooth effects on laminar flow. The second looked at uniform roughness on laminar flow. The third looked at sawtooth roughness in turbulent flow, and the fourth looked at varying pitch sawtooth roughness in laminar flow. Rough surfaces were formed in one of two ways. The first involved making structured repeating sawtooth ridges with a ball end mill on a CNC machine. The second was using sandpaper in a crosshatch pattern to make a more unpatterned roughened surface. In this study, the Reynolds number was varied from 30 to 15,000 with degassed, deionized water as the working fluid. The

experimental uncertainty in the experimental data is at worst 7.58% for friction factor and 2.67% for Reynolds number. Roughness structures varied from a lapped smooth surface with 0.2  $\mu\text{m}$  roughness height to sawtooth ridges of height 117  $\mu\text{m}$ . Hydraulic diameters from 198  $\mu\text{m}$  to 2,349  $\mu\text{m}$  were tested. The highest relative roughness tested was 24.8%.

As a result of the first and second experiments, it was shown that using constricted parameters, sawtooth and uniform roughness performance could be predicted in the laminar regime. In the third experiment, it was shown that certain sawtooth roughness samples cause the results to converge to a single line for friction factor. In the fourth experiment, the pitch of sawtooth elements was shown to be a key parameter in showing when each parameter is applicable. It was found that roughness has an effect even at relative roughness values less than 5%. Lapped smooth samples showed no departure from macroscale theory at all channel diameters tested, which implies that no departure from continuum mechanics occurred at the length scales tested. This fit with what was expected. Early transitions to turbulence were seen however, showing decreasing transition Reynolds number with increasing relative roughness. The lowest turbulent transition occurred at a Reynolds number of 210, with a relative roughness of 24.8%. Most all of the roughness structures studied were found to have experimental results that were well predicted with the use of constricted parameters. However, samples with roughness elements placed at higher pitches were

seen to have experimental results approaching theory calculated with root parameters of the channel.

## II. Table of Contents

I. Abstract.....	2
II. Table of Contents.....	5
III. Index of Tables and Figures.....	7
i. Figures.....	7
ii. Tables.....	8
IV. Nomenclature.....	9
1 Introduction.....	10
1.1 Previous Experimental Studies.....	10
1.1.1 Laminar and transition studies.....	10
1.1.2 Turbulent Flow.....	21
1.2 Numerical/Theoretical Work.....	23
1.3 Roughness Characterization.....	27
2 Theoretical Work.....	30
2.1 Current Roughness and Nikuradse.....	30
2.2 Derivation of Constricted Parameters.....	33
2.3 Application of Lubrication Theory.....	37
3 Experimental Work.....	44
3.1 Summary of experimental work.....	44
3.2 Initial Experimental Work - Sawtooth High.....	46
3.2.1 Experimental Loop Description for initial work.....	46
3.2.2 Experimental Schematics and Drawings.....	47
3.2.3 Samples used in First Experimentation.....	49
3.2.4 Experimental Procedure for the First setup.....	52
3.3 Second Setup - Low uniform RR testing.....	52
3.3.1 Experimental Setup for Low RR uniform elements.....	53
3.3.2 Samples used for low uniform roughness.....	55
3.4 Third Experiment - Fully Turbulent Flow.....	57
3.4.1 Experimental Schematics.....	57
3.4.2 Samples.....	58
3.4.3 Experimental Procedure.....	58

3.5 Fourth Experiment - Differing pitches of sawtooth roughness.....	59
3.5.1 Experimental Schematics.....	59
3.5.2 Samples.....	59
3.5.3 Experimental Procedure.....	62
3.6 LabVIEW.....	62
3.7 Experimental Uncertainties.....	67
4 Results.....	71
4.1 Summary and Major Findings.....	71
4.2 Results of first Experimentation.....	72
4.3 Results of second Experimentation.....	76
4.3.1 Experimental Results.....	76
4.3.2 Results of applying lubrication theory.....	78
4.4 Results of Third Experiment - Turbulent experiments.....	82
4.5 Results of fourth experimentation - varying pitch.....	84
4.6 Transition to turbulence.....	86
5 Conclusions.....	90
6 References.....	92
7 Appendices.....	96
7.1 Appendix A - First setup drawings.....	96
7.2 Second Experimental Setup.....	109

## III. Index of Tables and Figures

### i. Figures

Figure 1.1: Modified Moody Diagram by Kandlikar [28].....	25
Figure 1.2: Pressure drop v. pitch of sawtooth obstructions for $Re = 40$ , $h = 0.1$ , from Rawool [30].....	26
Figure 1.3: Generic roughness surface with parameters marked.....	29
Figure 2.1: Illustration of Idealized roughness surface from Nikuradse [2].....	32
Figure 2.2: Generic ribbed roughness with parameters illustrated.....	35
Figure 2.3: Illustration of Lubrication Problem.....	38
Figure 3.1: Schematic of the first test loop designed.....	49
Figure 3.2: Left: Exploded view of the setup Right: Assembled setup without cover piece.....	49
Figure 3.3: 405um pitch profile, taken with a stylus profilometer. The parameters are marked.....	51
Figure 3.4: 815um pitch profile, taken with stylus profilometer.....	51
Figure 3.5: Ground smooth sample surface, taken with a stylus Profilometer.....	52
Figure 3.6: Isometric Schematics of New Test section.....	54
Figure 3.7: Schematic of test loop used for low Relative roughness testing.....	56
Figure 3.8: 3D microscope images and stylus profilometer scans of the three roughnesses tested.....	58
Figure 3.9: Test loop for third experimentation.....	59
Figure 3.10: 3D Microscope compilations and 2D stylus profilometer scans of the samples.....	60
Figure 3.11: Interferometer scans (left) and apparent 2D profile scans (right) for the three samples tested.....	63
Figure 4.1: Smooth channel verification with $D_h = 565\mu\text{m}$ .....	74
Figure 4.2: Uncorrected - aligned sawtooth roughness $p=405\mu\text{m}$ , $D_h=1240\mu\text{m}$ , $b = 653\mu\text{m}$ .....	75
Figure 4.3: Corrected - aligned sawtooth $p=405\mu\text{m}$ , $D_{hcf}=847\mu\text{m}$ .....	76
Figure 4.4: Comparison of the two different pitches with the same constricted hydraulic diameter.....	76
Figure 4.5: Representative samples from the low uniform roughness testing plotted with (a) root parameters (b) constricted parameters.....	78

Figure 4.6: Illustration of all parameters used in experimentation applied to the 60 grit channel profile.....	79
Figure 4.7: Variation of $be_{ff,exp}$ with Reynolds Number.....	80
Figure 4.8: Parameters for separation normalized with experimental results.....	81
Figure 4.9: Results of turbulent testing with 405um samples (a) a single test plotted with a prediction of friction factor (b) all the samples.....	83
Figure 4.10: Comparing the two different sawtooth pitches.....	85
Figure 4.11: Constricted friction factor vs Reynolds number for 3 varying pitches .....	86
Figure 4.12: Constricted friction factor vs Reynolds number for the largest pitch, plotted with both root and constricted parameters.....	87
Figure 4.13: $f^*Re$ vs Beta for the samples with varying pitch.....	88
Figure 4.14: Transition Reynolds number vs Relative Roughness.....	90

## ii. Tables

Table 1.1: Summary of Experimental works on the effects of roughness on flow .....	21
Table 3.1: Summary of Roughness in First Experimentation.....	50
Table 3.2: Description of roughness surfaces used in low RR testing.....	57
Table 3.3: Summary of machining for the fourth set of samples.....	61
Table 3.4: State points to reference density.....	66
Table 3.5: Summary of max errors used in uncertainty analysis for the pressure and flow sensors.....	71
Table 4.1: Summary of all experimental work. Each row represents an individual test.....	72
Table 4.2: Repeatability.....	73
Table 4.3: Summary of experimental results from lubrication theory.....	80

## IV. Nomenclature

$\alpha$ = aspect ratio	$\dot{m}$ = mass flow rate
$\alpha_{cf}$ = constricted aspect ratio	$n$ = number of points in a roughness profile sample
$A$ = cross sectional area of channel	$p$ = pitch of roughness elements
$A_{cf}$ = constricted cross sectional area of channel	$P$ = perimeter or pressure in derivations
$a$ = channel base	$P_{cf}$ = constricted perimeter
$b$ = channel height	$\rho$ = density of the water
$b_{cf}$ = constricted channel height	$R_a$ = average roughness
$b_{eff}$ = separation from lubrication theory accounting for roughness effects	$Re$ = Reynolds number
$b_{eff,exp}$ = effective separation from experiments	$Re_c$ = critical Reynolds number
$b_{eff,theory}$ = effective separation from theory	$Re_{cf}$ or $Re_{cf}$ = Reynolds number, calculated from $D_{h,cf}$
$\epsilon$ = roughness element height	$Q$ = volumetric flow rate
$\epsilon_{FP}$ = roughness height - new parameters	$Re_o$ = Smooth channel turbulent transition
$\delta$ = used to show uncertainty in trailing variable	$R_p$ = maximum peak height
$D_h$ = hydraulic diameter	$RS_m$ = mean spacing of irregularities
$D_{h,cf}$ = constricted hydraulic diameter	$T_{mean}$ = mean fluid temperature in test section
$D_t$ = root diameter of circular tube	$u_x$ = fluid velocity component in the x direction
$f$ = friction factor	$u_y$ = fluid velocity component in the y direction
$f_{Moody}$ = turbulent friction factor from Moody diagram	$u_z$ = fluid velocity component in the z direction
$F_p$ = floor profile line	$V$ = flow velocity
$G$ = mass flow rate	$\dot{V}$ = Volumetric flow rate
$g$ = gravity vector	$w$ = width of silicon channels
$h$ = height of silicon channels	$x$ = distance from channel beginning
$L$ = a length along the channel in the flow direction	$Z$ = height at any given point along a roughness profile ( $\mu m$ )

# 1 Introduction

Work in the area of roughness effects on friction factors in internal flows was pioneered by Colebrook [1], Nikuradse [2], and Moody. Their work was limited to relative roughness values of less than 5%, a value which may be exceeded in microfluidics application where smaller hydraulic diameters are encountered. Many previous works have been performed through the 1990s with inconclusive and often contradictory results. No studies have been performed that systematically varied the roughness structures and relative roughness while collecting enough data necessary for any valid conclusions to be drawn. This study aims to conduct systematic experiments to evaluate the effects of these roughness elements on flow.

## 1.1 Previous Experimental Studies

### 1.1.1 Laminar and transition studies

Wu and Little [3] noticed an early transition to turbulent flow in microminiature refrigerators. Their channels were etched on glass and silicon with  $D_h$  from 45.46 to 83.07 $\mu\text{m}$ . Wu and Little [4] fabricated microchannels with the same process, but varied  $D_h$  from 134 $\mu\text{m}$  to 164 $\mu\text{m}$ , and found unusually high frictional factors. They found these to contribute to low critical Reynolds numbers from  $\sim 400$ -900.

Peng *et al.* [5] machined five different microchannels in stainless steel, with  $D_h$  ranging from 133 $\mu\text{m}$  to 343 $\mu\text{m}$  and aspect ratio varying from

0.333 to 1. The error was  $\pm 10\%$  on friction calculations and  $\pm 8\%$  on Reynolds number. The fluid used was water, with Reynolds numbers varying from 50 to 4000. Critical Reynolds numbers were found to be between 200 and 700, or much lower than conventional macroscale theory. In this study, Peng stresses the effect of the aspect ratio and hydraulic diameter on  $Re_c$  and  $f$ . He found that the lowest friction factor, lower than macroscale theory, occurs at aspect ratios nearest to 0.5. The  $Re_c$  value was related to  $D_h$ , but no relationship was given. Also noted is a deviation from classical theory and suggestion that different laminar and turbulent flow mechanisms are occurring, along with a decrease in the transition region with decreasing  $D_h$ . As such, an empirical relationship for friction factor is proposed in equation 1.1, where  $C_f$  and  $C_{f,t}$  are empirical constants that are depended on channel aspect ratio and fluid species.

$$\begin{aligned}
 f_{laminar} &= \frac{C_f}{Re^{1.98}} \\
 f_{turbulent} &= \frac{C_{f,t}}{Re^{1.72}}
 \end{aligned}
 \tag{1.1}$$

Pfund *et al.* [6] used a variable depth microchannel along with pressure drop sensors and flow visualization to study the same phenomena.

Overall the setup is similar in nature to the setup in use for this thesis.

The samples used to construct the channel were characterized with an optical profilometer, however for the rough channel only one side of the

rectangular channel's 128  $\mu\text{m}$  – 1,050  $\mu\text{m}$  by 10 mm dimensions were roughened. Uncertainties as found with a Monte-Carlo simulation were stated to be between  $\pm 5.4\%$  and  $\pm 11.1\%$ , although it is stated that RMS calculations yield 1% higher uncertainties. Uncertainties in Reynolds number were between  $\pm 1.6\%$  and  $\pm 3.4\%$ . It was found that every channel used in the study exhibited higher than theoretical predictions in the laminar region, even for the smooth channels. For the roughened channels, the discrepancy was even more pronounced.  $Re_c$  was again observed to be lower than theory, but not as extreme as those reported by Peng *et al.* [5]. Again, a dependence of  $Re_c$  on hydraulic diameter was observed. Utilizing flow visualization, eddy currents around surface features are proposed to be the mechanism for transition, and also for the shorter but continuous transitions reported elsewhere.

Tu *et al.* [7] performed tests on five microchannels with hydraulic diameters from 69.5  $\mu\text{m}$  to 304.7  $\mu\text{m}$  and aspect ratio from 0.09 to 0.24. Working fluid was R134a liquid or vapor depending on the test. The test sections were manufactured such that the surfaces were as smooth as possible. Errors were reported as  $\pm 6.3\%$  max for  $f$  and  $\pm 2\%$  max for  $Re$ . It was found that for the four channels with relative roughness less than 0.3%, no deviation occurred from conventional  $f$  or  $Re_c$  macroscale theory ( $Re_c$  2150 to 2290 was reported). For the one channel with a relative

roughness of 0.35%, the friction factor was observed to be 9% higher than predicted, accompanied by a significantly lower  $Re_c$  of 1570.

Wu *et al.* [8] used thirteen fabricated trapezoidal silicon channels with pairs of geometrically similar channels with varying surface roughness and hydrophobicity (through use of  $SiO_2$ ). An increased friction factor was observed in the laminar flow regime due to surface roughness when compared to the smooth channel. Increasing discrepancies were noted with increasing  $Re$  for the smooth versus roughened channels. The coating of  $SiO_2$  also slightly increased friction factor values from the smooth channel. The oxide also increased the convective heat transfer. Wu also describes empirical correlations for  $Nu$  and  $f_{app}Re$  for the geometric ratios relating to trapezoidal channels.

Celata *et al.* [9] used capillary glass tubes with hydraulic diameter ranging from 70  $\mu m$  to 326  $\mu m$  with water as the working fluid. The inside of the capillaries were roughened by flowing particulates through the channels. It was observed that even the low relative roughness values seemed to increase friction factor in the laminar region in comparison to the smooth channel results. Additionally, earlier transitions were seen with the roughened channels.

Mala *et al.* [10] conducted a study on 13 capillary tubes with hydraulic diameter ranging from 50 $\mu m$  to 254 $\mu m$ . This study has a reported

roughness height values of  $1.75\mu\text{m}$ . These channels are considered smooth in this study, which is interesting when it is noticed these are rougher than the “rough” capillaries used by Celata *et al.* [9]. Mala explains the discrepancy with a modified roughness-viscosity theory. This model varies the viscosity of the fluid going around the roughness elements and increases the pressure drop prediction. This modified model is based on an older aerodynamic model by Merkle *et al.* [11] and Tani [12]. The model relies on the results of CFD experimentation, and is not applicable to any surface.

Kandlikar *et al.* [13] studied heat transfer and pressure drop in stainless steel capillary tubing of diameters  $620\mu\text{m}$  and  $1067\mu\text{m}$ . Three different surface types for each diameter were created using varying acid etching techniques on the inside of the capillaries. For the larger diameter, little effect on friction factor or heat transfer performance was discernible from even the largest relative roughness value of 0.23%. It was suggested that this diameter is not truly microscale, and thus macroscale theories are more applicable. For the smaller diameter, the highest relative roughness value of 0.36% yielded the highest friction factors and highest heat transfer performance. The capillaries with successively smoother walls showed less extreme friction factor and heat transfer.

Baviere *et al.* [14] studied both the effect of roughness and the effect of the electrical double layer on internal flows. The study used silicon

etched channels for hydraulic diameters less than 100 $\mu\text{m}$  and a bronze block setup for hydraulic diameters greater than 100 $\mu\text{m}$ . Roughness elements were created by embedding SiC particles in a thin nickel wall coating. They found no deviation from conventional theory for smooth channels. In roughened channels, higher friction factors were observed. However, in contrast to other studies, the addition of roughness elements in this setup stabilized flow, and created higher values for the transition to turbulence.

Hao *et al.* [15] performed an experimental study with etched silicon rectangular microchannels which had three artificially created roughness elements on one side of the channel, measuring 50 $\mu\text{m}$  square and spaced between 7 and 8 mm from each other. Hydraulic diameters ranged from 153 $\mu\text{m}$  -191 $\mu\text{m}$ , and Reynolds numbers were tested with values less than 2400. Flow visualization was also included to observe the flow as it traversed the artificially created roughness. Smooth channels were observed to follow conventional theory for friction and transition. The artificially roughened channels, however, followed conventional theory to  $\text{Re} = 900$ , then departed into transition. This study showed that these elements are able to trigger early transition from laminar by imparting additional disturbances to the flow. The friction factor remained constant, which can be explained by the few and sparsely spaced roughness elements. These did not have a significant effect on the friction factor.

Finally, Hao also concludes that similar features of macroscale turbulence are also visible in microscale fluid turbulence.

Weilin *et al.* [16] fabricated trapezoidal channels using micromachining techniques on silicon substrates. Due to the silicon's surface finish, relative roughness values varied from 2.4% to 3.5%. Experimentation was limited to a 1,723 kPa maximum pressure drop, beyond the silicon substrate failed. The resulting Reynolds numbers were less than 1500. They found friction factors that were higher than theory would predict, and also found linear relationships between pressure drop over length and Reynolds number to possess higher than theoretical slopes. Using this data, they applied the modified roughness-viscosity model of Mala and Li [10] and obtained good correlation with experimental data. A complicated formulation for a coefficient inherent to the model is determined using variables such as channel geometry, roughness distribution, and shape of roughness elements. The coefficients obtained have limited applicability past the channels used in this study.

Shen *et al.* [17] machined 26 parallel microchannels of 300 $\mu\text{m}$  width and 800 $\mu\text{m}$  depth in a copper block. They studied the effects of 4% relative roughness on friction factor and Nusselt number. No effect on the transition to turbulence was found, however Reynolds numbers were tested only to 1257, which severely restricts any conclusions of this nature. It was also found that for low Reynolds numbers no departure

from macroscale theory was observed. With increasing  $Re$ , the Poiseuille number increased along with  $Re$  rather than remaining constant. They proposed the correlation given in equation 1.2 for roughened rectangular microchannels and laminar flow.

$$f Re^{0.4743} = 4.0922 \quad (1.2)$$

Celata *et al.* [18] used a parallel microtube setup ( $D_h=130\mu\text{m}$ ) with steam condensation heating to study the effects of roughness on heat transfer and fluid flow. It was found that below  $Re = 583$  the roughness did not play a major role, and friction factor agreed with macroscale theory. The critical Reynolds number was found to range from 1881-2479 for laminar to turbulent transition. They also observed poor fit of experimental heat transfer performance with established correlations.

Li *et al.* [19] used a variety of stainless steel, glass, and fused silica capillary tubes to study the effects of roughened tubes. Hydraulic diameters ranged from  $79.9\text{-}449\mu\text{m}$ . The fused silica and glass tubes were considered to be smooth tubes for this experimentation, as the roughness was negligible. The stainless steel tubes had relative roughness ranging from 3-4%. No deviation from macroscale theory was found in the smooth microtubes. For the rough stainless steel tubes,  $f*Re$  was found to be much higher. As the relative roughness increased, larger discrepancies were observed. The parameter  $f*Re$  was again shown to

vary with Reynolds number in this work instead of remaining constant as macroscale theory would predict.

Bucci *et al.* [20] tested stainless steel capillaries with hydraulic diameters from 172 $\mu\text{m}$  to 520 $\mu\text{m}$ . The study used vapor condensation heating for the heating source. It was shown that for low relative roughness, the tubes behaved as macroscale theory predicts, with both experimental friction factor and laminar-turbulent transition agreement. For rougher tubes with smaller diameters, the laminar-turbulent transition was observed at higher Reynolds numbers and very abrupt rather than smooth.

Schmitt and Kandlikar [21] performed work in this area using rectangular minichannels of hydraulic diameters ranging from 325 $\mu\text{m}$  to 1819 $\mu\text{m}$  with air and water as the working fluids. They found early turbulent transition and higher pressure drops when compared to conventional values. They also found that the laminar friction factor could be calculated by using the constricted hydraulic diameter,  $D_{h,cf}$ . Use of this constricted area takes into account only the area of the channel that has no roughened protrusions into the flow. They also found a relationship between the critical Reynolds number and the relative roughness.

Wibel *et al.* [22] performed experimentation on varying aspect ratio microchannels, fabricated with an end mill in metal. The hydraulic diameters were intended to be a constant  $133\mu\text{m}$ , but manufacturing inaccuracies led to minor variations. Three aspect ratios were investigated, unity, 1:2 and 1:5. An increasing critical Reynolds number was found with decreasing aspect ratio, with  $Re_c=1800-2000$  for a unity aspect ratio and  $Re_c=2300-2800$  for 1:5. It was also found that decreasing aspect ratio increased the length of the laminar turbulent transition. Good correlation was found with conventional macroscale theory for friction factors, however the channels were relatively smooth.

Campbell *et al.* [23] showed that the type of entrance to the mini- or micro-channel has little effect on pressure drop or laminar turbulent transition. This result verifies that the above studies can indeed be compared as they all implement differing test setups and entry conditions.

A summary of experimental works is presented in Table 1.1.

	Year	Material	Roughness	Shape	# Tests	Dh ( $\mu\text{m}$ )	h/w	Re	f	Fluid	Re <sub>c</sub>	Error
<b>Mala and Li [10]</b>	1999	SS and Fused Silica	1.75 $\mu\text{m}$	Capillaries	13	50-254	~	<2100	greater than predicted, increases w/ decreasing Dh	Water		9.2%f 3%Re
<b>Celata et al. [18]</b>	2000	SS	0.0265	Capillaries	1	130	~	100-800	Re<583 classical, greater with higher Re numbers	R114	1881-2479 is transition region	9%f 5%Re 20%Nu
<b>Li et al. [19]</b>	2000	SS, fused silica, glass	0.1%RR to 4%RR	Capillaries	12	79.9-449	~	<2400	Smooth Tubes follow macroscale, Rough have 15-37% higher f	Water	1700~1900 for rough tubes	
<b>Kandlikar et al. [13]</b>	2001	SS	1.0-3.0	Capillaries	6	620 and 1067	~	<2300	no effect on Dh 1067, highest f and Nu from roughest 620	Water	Lowered w/ roughness	
<b>Bucci et al. [20]</b>	2003	SS	0.3% to 0.8% RR	Capillaries	3	172-520	~	200-600	Re<800-1000 follows classical	Water	1800-3000, abrupt transition for high RR	8.36%f 1.8%Re 22.25%Nu
<b>Celata et al. [9]</b>	2004	glass, Teflon	.05 $\mu\text{m}$ smooth, .2-.8 $\mu\text{m}$ rough	Capillaries	10	31-326	~		tentatively propose higher than normal friction	Water		
<b>Peng et al. [5]</b>	1994	SS	~	Rectangular	7	.133-.343	.333-1	50-4000	$\alpha$ makes some +, some -	Water	200-700	10%f, 8%Re
<b>Pfund et al. [6]</b>	2000	Lexan and Polyimide	.16 and .09 $\mu\text{m}$ , rough 1.9 $\mu\text{m}$	Rectangular	6	252.8-1900	.0128-.105	<3600	higher, highest for rough	Water	approach 2800 w/ larger	11.1%f 3.4%Red
<b>Tu et al. [7]</b>	2003	Silicon	Ra < 20nm	Rectangular	5	69.5-304.7	.09-.24	112-9180	RR<.3%, conventional, RR=.35% f is 9% higher	RF134a	2150-2290 w/ RR<.3%, 1570 for .35%	6.3%f 2%Re
<b>Baviere et al. [14]</b>	2004	Bronze, Ni, SiC, Silicon	5-7 $\mu\text{m}$	Rectangular	10			01-8000	increased laminar friction	Water	increased with roughness	
<b>Hao et al. [15]</b>	2006	Silicon	Artificial 50x50 $\mu\text{m}$ RR 19%	Rectangular	4	153-191	0.39-0.55	<2400	follows theory until Re=900, then higher, indicating trans.	Water	Transition ~900	
<b>Shen et al. [17]</b>	2006	Copper	4% RR	Rectangular	1	436	0.375	162-1257	Higher, and Po number increases with Re, nothing at low Re	Water	N/A	7.1%f 6.95%Re 5.93%Nu
<b>Wibel et al. [22]</b>	2006	metal	1.3 $\mu\text{m}$ (~0.97%RR)	Rectangular	6	~133	0.2-1	<4000	near classical values	Water	1800-2300 - varies with aspect ratio	
<b>Wu et al. [3]</b>	1983	Glass	0.05-0.30 height	Trapezoidal		45.5-83.1	~	~	greater than predicted	Gas		
<b>Wu et al. [4]</b>	1984	Glass	0.01 height	Trapezoidal		134-164	~	~	greater than predicted	Gas	1000-3000	
<b>Weilin et al. [16]</b>	2000	Silicon	2.4%-3.5%	Trapezoidal	6	51-169	~	<1500	Higher and larger slope for Px-Re (18-32%)	Water	N/A	7.6%f 4.6%Re
<b>Wu et al. [8]</b>	2003	Silicon and SiO <sub>2</sub>	3.26e-5-1.09e-2	Trapezoidal	13	~100	.0382-.3573	14-1100	roughness increased it, surface type varied it	Water	N/A	10.3%fappRe 7.8%Nu

**Table 1.1: Summary of Experimental works on the effects of roughness on flow**

### 1.1.2 Turbulent Flow

The effects of roughness in turbulent flow in microchannels is rarely studied, due to the high pressure drops that this regime requires in small channels. In addition, most processes of interest in microfluidics work with laminar flow. Because of this, few studies ever cover this range and those will be outlined below.

Celata *et al.* [24] studied the heat transfer on 6 capillary tubes of diameter 130  $\mu\text{m}$ . The roughness element height in these channels was 3.45  $\mu\text{m}$ , leading to a relative roughness of 2.65%. In the laminar regime, the experimental results follow closely with theory, however nearly all the data points collected fall above this line, in agreement with the author's past work on the laminar regime. In the turbulent regime, the experimental data fall between the Blasius correlation (smooth tubes) and Colebrook (for the roughened parameters) predictions. They found that the Colebrook equation over predicted the results in the turbulent regime.

Bucci *et al.* [25] used stainless steel capillary tube ranging from 172  $\mu\text{m}$  to 520  $\mu\text{m}$  with water Reynolds numbers up to 6000. The roughness in these capillaries varied from 1.49  $\mu\text{m}$  to 2.17  $\mu\text{m}$ . For the largest two capillary tubes where the turbulent flow regime could be easily reached, the results matched results that were obtained using the Colebrook equation.

Tu and Hrnjak [26] tested R134a in 5 different rectangular channels with differing aspect ratios. Their relative roughnesses varied from 0.14% to 0.35%. They found excellent agreement with macroscale theory in all regimes of flow. The turbulent data was found to fit the Colebrook equation at all roughnesses tested.

Bavier *et al.* [27] examined friction factor in channels varying from 7  $\mu\text{m}$  to 500  $\mu\text{m}$ . Based on plots presented in the work, it appears that their experimental results in the turbulent region correlate well to macroscale theory, however it was never explicitly summarized.

Most all previous work on roughness, even in macroscale focuses on channels with less than 5% relative roughness. Most fluidic devices fall within this region, however surpassing this limitation is possible and likely as fluid devices' channel size decreases. Kandlikar *et al.* [28] proposed using a constricted parameter,  $\epsilon_{FP}$  to model roughness in channels. First, the use of a new roughness element height is proposed by the parameter  $\epsilon_{FP}$ . By changing the base dimension of the channel and recalculating parameters, one can obtain a set of constricted parameters. Using this method, they proposed a modified Moody diagram to account for the effect of roughness essentially decreasing the free flow area of a circular channel. They propose replacing the friction term in the Colebrook turbulent friction factor equation with the following relation. In this equation,  $D_t$  is the root diameter of the tube

$$f_{Moody,cf} = f_{Moody} \left[ \frac{(D_t - 2 \epsilon_{FP})}{D_t} \right]^5 \quad (1.3)$$

When this is used to replot the Moody diagram, all values of relative roughness between 3-5% plateau to a friction factor of  $f=0.042$  for high Reynolds numbers. It is difficult to find a work that tests relative roughness up to or over 3%, part of this thesis aims to test past this region.

## 1.2 Numerical/Theoretical Work

Kandlikar, *et al* [29] report laminar-to-turbulent transitions at far lower values than the accepted value of  $Re=2300$ . It was shown, citing work by Schmitt and Kandlikar [21] that increasing relative roughness values resulted in decreasing critical Reynolds numbers. They give the relation governing the critical Reynolds number in equation 1.4. Also resulting from this work is a modified Moody Diagram, based on constricted hydraulic diameter determining the friction factor. This is shown in Figure 1.1.

$$\begin{aligned} 0 < \frac{\epsilon}{D_{h,cf}} < 0.08 & \quad Re_{crit,cf} = 2300 - 18,750 \left( \frac{\epsilon}{D_{h,cf}} \right) \\ 0.08 < \frac{\epsilon}{D_{h,cf}} < 0.15 & \quad Re_{crit,cf} = 800 - 3,270 \left( \frac{\epsilon}{D_{h,cf}} - 0.08 \right) \end{aligned} \quad (1.4)$$

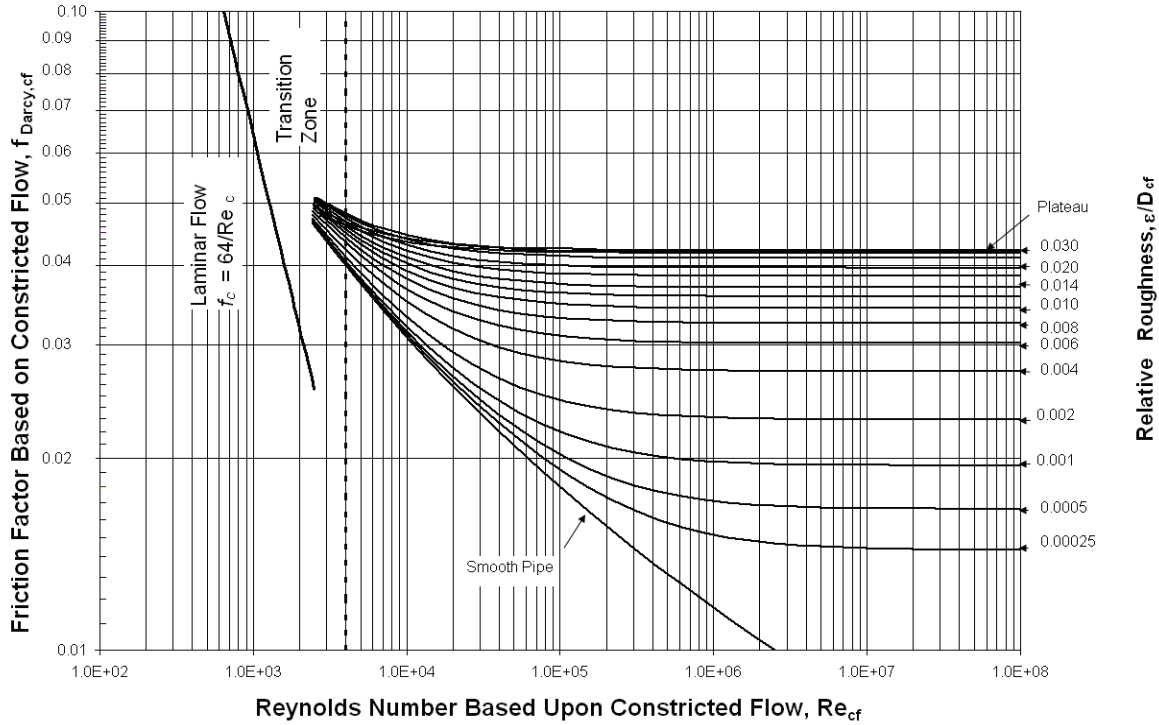


**Figure 1.1: Modified Moody Diagram by Kandlikar [28]**

Rawool *et al.* [30] performed a numerical simulation of sawtooth roughness elements, similar in nature to those used in this experiment. In the simulation, serpentine channels were examined. They found that differing pitches of identical triangular roughness elements led to variations in pressure drop, and velocity profiles. Pressure drop decreases with an increase in the pitch of the elements. A diagram of this discrepancy can be found in Figure 1.2.

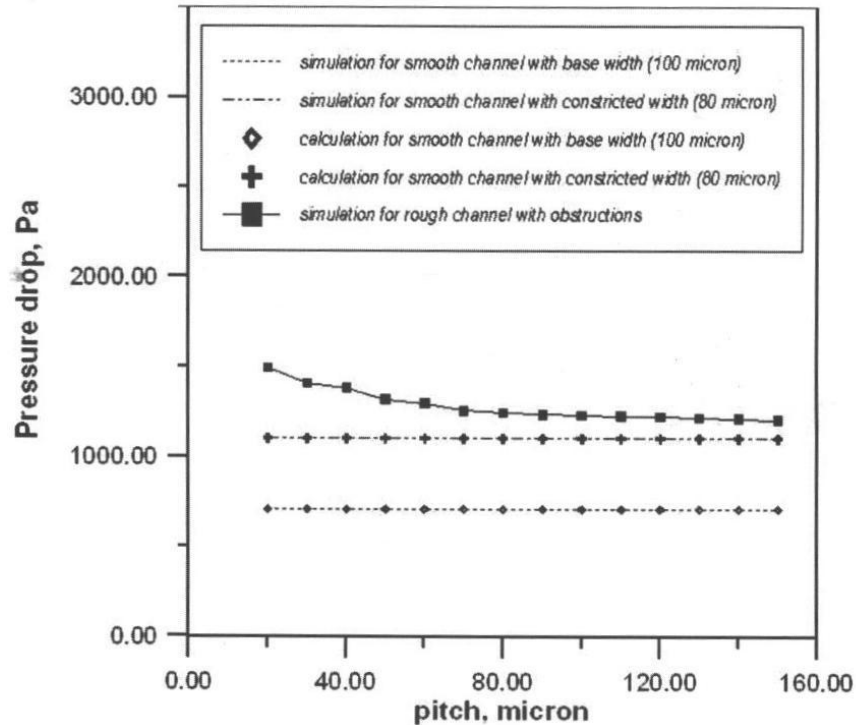


**Figure 1.2: Pressure drop v. pitch of sawtooth obstructions for  $Re = 40$ ,  $h = 0.1$ , from Rawool [30]**

Kandlikar [29] performed a review of available literature and commented on past and current work in roughness and pressure drop. He concluded that work much older than the 1990s on microscale pressure drop included uncertainties that prevented accurate conclusions from being drawn. It also reaffirmed the effect of surface roughness on friction factor and early turbulent transition, while calling for more low relative roughness experimentation.

Chen and Cheng [31] created a fractal and an empirically based model to determine the pressure drop in roughened microchannels. They determined a parameter  $D$ , that is based on the number of boxes ( $N$ ) in a

uniform square mesh which contains a piece of a superimposed roughness profile. They systematically decreased the mesh spacing and plotted the results to obtain an empirical constant. Two additional empirical constants are then derived from experimental data by Pfund [6].

Bahrami *et al.* [32] modeled a randomly roughened surface on the walls of circular microtubes using a Gaussian distribution in both the angular and longitudinal directions. The total surface shape was represented by a superposition of these distributions. After solving the NS equations for this geometry, they arrived at a modification factor that is based on simply the constantly changing radius. It is then manipulated to an easily applied form when the roughness height and some additional modification correlations are given. Using this model Bahrami found agreement with data published by Celata [18], Jiang [33], Kandlikar [13], Li [19], and Mala and Li [10]. Although error from the model is never presented in numerical fashion, average error from the model's results is about 7% judging from the 10% error bars used. The error range is from 0-20%.

Zou and Peng [34] used constricted flow parameters with an additional factor to predict the frictional behavior of flows. To represent the roughness, they used  $R_z$  roughness, or mean peak height. Using just this constriction in the flow area they described friction factor as a modification of the standard friction factor,  $f_0$ . They further modified this constricted flow parameter by adding empirical correction factors for the

separation between the roughness elements. The separation correction effectively decreases the original modification factor by adding another coefficient. Using the height of the roughness elements, the distance between elements, and the distance to reattachment behind the elements from backwards facing step results, they then further modified the model.

Mala and Li [10] proposed a roughness viscosity model based on work by Merkle [11]. The goal of this model is to treat the roughness effects as a higher apparent viscosity in the fluid near the rough walls. Using this modified viscosity they rewrote the momentum equation to account for the roughness effect. The resulting equation is difficult to solve analytically and as such Mala and Li developed a numerical scheme to solve it. Using experimental data and CFD results, some empirical constants are introduced to account for the observed effects.

Some of the models described above account for geometric shape, however none account for flow effects with anything other than empirical correction factors. The work presented here is a continuation of our efforts to develop a model that will account for the fluid flow intricacies, beginning with lubrication theory.

### **1.3 Roughness Characterization**

Recently, Kandlikar *et al.* [28] proposed new roughness parameters of interest to roughness effects in microfluidics. These parameters are

illustrated graphically in Figure 1.3. The parameters are listed below, as well as how all were calculated. These values are established to correct for the assumption that different roughness profiles with equal values of  $R_a$ , average roughness, may have different effects on flows with variations in other profile characteristics. For example, a roughness surface with twice the pitch but the same  $R_a$  may have different pressure drops.

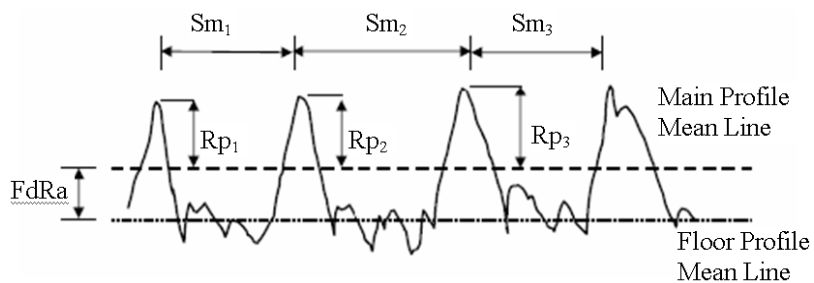


**Figure 1.3: Generic roughness surface with parameters marked**

- The Mean Line is the arithmetic average of all the points from the raw profile, which physically relate to the height of each point on the surface. It is calculated by equation 1.5. Note that  $Z$  is the height of the scan at each point,  $i$ .

$$Mean\ Line = \frac{1}{n} \sum_{i=1}^n Z_i \quad (1.5)$$

- $R_p$  is the maximum peak height from the mean line, which translates to the highest point in the profile sample minus the mean line. It is calculated by equation 1.6.

$$R_p = \max(Z_i) - Mean\ Line \quad (1.6)$$

- $R_{S_m}$  is defined as the mean separation of profile irregularities, or the distance along the surface between peaks. This is also defined in this

paper as the pitch of the roughness elements. It can be seen in Figure 1.3.

- $F_p$  is defined as the floor profile. It is the arithmetic average of all the points that fall below the mean line value. As such, it is a good descriptor of the baseline of the roughness profile. It can be calculated from equation 1.7. This value defines the unconstricted parameters.

*Let  $z \subseteq Z$  s.t. all  $z_i = Z_i$  iff  $Z_i < \text{Mean Line}$*

$$F_p = \frac{1}{n_z} \sum_{i=1}^n z_i \quad (1.7)$$

- $FdRa$  is defined as the distance of the floor profile ( $F_p$ ) from the mean line. It is found with equation 1.8.

$$FdRa = \text{Mean Line} - F_p \quad (1.8)$$

- $\epsilon_{FP}$ , or the value of the roughness height, is determined by equation 1.9.

$$\epsilon_{FP} = R_p + FdRa \quad (1.9)$$

## 2 Theoretical Work

### 2.1 Current Roughness and Nikuradse

A brief look will be taken at the method used by Nikuradse [2] to generate the original data on roughness in 1933. Nikuradse collected pressure drop data on roughened pipes, using sand grains as roughness elements in commercially available smooth tubes. He defined roughness height to be the diameter of the grains of sand coating the walls of the pipe. Unfortunately, relating a real life roughness profile to a sand grain diameter for calculations is nearly impossible. Therefore, a parameter to relate roughness encountered in microchannels and minichannels to the data collected by Nikuradse needs to be determined. To begin, the method Nikuradse used to create his roughness must be examined.

Nikuradse [2] first sifted grains from ordinary building sand to obtain grains that were 800 $\mu\text{m}$  in diameter using an 820 $\mu\text{m}$  and a 780 $\mu\text{m}$  sieve. These grains were then put under a micrometer to verify the desired size. Pipes used in the experiments were filled with a lacquer, drained, and allowed to become tacky. When the lacquer became tacky, the pipes were filled with the sieved sand, and then emptied again. He then again filled the tubes with lacquer and emptied them, in the interest of achieving better adhesion of sand grains to the walls of the tubes. To allow the lacquer to properly dry, heat lamps were applied over an extended amount of time. These pipes were then tested in the

experimental apparatus. The resulting surface of the pipes looks something like the ideal surface given in Figure 2.1 (b).

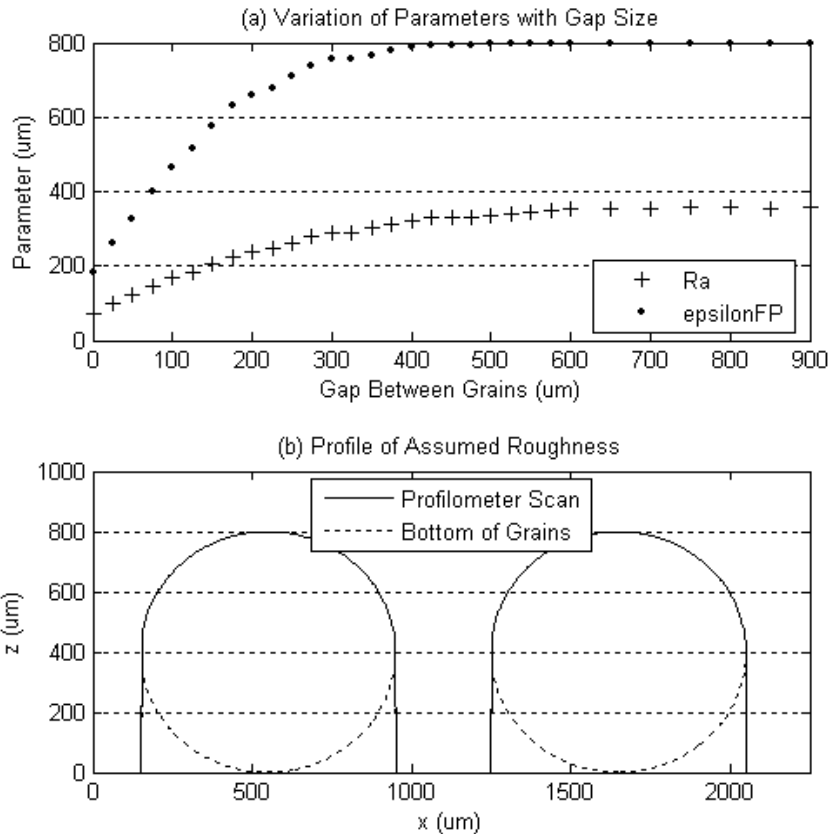


**Figure 2.1: Illustration of Idealized roughness surface from Nikuradse [2]**

A question this process brings to mind is whether a coating of lacquer over the sand grains would appreciably change their diameter. To alleviate this worry, Nikuradse applied this same procedure to a flat plate, and measured the height of the resulting roughness formations post-lacquering with a micrometer. Confirmation of the height of roughness was expressed in his work. A microscope picture of these grains was taken, and it showed that small gaps were present in between

the sand grains, however this illustration was included only to show that the hydrodynamic influence of these grains was indeed the diameter. Thus the gap size between the grains is of definite variability from grain to grain, but from the microscope photo shown in Nikuradse's work it appears to be at most 400 $\mu\text{m}$  and at least 100 $\mu\text{m}$  as a rough estimate.

A model is made, assuming the sand grains are perfect spheres, of an ideal representation what a 2D stylus profilometer scan of this surface would look like. This model is implemented in a spreadsheet. Using this ideal example profile, just as one would use the results of a stylus profilometer, parameters of the surface can be determined. Since the average gap distance between grains is not noted in the paper, the exercise was performed for many gap sizes. With a reasonable assumption that the average distance between grains is taken to be 300 $\mu\text{m}$ ; the resulting Ra is 291 $\mu\text{m}$  and the proposed parameter  $\epsilon_{FP}$  is 756 $\mu\text{m}$ . The value that Nikuradse would have used for this profile is 800 $\mu\text{m}$ , and thus that is what the currently compiled body of data for friction factor relies on. This alone shows the inadequacy of using the Ra parameter as roughness height. Both the profile of roughness (at 300 $\mu\text{m}$  gaps between sand grains) and the plot of the parameters versus the gap size can be seen in Fig. 2. In addition, Figure 2.1 (a) shows clearly that using  $\epsilon_{FP}$  the roughness height asymptotically approaches 800 $\mu\text{m}$ , which would be the value that the modern Moody Diagram is based on. Using Ra

as the roughness parameter will give a smaller value of roughness than intended, and will introduce large errors in the Moody diagram representation.

Note that with increasing gap size,  $\epsilon_{FP}$  approaches the actual sand grain size. One could observe that use of the peak-to-valley roughness parameter, which is simply the maximum point in the profile subtracted by the minimum point, would yield the correct size of  $800\mu\text{m}$ . However practical applications with non-ideal roughness require a parameter that is easy to calculate with simple algorithms, and peak-to-valley would be wrong in any case where a profile contained errant peaks or valleys. This simple exercise shows that  $\epsilon_{FP}$  can characterize roughness height well on a theoretical level, whereas the use of  $R_a$  is a poor choice.

## 2.2 Derivation of Constricted Parameters

The derivation of constricted parameters is paramount to determining important predictors for the friction factor in high roughness channels. First, we have to define the constricted channel height. An ordinary channel has a cross section of height  $b$ , and width  $a$ . However, with roughness on 2 sides of the channel we will introduce the parameter  $b_{cf}$ , to be the new constricted channel height. These parameters are illustrated with generic ribbed roughness in Figure 2.2.

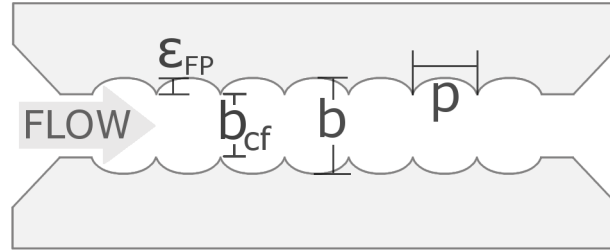


**Figure 2.2: Generic ribbed roughness with parameters illustrated**

Now, to recalculate new constricted parameters, we will use  $b_{cf}$  in place of  $b$ .

The constricted height,  $b_{cf}$  is simply  $b$  minus  $2\epsilon_{FP}$ . Where area is given by equation 2.1, constricted area,  $A_{cf}$ , will be defined by equation 2.2.

$$A = ab \quad (2.1)$$

$$A_{cf} = a b_{cf} \quad (2.2)$$

Perimeter of the rectangular channels is found using equation 2.3. The

constricted perimeter is found using  $b_{cf}$  again instead of  $b$  in equation 2.4.

$$P = 2a + 2b \quad (2.3)$$

$$P_{cf} = 2a + 2b_{cf} \quad (2.4)$$

Hydraulic diameter is calculated using equation 2.5. The constricted hydraulic diameter is found by using the constricted area given in equation 2.6.

$$D_h = \frac{4A}{P} \quad (2.5)$$

$$D_{h,cf} = \frac{4A_{cf}}{P_{cf}} \quad (2.6)$$

Using these constricted parameters, we can now find the theoretical experimental friction factors. In the laminar regime, friction factor for rectangular channels is predicted by Kakac, *et al* [35] by equation 2.7.

The aspect ratio  $\alpha$  is defined by equation 2.8. Again, the constricted aspect ratio,  $\alpha_{cf}$ , is defined with the constricted channel height in equation 2.9.

$$f = \frac{24}{Re} (1 - 1.3553\alpha + 1.9467\alpha^2 - 1.7012\alpha^3 + 0.9564\alpha^4 - 0.2537\alpha^5) \quad (2.7)$$

$$\alpha = \frac{b}{a} \quad (2.8)$$

$$\alpha_{cf} = \frac{b_{cf}}{a} \quad (2.9)$$

The theoretical friction factor is calculated using equation 2.10 from Colebrook [1].

$$\frac{1}{f_{Moody}^{0.5}} = -2.0 \log \left( \frac{\epsilon_{FP}/D_h}{3.7} + \frac{2.51}{Re f_{Moody}^{0.5}} \right) \quad (2.10)$$

To relate the turbulent friction factor we have to look at the governing equation determining friction factor. From the pressure drop equation, we perform the following derivation for equation 2.11 with channel dimension based parameters of the terms pulled outside the parentheses.

$$\begin{aligned} \Delta P &= \frac{2f_{moody} L \rho v^2}{D_h} \\ f_{Moody} &= \frac{\Delta P}{\Delta x} \frac{D_h}{2\rho \left(\frac{Q}{A}\right)^2} \\ f_{Moody} &= \frac{\Delta P}{\Delta x} \frac{D_h A^2}{2\rho Q^2} \\ f_{Moody} &= \left( \frac{\Delta P}{\Delta x} \frac{1}{2\rho Q^2} \right) D_h A^2 \end{aligned} \quad (2.11)$$

$$f_{Moody,cf} = \left( \frac{\Delta P}{\Delta x} \frac{1}{2\rho Q^2} \right) D_{h,cf} A_{cf}^2 \quad (2.12)$$

To compare the friction factor of the constricted channel, we will substitute  $D_{h,cf}$  for  $D_h$  and  $A_{cf}$  for  $A$ . Then, equation 2.11 for  $f_{Moody}$  will be divided by equation 2.12 for  $f_{Moody,cf}$  to obtain a correlation for the constricted friction factor. This is given in equation 2.13.

$$\begin{aligned} \frac{f_{Moody,cf}}{f_{Moody}} &= \frac{\left( \frac{\Delta P}{\Delta x} \frac{1}{2\rho Q^2} \right) D_{h,cf} A_{cf}^2}{\left( \frac{\Delta P}{\Delta x} \frac{1}{2\rho Q^2} \right) D_h A^2} \\ f_{Moody,cf} &= f_{Moody} \frac{\frac{4ab_{cf}}{2a+2b_{cf}} a^2 b_{cf}^2}{\frac{4ab}{2a+2b} a^2 b^2} \\ f_{Moody,cf} &= f_{Moody} \frac{(a+b)}{(a+b_{cf})} \frac{b_{cf}^3}{b^3} = f_{Moody} \frac{P}{P_{cf}} \frac{b_{cf}^3}{b^3} \end{aligned} \quad (2.13)$$

Now we calculate the constricted Reynolds number. It is given by equation 2.14. To calculate the constricted Reynolds number, simply substitute the constricted perimeter in for perimeter. This is given in equation 2.15.

$$Re = \frac{4\dot{m}}{\mu P} \quad (2.14)$$

$$Re_{cf} = \frac{4\dot{m}}{\mu P_{cf}} \quad (2.15)$$

## 2.3 Application of Lubrication Theory

The application of the constricted parameter set is based on theory, in addition to being a practical method for predicting channel performance. A simple derivation from the Navier-Stokes equation with lubrication approximations yields a very similar concept. Originally intended for looking at hydrodynamic effects in fluid bearings, lubrication theory allows one to account for slight wall geometry variances while keeping the solution analytical. The structure of the problem is as follows. A rectangular duct is formed in two dimensions using unknown functions  $f(x)$  for the bottom face and  $h(x)$  for the top face. The simple diagram for analysis can be seen in Figure 2.3.

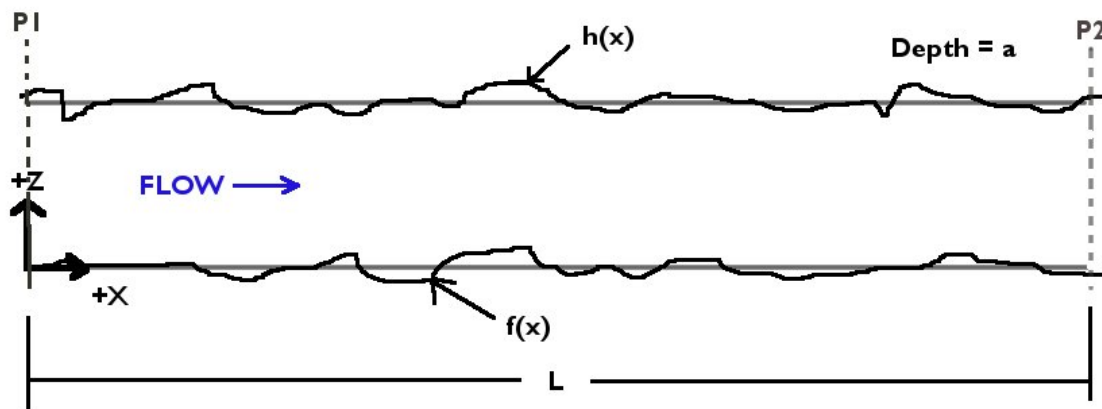


**Figure 2.3: Illustration of Lubrication Problem**

To analyze the system, we begin by stating the appropriate assumptions. Since the separation of the system is much smaller than the length and the slope of the roughness is small, we can assume the

lubrication assumption. We will also assume the slope of roughness elements is small and also that gravity effects are negligible compared to pressure drop in the x direction. The flow is assumed to be incompressible and steady, with entry and exit regions ignored. Ignoring the entrance and exit regions is valid, since these regions are purposely not tested in the experimental results. It is also assumed that there is no velocity in the y direction, and also that the flow does not vary in the x direction.

1.  $(h-f) \ll L$  for all x
2.  $u_y = 0$  - No flow into/out of page
3. Lubrication approximation - neglect  $u_z$  in NS equations
4. Incompressible Flow
5. Ignore gravity -  $(h-f)$  is small for all x
6.  $\frac{\partial u_x}{\partial x} = 0$
7. Flow doesn't vary in y direction
8. Steady Flow
9. Ignore Entry and Exit regions, flow is unidirectional

Next, we start with the continuity equation in 2.16. Using the assumption of incompressibility and no flow in y direction the continuity equation simplifies to 2.17.

$$\frac{\partial u_x}{\partial x} + \frac{\partial u_y}{\partial y} + \frac{\partial u_z}{\partial z} = 0 \quad (2.16)$$

$$\frac{\partial u_x}{\partial x} + \frac{\partial u_z}{\partial z} = 0 \quad (2.17)$$

Now the Navier-Stokes equations are written and simplified in each direction. The simplified forms are given in equations 2.18 to 2.20.

$$x\text{-direction} \quad \frac{1}{\mu} \frac{\partial P}{\partial x} = \frac{\partial^2 u_x}{\partial z^2} \quad (2.18)$$

$$y\text{-direction} \quad \frac{\partial P}{\partial y} = 0 \quad (2.19)$$

$$z\text{-direction} \quad \frac{\partial P}{\partial z} = \rho g_z = 0 \quad (2.20)$$

Next, the boundary conditions of the problem must be set. We require a no slip boundary condition at both the top and bottom surfaces,  $f(x)$  and  $h(x)$  respectively. The pressure at each end of the channel is also defined. Since the pressure variation in the  $y$  direction is negligible compared to variation in the  $x$  direction, gravity is neglected, and the form of the pressure boundary conditions is simply defining a single static pressure of both entrance and exit. The boundary conditions are listed in enumerated form below.

1.  $u_x = u_z = 0 @ z=f(x)$
2.  $u_x = u_z = 0 @ z=h(x)$
3.  $P = P_1 @ x = 0$
4.  $P = P_2 @ x = L$

With the NS equations, continuity equation, and boundary conditions, we have enough information to analytically solve this problem. First, the velocity in the  $x$  direction is found. After integrating the  $x$  direction, two

constants arise, which are found with BCs 1 and 2. The resulting form of flow in the x direction is given by equation 2.21.

$$u_x = \frac{1}{2\mu} \frac{\partial P}{\partial x} [(z-f)^2 - (h-f)(z-f)] \quad (2.21)$$

Now to account for the velocity in the z direction, we integrate the continuity equation over the gap spacing. The formation of this is given in equation 2.22.

$$\int_f^h \frac{\partial u_x}{\partial x} dz + \int_f^h \frac{\partial u_z}{\partial z} dz = 0 \quad (2.22)$$

$$\int_f^h \frac{\partial u_x}{\partial x} dz + u_z|_f^h = 0$$

From BC 1 and 2, we see that  $u_z$  evaluated at both  $f$  and  $h$  is 0, which removes that term. To integrate the remaining term, we apply Leibnitz' Rule to rewrite the first term as is shown in equation 2.23.

$$\frac{d}{dx} \int_f^h u_x dz = \int_f^h \frac{\partial u_x}{\partial x} dz + \frac{dh}{dx} u_x|_h + \frac{df}{dx} u_x|_f \quad (2.23)$$

At this point, we again use boundary conditions 1 and 2 to eliminate the last two terms in equation 2.23. We can now rewrite equation 2.22 in a form that is easy to integrate, given in equation 2.24.

$$\frac{d}{dx} \int_f^h u_x dz = 0 \quad (2.24)$$

This equation is integrated once to get the form shown in equation 2.25.

It can be intuitively seen that integrating x velocity across the gap will

give volumetric flow rate ( $Q$ ) per width of the channel ( $a$ ). As such, the constant of integration is expressed as  $Q/a$ .

$$\int_f^h u_x dz = \text{constant} = \frac{Q}{a} \quad (2.25)$$

The expression derived in equation 2.25 is substituted in for  $u_x$  from equation 2.21 and then integrated. The result of this integration gives the relation in equation 2.26.

$$\frac{Q}{a} = \frac{-(h-f)^3}{12\mu} \frac{dP}{dx} \quad (2.26)$$

This equation is very similar to the equation encountered when simple solving the unidirectional problem of flow through a narrow gap, while neglecting end effects. Now to have a more useful form of this expression, equation 2.26 is solved for the partial derivative of pressure in the  $x$  direction. In actuality, this partial derivative is in fact a normal derivative, since the NS equations cancel the pressure terms in the  $y$  and  $z$  directions. Since the problem is steady, pressure is only a function of the  $x$  direction. This allows us to integrate to obtain equation 2.27.

$$P_2 - P_1 = \frac{-12\mu Q}{a} \int_0^L \frac{1}{(h-f)^3} dx \quad (2.27)$$

For analysis purposes, we can now define a channel height,  $b_{\text{eff}}$  that will be able to predict what friction factor will be present when two samples of known roughness profiles are placed into the test apparatus. If we look

back to equation 2.27 and use  $b_{\text{eff}}$  defined as  $b_{\text{eff}} = h - f$ , we can rewrite it as shown in equation 2.28.

$$\frac{Q}{a} = \frac{-b_{\text{eff}}^3}{12\mu} \frac{dP}{dx} \quad (2.28)$$

Integrating this function as we did before, we can obtain a function for change in pressure using the effective height, given in equation 2.29.

$$P_2 - P_1 = \frac{-12\mu L Q}{a(b_{\text{eff}})^3} \quad (2.29)$$

To obtain a relationship to determine the effective height, we can equate the right sides of equations 2.27 and 2.29. When simplified, we are left with the expression in equation 2.30.

$$b_{\text{eff}, \text{theory}} = \left[ \frac{L}{\int_0^L \frac{1}{(h-f)^3} dx} \right]^{1/3} \quad (2.30)$$

To derive an  $b_{\text{eff}}$  value from experimentation, all that is needed is a rearrangement of equation 2.29 into the form of equation 2.31. Since  $P_1$ ,  $P_2$ ,  $Q$ ,  $a$ ,  $L$ , and  $\mu$  are known in the experiment, it is easy to find  $b_{\text{eff}}$  in equation 2.31.

$$b_{\text{eff}, \text{exp}} = \left[ \frac{-12\mu L Q}{a(P_2 - P_1)} \right]^{1/3} \quad (2.31)$$

This theory should be able to predict the effects of small roughness elements of low slope. Once we surpass the assumptions of this theory, that is have roughness heights that are not much less than the channel

gap, irreversible effects will cause the uniform flow assumption to break down. To further this theory to apply to truly two dimensional flows, a model needs to be added to account for for these added effects on flow.

## 3 Experimental Work

### 3.1 Summary of experimental work

The testing has been performed over a three year period, and because of that multiple tests have been run to test different aspects of the roughness. A brief summary of these four different experiments will be given here, then the full length explanations of the different experiments will be given in the following sections.

The first test that was run was similar to work performed by Derek Schmitt in this same lab. He experimented on the effects of having aligned and offset sawtooth roughness structures in a similar two sample test apparatus. He experimented with water and air as the working fluid. The initial work performed is very similar in nature, and obtained very similar results in both the modification to friction factor, and early transition to turbulence. The relative roughness studied in this thesis varied up to 24% relative roughness, with roughness element heights on the order of 100 $\mu$ m. The work was mainly in the laminar regime.

The second work aimed to establish whether the correlation established with the patterned sawtooth roughness of the previous work still applied to a uniform field of random roughness, or something more like you might find in a channel. The samples were created with two different grits of sandpaper, and the roughness element heights were 9.17 $\mu$ m and

23.19 $\mu\text{m}$  for the two grits. It was found that the correlations that were obtained from the sawtooth work still applied to these roughness structures in the laminar and transition regimes. The relative roughness in this work were all below 6%.

The third work used samples from the two previous tests, and tested them further into the turbulent flow regime to observe the effects. A larger pump was added, and some of the pressure restrictions in the setup were removed to get to higher Reynolds numbers. In this work, one pressure sensor in a differential configuration was used rather than having 2 gage pressure measurements and a subtraction operation. Reynolds numbers as high as 15,000 were obtained with a high differential pressure pump and a  $\frac{1}{2}$  horsepower electric drive.

Finally, a set of sawtooth samples with the same element height (about 50 $\mu\text{m}$ ) but differing pitches were machined. There were 4 sets of samples in this testing, with pitches varying from 503 $\mu\text{m}$  to 2,032 $\mu\text{m}$ . These samples were also tested with a differential pressure sensor, only in the laminar regime. Relative roughness for this experimentation was under 10% relative roughness. This work was performed in the laminar and transition regime.

## 3.2 Initial Experimental Work - Sawtooth High

### 3.2.1 Experimental Loop Description for initial work

The initial test setup was designed and machined three years ago. The system was designed to allow for easy interchange of samples, but had a few operational difficulties. These difficulties arose from the time required to test each sample and the manual nature of controlling the flow with rotameters. All the data had to be manually recorded, which made data collection time consuming.

A schematic of the setup is shown in Figure 3.1. Distilled water is used as the experimental fluid and is stored in a stainless steel reservoir. From the reservoir, it is delivered to a bronze gear pump, Oberdorfer N991RM-FO1 which is driven by a Dayton 5K918C electric motor. It then branches through a 1 $\mu$ m woven filter (Shelco OSBN-384DUB) or goes through the pass-through back to the reservoir. From here, it is delivered to a bank of 3 rotameter flow meters, parts Omega FL-5551C. The distilled water then enters the test section. It then exits the test section and is released back into the reservoir.

The test section is rectangular in shape, with a fixed width of 12.2 mm (0.48in) and a variable height, fixed by four set screws. The test section is 88.9 mm (3.5 in) long and has static pressure taps along the length of the channel. These taps are spaced 6.35 mm (0.25 in) apart for a total of 16 taps along the channel length, and are formed with a #60 drill (diameter

= 1.016 mm) in the wall of aluminum. Care was taken to leave no burrs protruding into the flow. The taps are all connected to a pressure manifold, with a separate valve for each tap. At the end of the pressure manifold is a Honeywell 0-690 kPa (0-100 psi) differential pressure sensor powered by an Electro Industries Laboratory DC power supply. At the inlet and outlet, two K type thermocouples measure the temperature of the water. To control the separation, two Mitutoyo Digimatic Micrometer heads with  $\pm 2.54 \mu\text{m}$  accuracy are used to set the separation, which is then fixed in place with screws.

The pressure sensor is connected to one channel of a simple LM324 operational amplifier circuit, with the gain set at 67. The design used is a basic non-inverting amplifier circuit. The op-amp circuit is powered by an Electro Industries Laboratory DC power supply (at +31VDC). The amplified voltage reading is calibrated to a pressure using an OMEGA DPS-610 Pressure calibrator. Pressure readings are then obtained using the voltage recorded by a Craftsman 82040 Multimeter.

### **3.2.2 Experimental Schematics and Drawings**

A simple schematic of the setup can be seen in Figure 3.1.

The test section itself was machined from 6061 aluminum stock. An exploded view of the test section makeup is given in Figure 3.2.

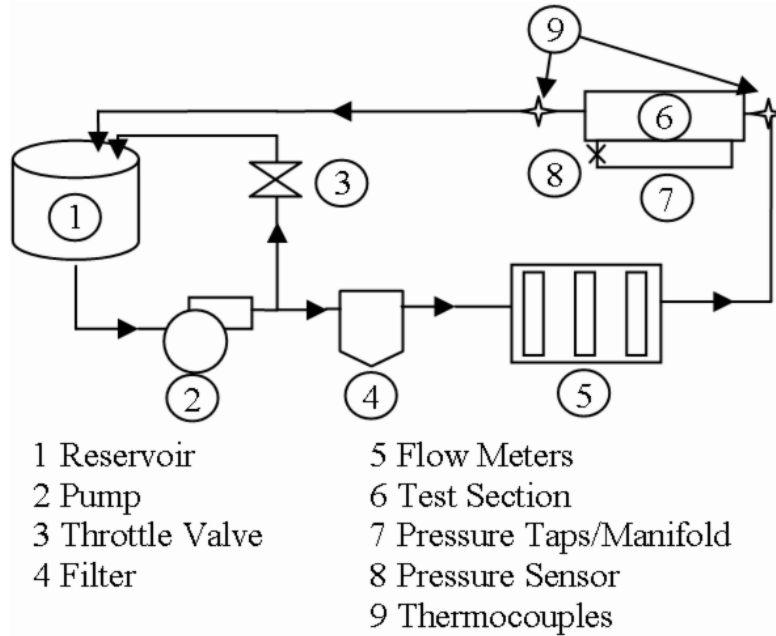


**Figure 3.1: Schematic of the first test loop designed**

In Figure 3.2 the two red blocks are the samples that form the microchannel. The yellow block on the top holds the top sample fixed. The yellow block on the bottom holds 2 screws and 2 micrometer positioning heads that allow the separation of the setup to be varied. This

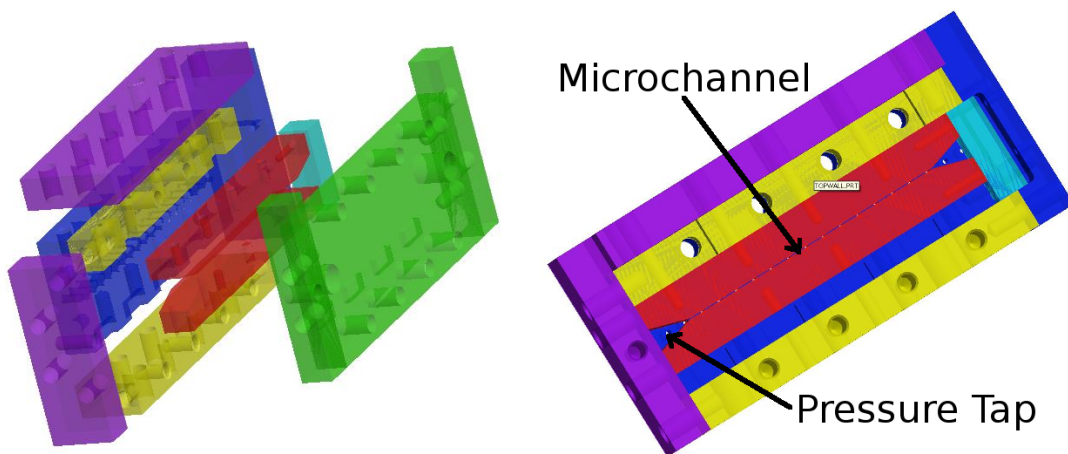


**Figure 3.2: Left: Exploded view of the setup Right: Assembled setup without cover piece**

allows the same samples to be used in channels of varying diameters, essentially varying the relative roughness. The blue piece comprises one

wall of the channel and features pressure taps for measuring static pressure along the channel. The end of the channel is made up of the light blue piece. Finally, the green cover comprises another wall, and holds the inlet and outlet of the channel.

### 3.2.3 Samples used in First Experimentation

With this setup, the effects of sawtooth roughness with high relative roughness was examined. Two sample sets were used for the roughened channels. They had similar roughness heights, but differed in the pitch of the roughness elements. First however, the experimental setup is validated using samples that were ground to be flat and smooth. The smooth channel profile as obtained by a stylus profilometer can be seen in Figure 3.5. The height of roughness from the grinding process is around  $\epsilon=2 \mu\text{m}$ . The values obtained from these smooth channel tests are expected to match theoretical values for smooth rectangular channels.

	Pitch $\mu\text{m}$	$\epsilon_{FP}$ $\mu\text{m}$	Ra $\mu\text{m}$	Fp $\mu\text{m}$
Smooth	N/A	2	0.31	N/A
405 $\mu\text{m}$ Sawtooth	405	99.71	27.43	23.34
815 $\mu\text{m}$ Sawtooth	815	105.55	24.19	21.52

**Table 3.1: Summary of Roughness in First Experimentation**

Two different sample sets were machined using a ball end mill of appropriate diameter. The ball end mill was run perpendicular to the test samples to machine grooves at a shallow depth. The ball end mill diameter was 762  $\mu\text{m}$ .

For this experiment, two pitches of 415  $\mu\text{m}$  and 815  $\mu\text{m}$  were employed. The profile of the  $p=415 \mu\text{m}$  sample is shown in Figure 3.3, and was obtained with a Mitutoyo stylus profilometer. It can be seen from measuring eight different parts of the sample in 2 mm samples that the height of the roughness elements are  $\epsilon = 99.71 \mu\text{m}$ . The 815  $\mu\text{m}$  pitch sample had a roughness profile that is shown in Figure 3.4. Every other

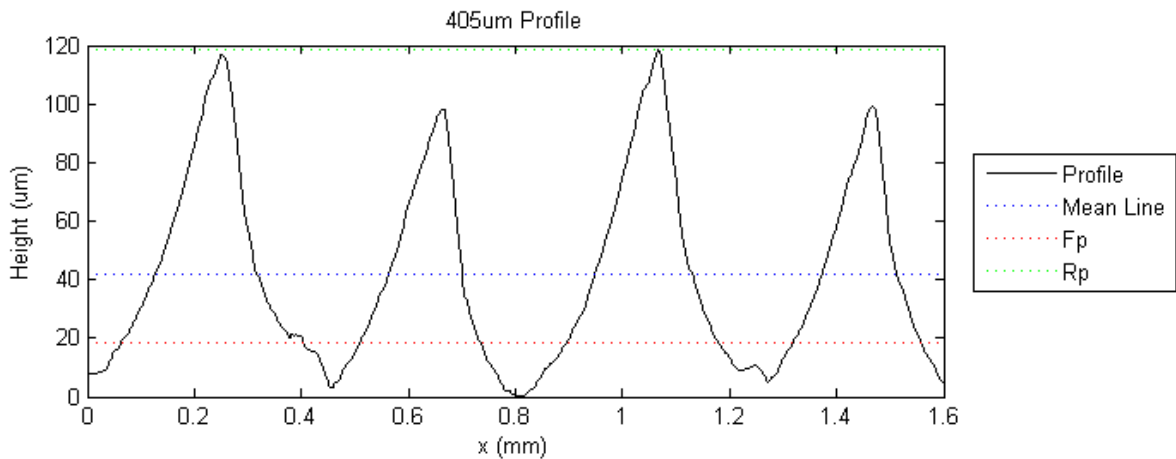


**Figure 3.3: 405um pitch profile, taken with a stylus profilometer. The parameters are marked**

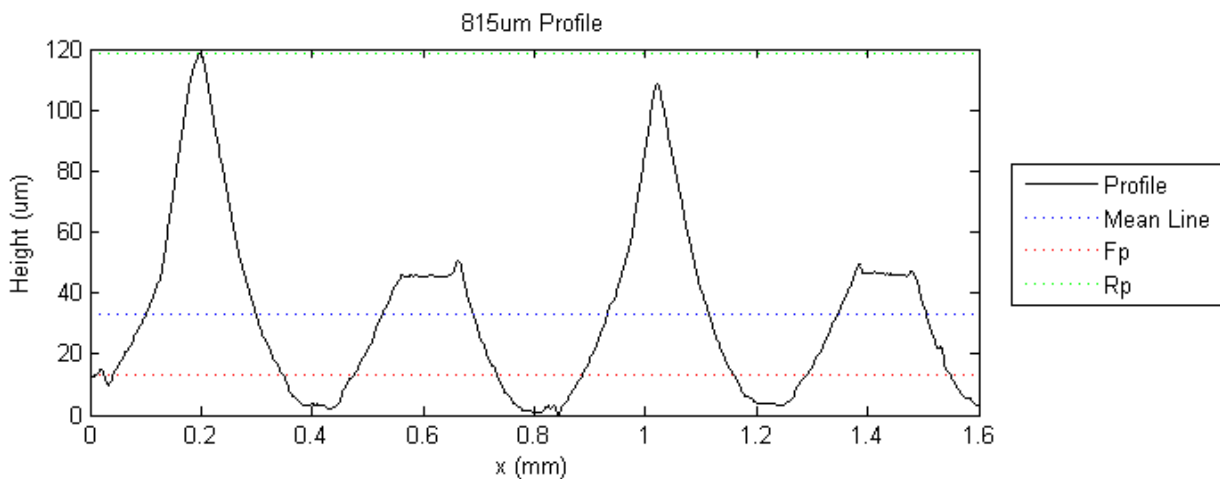


**Figure 3.4: 815um pitch profile, taken with stylus profilometer**

roughness element on these samples was machined somewhat

differently. Only the tops of every other element were removed, rather than the entire element. On these samples the height of the roughness elements is  $\epsilon=105.55 \mu\text{m}$ .

The geometries of the samples are summarized in Table 3.1. The value of  $R_a$  is calculated from the raw profilometer data by averaging the heights according to ASME standards. The value of  $F_p$  was then obtained with a simple program that ignored all data above  $R_a$  and found the average of the rest of the data.  $F_p$  is then the distance from the average roughness to the floor profile line.

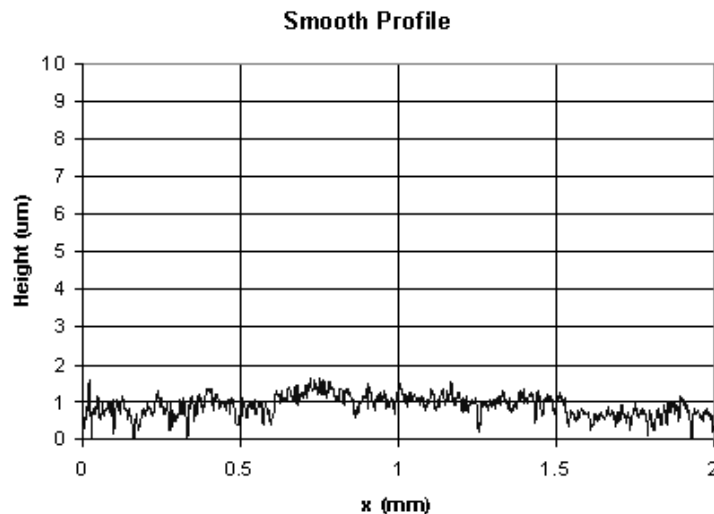


**Figure 3.5: Ground smooth sample surface, taken with a stylus Profilometer**

### **3.2.4 Experimental Procedure for the First setup**

First, the samples to be tested are put in the test apparatus, which is sealed with small quantities of gray putty tape. The constricted height (bcf) of the channel is calibrated at zero by placing two gage blocks of equal size between the samples, then zeroing the micrometers when the samples are touching the gage blocks. After removing the gage blocks, the height is set to the desired distance and secured in the set position with screws. The bypass valve in the water flow loop is then opened the entire way to allow excess flow back into the reservoir. The pump is then turned on. The flow through the test channel is set with the bank of flow meters. When the flow stabilizes, the static pressure at each tap is measured successively using a bank of connecting valves appropriately. The flow rate is then changed over the desired range of Reynolds numbers to obtain the flow characteristics at each hydraulic diameter. This is performed for each set of samples, with the flat samples used to validate the experimental setup.

### **3.3 Second Setup - Low uniform RR testing**

The purpose of this testing is to look at the effect of less patterned roughness, or more similar to roughness that would be encountered in actual channels. The purpose of this testing is to verify that the constricted parameters apply to roughness structures other than sawtooth elements.

### 3.3.1 Experimental Setup for Low RR uniform elements

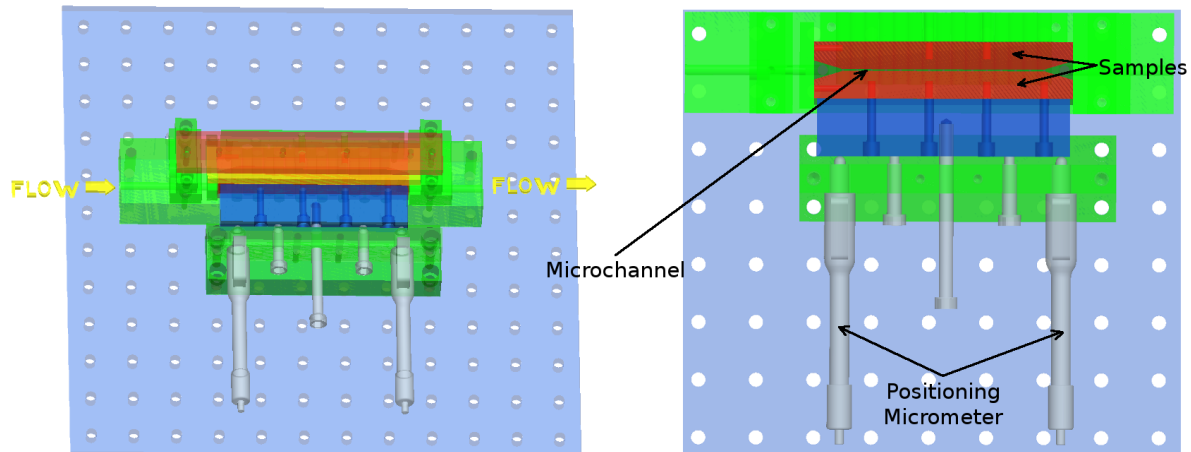


**Figure 3.6: Isometric Schematics of New Test section**

The experimental setup was developed based on insight gained from the use of the previous setup. An isometric view of this new improved system can be seen in Figure 3.6. Improvements were made in many areas to accommodate for easier and less time consuming testing. Any metallic surface critical to accurate measurements was ground smooth, planar, and square in a precision surface grinder. The channel is sealed with sheet silicone gaskets around the outside of the samples to prevent leaks. The base block acts as a fluid delivery system and also houses 15 pressure taps, each drilled with a #60 drill (diameter of 1.016mm) along the channel. The taps begin at the entrance to the channel and are spaced every 6.35mm along the channel's 88.9mm length. Each tap is connected to a 0-689kPa (0-100psi) differential pressure sensor with 0.2% FS accuracy. The pressure sensor outputs are put through independent linear 100 gain amplifiers built into the NI SCXI chassis to increase

accuracy. The separation of the samples is controlled by two Mitutoyo micrometer heads, with  $\pm 2.54\mu\text{m}$  accuracy. There is a micrometer head at each end of the channel to ensure parallelism.

Water is delivered via a Micropump motor drive along with two Micropump metered pump heads, one for low flows (0-100mL/min) and one for high flows (76-4000mL/min). The flow rate is verified with three flow meters, one each for 13-100mL/min, 60-1000mL/min, and 500-5000mL/min. Each flow meter is accurate to better than 1% FS. Furthermore, each flow meter was calibrated by measuring the weight of water collected over a period of time. Thermocouples are mounted on the inlet and outlet of the test apparatus. Fluid properties are calculated at the average temperature. All of the data is acquired and the system controlled by a LabVIEW equipped computer with an SCXI-1000 chassis. Testing equipment allows for fully automated acquisition of data at set intervals of Reynolds number. A test setup schematic can be found in Fig. 4. All of the circles with P's are pressure sensors.

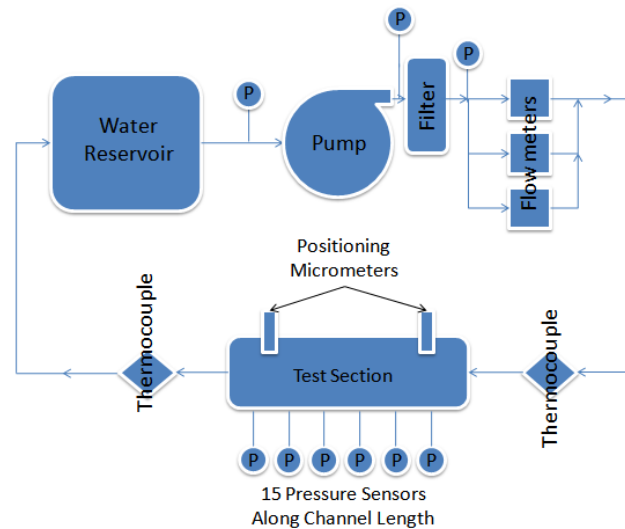


**Figure 3.7: Schematic of test loop used for low Relative roughness testing**

### 3.3.2 Samples used for low uniform roughness

The sample blanks are machined to near-dimensions, and then are precision ground to exact dimensions. The parallelism and flatness are then verified to ensure proper channel geometry. The smooth channel samples were then lapped first with 5 $\mu$ m lapping compound and then 1 $\mu$ m lapping compound to create a mirrored smooth surface.

The first roughened channel set is then formed by using 100 grit sandpaper in a perpendicular crosshatch pattern. The uniform roughness is formed sanding 45 degrees in both directions from the axis along the length of the channel. The profile of this surface is then taken with a stylus profilometer, and parameters are determined using both  $\epsilon_{FP}$  and the conventional Ra. The results of 8 tests are averaged and a value  $\epsilon_{FP} = 9.17\mu$ m is found for the roughness element height. The procedure is repeated on another sample set, except 60 grit sandpaper is used instead

of 100 grit sandpaper. This yielded a much higher value of  $\epsilon_{FP} = 23.19\mu\text{m}$  for the roughness element height. An example profile of each sample used in testing can be seen in Figure 3.8, along with a 3D digital microscope scan of the surfaces. Note that the charts given in Figure 3.8 represent the results of one profilometer scan, and thus the values for each of these calculated parameters may vary slightly from the presented average of all 8 scans.

	<b>Ra</b> <b><math>\mu\text{m}</math></b>	<b>Rp</b> <b><math>\mu\text{m}</math></b>	<b>Rv</b> <b><math>\mu\text{m}</math></b>	<b>FdRa</b> <b><math>\mu\text{m}</math></b>	<b><math>\epsilon_{FP}</math></b> <b><math>\mu\text{m}</math></b>
Smooth	0.06	0.15	0.08	0.05	0.2
100 Grit	2.64	6.87	7.66	2.3	9.17
60 Grit	6.09	17.09	20.81	6.09	23.19

**Table 3.2: Description of roughness surfaces used in low RR testing**

The roughness parameter Ra has often been used in studies to represent the height of the roughness elements. For comparison, this parameter was calculated by the profilometer used in this study. Both parameters for all samples used in testing can be seen in Table 3.2. For a more in depth look at the parameterization of different machined surfaces using this method, refer to Young *et al* [36].

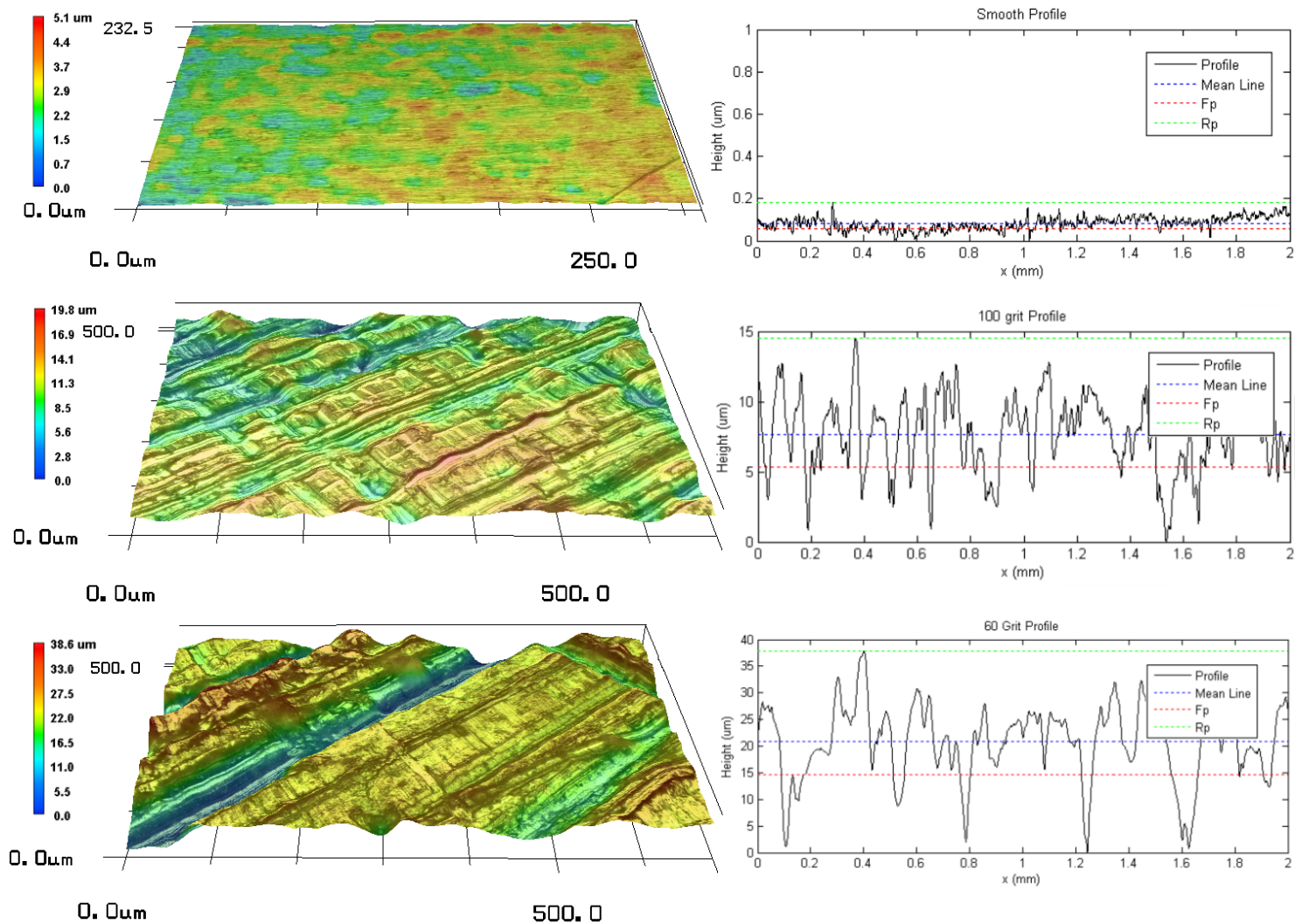


**Figure 3.8: 3D microscope images and stylus profilometer scans of the three roughnesses tested**

### 3.4 Third Experiment - Fully Turbulent Flow

#### 3.4.1 Experimental Schematics

The experimental setup for this series of tests is similar to the second experiment, however some modifications are made to allow for less pressure drop along the fluid path, which enables the testing to continue to higher Reynolds numbers. Manifolds are bypassed, and only the highest flow sensor is used. In addition, rather than using all 15 taps along the length of the channel, 1 sensor in differential mode is used so

the pressure limit of each individual sensor is not exceeded. The test section is also modified slightly to let the flow exit the test section in a straight line. A schematic of the test loop can be seen in Figure 3.9.

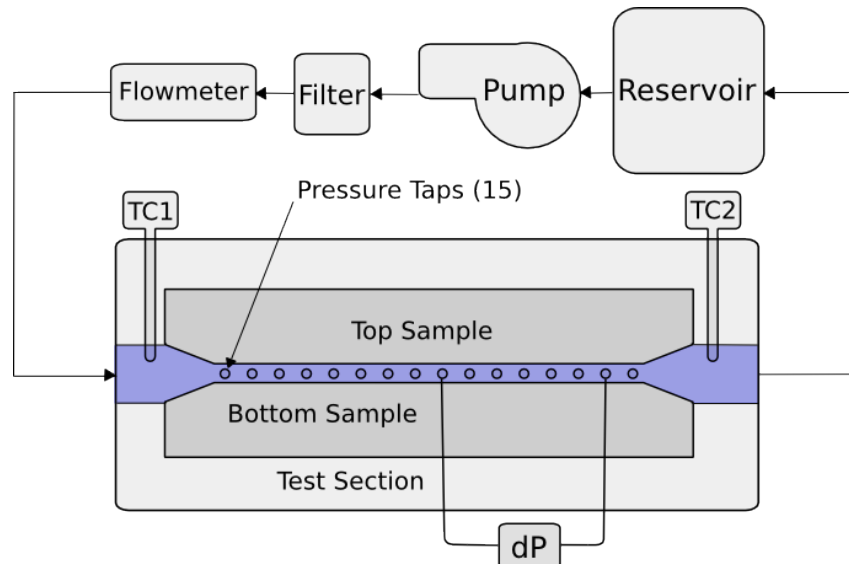


**Figure 3.9: Test loop for third experimentation**

### 3.4.2 Samples

For this experimentation, samples were used from the previous two tests. The 405 $\mu\text{m}$  sawtooth samples from the first experiment were used for higher relative roughnesses (above 5%) and 1008  $\mu\text{m}$  sawtooth samples from the next set of samples were used. The samples are imaged with a 3D microscope and a 2D stylus profilometer, and these views are given in Figure 3.10.

### 3.4.3 Experimental Procedure

Experimental procedure for this set of experimentation is identical to that of the second experiment, with some slight modification to the LabVIEW code to make it work with a single differential pressure sensor.

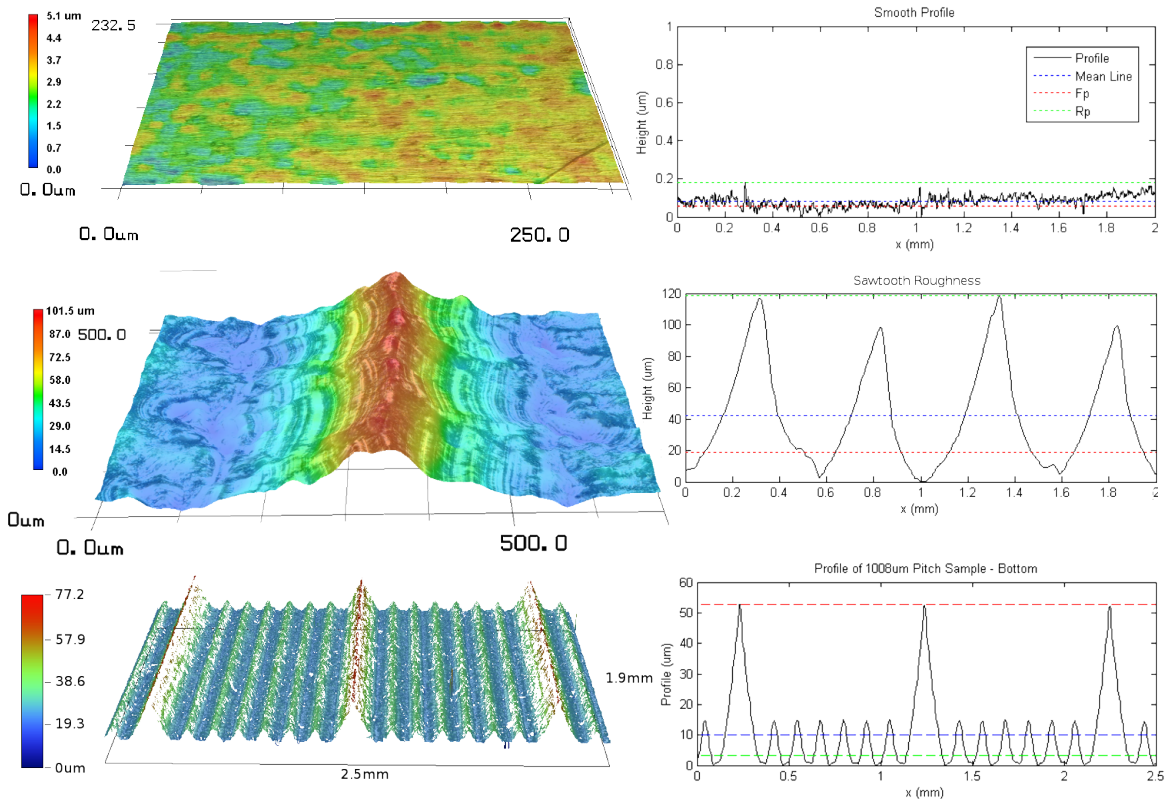


**Figure 3.10: 3D Microscope compilations and 2D stylus profilometer scans of the samples**

## 3.5 Fourth Experiment - Differing pitches of sawtooth roughness

### 3.5.1 Experimental Schematics

The schematic and test apparatus has no change from those of the second experiment. All the hardware and the loop setup is the same.

### 3.5.2 Samples

The samples were made similar to the first experiment, by using a ball end mill in close cuts. This time a more accurate CNC mill was used for more repeatable cutting. Four sets of samples were machined, with the intent of achieving roughness elements with a height of  $50\mu\text{m}$ . What was

varied is the pitch or separation of the elements. The pitch varied from around 500 to 2000 $\mu\text{m}$ .

The results from the machining varied slightly. The two smaller of the four pitches and the largest pitch were machined correctly, but the third largest of the samples was far off. As such, it was not tested. A summary of the roughness machined can be seen in Table 3.3.

Design Pitch Inches	Design Pitch $\mu\text{m}$	Actual Pitch $\mu\text{m}$	Holes in Sample ~	$\epsilon_{FP}$ $\mu\text{m}$	Ra $\mu\text{m}$	Pitch to Height Ratio
0.02	508	503	2	46.24	7.05	11.0
0.02	508	504	4	46.58	6.73	10.9
0.04	1016	1008	2	55.31	6.60	18.4
0.04	1016	1008	4	49.7	6.11	20.4
0.06	1524	1513	2	44.54	5.23	34.2
0.06	1524	1479	4	77.82	4.38	19.6
0.08	2032	2015	2	53.38	4.39	38.1
0.08	2032	2015	4	44.83	4.84	45.3

**Table 3.3: Summary of machining for the fourth set of samples**

The samples were verified with an interferometer. Using the raw data from a 640x480 matrix of diffraction heights, the samples are averaged into one complete 2D axial profile, similar to that that would be obtained from a stylus profilometer. Using this apparent 2D scan, the parameters of the surface can be obtained, and are summarized in Table 3.3. The interferometer scan and apparent 2D scan can be seen in Figure 3.11. The MATLAB code that processes this raw matrix is given below. It can be called to obtain the 2D equivalent as its output.

```

function [output] = simplify_interferometer(rawdata)
% this function accepts a matrix output from the interferometer
instrument
% (after being manually modified to remove the headers and the
"intensity"
% section. It outputs an average profile.

% Constants
bad_value = -6900; % Set to what number you used instead of "Bad"

% Find Dimensions
[nr nc] = size(rawdata);
% Make grid
[X,Y] = meshgrid([1:1:nc],[1:1:nr]);

for n = 1:nr
    %zero things
    sum = 0;
    count = 0;
    for m = 1:nc
        if rawdata(n,m) == bad_value
            hooray = 1;
        else
            sum = sum + rawdata(n,m);
            count = count + 1;
        end
    end
    output(n) = sum / count;
end

return

```

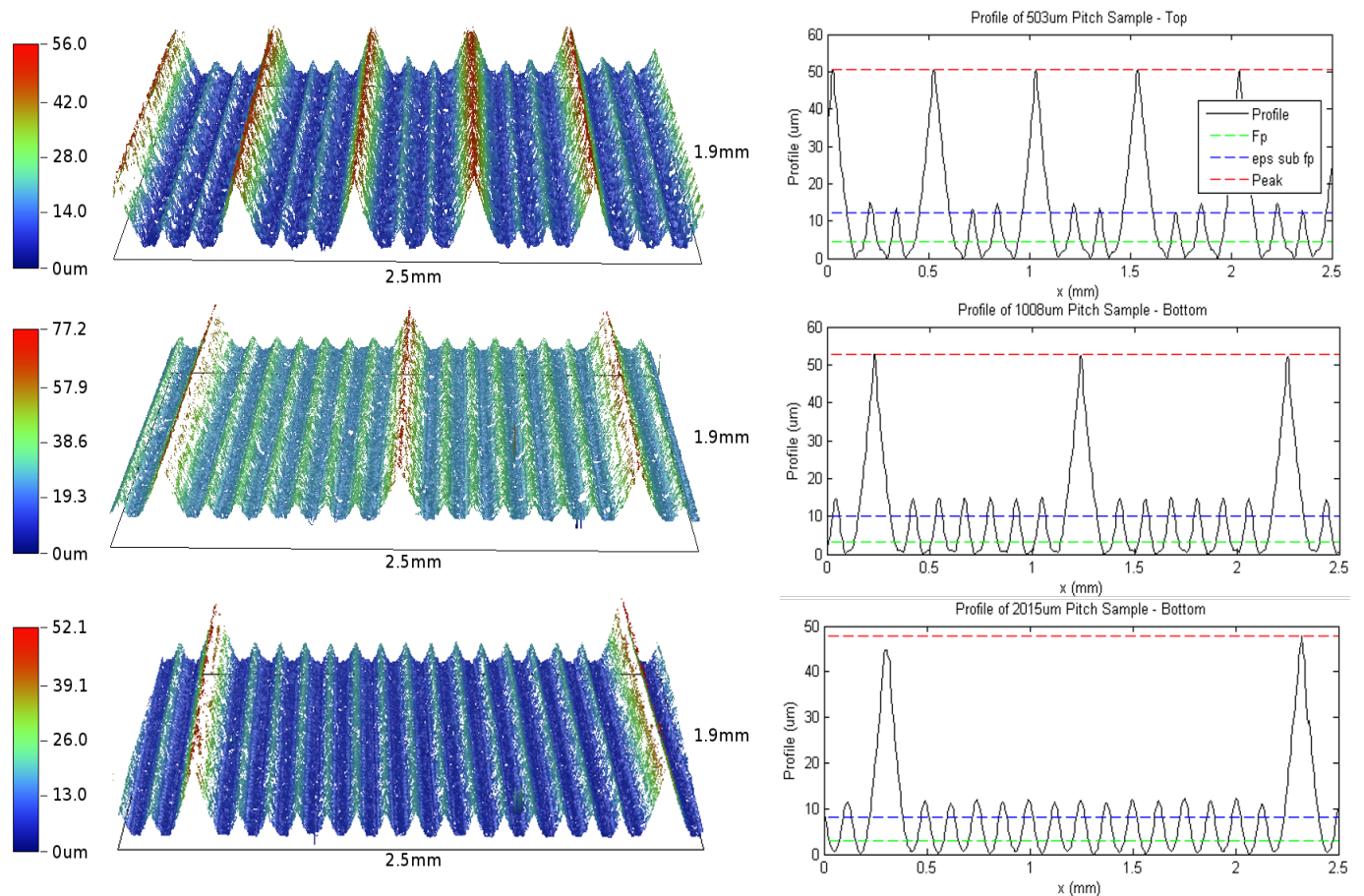


**Figure 3.11: Interferometer scans (left) and apparent 2D profile scans (right) for the three samples tested**

### 3.5.3 Experimental Procedure

Again, this experiment followed the procedure laid out in the second set of experimentation.

## 3.6 LabVIEW

LabVIEW was used to control the experiment, as well as record the data. An in depth virtual instrument (VI) was coded to control all aspects of the experimentation. The VI used went through 12 iterations to get to the point that it can properly and accurately control the experiment. At its current state, the separation and experimental parameters can be set,

then the code assumes control of the experiment and runs it on its own. When finished, it outputs a sheet of the properties and results at all the Reynolds numbers tested.

Given the parameters of the test setup, mainly surface roughness height and test block separation, the VI can control the flow rate from the pump through a desired Reynolds number range at prescribed increments. The LabVIEW motor controller holds the flow rate at a prescribed value, and when a steady state value is achieved the pressure drop and temperature data is recorded. In addition, the LabVIEW VI calculates other parameters, such as finding density and viscosity from the average temperature in the test section. All of the constricted parameter calculations are performed in LabVIEW and exported as an Excel or MATLAB readable file. MATLAB is preferred for more involved calculations. Below, the procedure LabVIEW executes for calculating all of the parameters of interest is outlined.

First constricted area of the channel is found, with a constant and the set value of constricted separation. The width of the samples is  $12,192\mu\text{m}$ , and the  $1\text{e-}12$  is a conversion factor from square micrometers to square meters. In this case, the  $b$  values are entered in micrometers. Because of this, conversion factors are prevalent throughout the first few stages of calculations, until everything has been reduced to SI units.

$$A_{cf} = 12192 (b_{cf}) (1e-12) \quad (3.1)$$

Knowing the roughness height, another constant, we can find the root dimension of the channel as:

$$b = b_{cf} + 2\epsilon_{FP} \quad (3.2)$$

The non constricted area and root area are found with the following.

$$A = 12192 (b) (1e-12) \quad (3.3)$$

$$A_{cf} = 12192 (b_{cf}) (1e-12) \quad (3.4)$$

Then, we calculate the non-constricted and constricted perimeter of the channels with the following equations.

$$P = \frac{2 * 12192 + 2 * b}{1,000,000} \quad (3.5)$$

$$P_{cf} = \frac{2 * 12192 + 2 * b_{cf}}{1,000,000} \quad (3.6)$$

With the areas determined, we can now find the hydraulic diameters.

Since both the areas and perimeters are now in SI units, the calculations are simple as follows.

$$D_h = \frac{4A}{P} \quad (3.7)$$

$$D_{h,cf} = \frac{4A_{cf}}{P_{cf}} \quad (3.8)$$

Next the relative roughnesses are calculated with the following equations.

$$RR = \frac{(\epsilon_{FP} * 1e-6)}{D_h} \quad (3.9)$$

$$RR_{cf} = \frac{(\epsilon_{FP} * 1e-6)}{D_{h,cf}} \quad (3.10)$$

The aspect ratio of the channels is also calculated.

$$\alpha = \frac{b}{a} \quad (3.11)$$

$$\alpha_{cf} = \frac{b_{cf}}{a} \quad (3.12)$$

The volumetric flow rate from the sensors needs to be converted to mass flow rate. This requires the density, which varies as a function of temperatures. As such, the following table converts mean temperature in the channel (as measured by a TC at the entrance and exit of the channel) to density of water. This is performed via a built in linear interpolation function that references a table. The table used over the range of temperatures in this experiment is given below.

Temperature Celsius	Density kg/m <sup>3</sup>
0	999.9
10	999.7
20	998.2
30	995.7
40	992.2
50	988.1
60	981.3

**Table 3.4: State points to reference density**

The second parameters of water we require is the dynamic viscosity, which also varies with temperature. To calculate this we use the following equation.

$$\mu = 0.001005 \left( \frac{T_{mean} + 273.15}{293.15} \right)^{8.9} e^{4700 \left( \frac{1}{T_{mean} + 273.15} - \frac{1}{293.15} \right)} \quad (3.13)$$

With the density at the particular temperature calculated, we can convert the output from the water flow sensors from their native mL/min to kg/s.

To convert, the following equation is used.  $G$  is mass flow (kg/s),  $\dot{V}$  is volumetric flow rate, and  $\rho$  is the density found from table interpolation. Note that a factor of 60,000,000 converts mL/min to cubic meters per second.

$$G = \frac{\dot{V} \rho}{60,000,000} \quad (3.14)$$

Now the Reynolds number and constricted Reynolds number can be found.

$$Re = \frac{4G}{\mu P} \quad (3.15)$$

$$Re_{cf} = \frac{4G}{\mu P_{cf}} \quad (3.16)$$

The code then uses these Reynolds number values to calculate the theoretical laminar friction factor using the corrected empirical rectangular duct equation. This is:

$$f = \frac{24}{Re} (1 - 1.3553\alpha + 1.9467\alpha^2 - 1.7012\alpha^3 + 0.9564\alpha^4 - 0.2537\alpha^5) \quad (3.17)$$

Turbulent theory is predicted using the closed form version of the Colebrook equation, the Haaland Equation. This data is not ever plotted in the output, as a recursive MATLAB function is used instead to solve the Colebrook equation. Additionally, the theoretical friction factor that results from this calculation is not corrected for rectangular ducts as suggested by Kakac [35]. However, the Haaland equation is given below, converted from Darcy to Fanning friction by dividing by four.

$$f = \frac{0.25 \log \left( \frac{\frac{\epsilon_{FP}/10^6}{D_h} + \frac{5.74}{Re^{0.9}}}{3.7} \right)^{-2}}{4} \quad (3.18)$$

$$f_{cf} = \frac{0.25 \log \left( \frac{\frac{\epsilon_{FP}/10^6}{D_{h,cf}} + \frac{5.74}{Re_{cf}^{0.9}}}{3.7} \right)^{-2}}{4} \quad (3.19)$$

The developing length of the channel is also checked, to ensure that measured pressures lie outside the developing range. The equation to determine this length is given by:

$$L_d = 0.05 Re D_h \quad (3.20)$$

Finally, an experimental fanning friction factor can be determined using the above parameters along with a term for the pressure gradient. This is calculated using the following:

$$f_{\text{exp}} = \frac{dP}{dx} \frac{D_h A^2}{2\rho \left(\frac{G}{\rho}\right)^2} \quad (3.21)$$

$$f_{\text{exp},cf} = \frac{dP}{dx} \frac{D_{h,cf} A_{cf}^2}{2\rho \left(\frac{G}{\rho}\right)^2} \quad (3.22)$$

### 3.7 Experimental Uncertainties

The uncertainty in the measure of friction factor is now to be determined.

First the equation for the friction factor is stated.

$$f = \frac{P_2 - P_1}{x} \frac{\rho D_h A^2}{2 G^2} \quad (3.23)$$

To find the error, the propagation of errors in  $f$  ( $\delta f$ ) by the changes in each of the variables was found by the following differentiation:

$$\delta f = \frac{\partial f}{\partial P_1} \delta P_1 + \frac{\partial f}{\partial P_2} \delta P_2 + \frac{\partial f}{\partial x} \delta x + \frac{\partial f}{\partial D_h} \delta D_h + \frac{\partial f}{\partial A} \delta A + \frac{\partial f}{\partial G} \delta G \quad (3.24)$$

Now, the uncertainty in each variable, depicted here as an arbitrary  $y_1$ , is then defined as is shown in the following equation.

$$u_{y_1} = \frac{\delta y_1}{y_1} \quad (3.25)$$

The error propagation equation is then divided through by the friction factor, and rearranged into uncertainties.

$$\begin{aligned} \frac{\delta f}{f} &= \frac{P_1}{f} \frac{\partial f}{\partial P_1} \frac{\delta P_1}{P_1} + \frac{P_2}{f} \frac{\partial f}{\partial P_2} \frac{\delta P_2}{P_2} + \frac{x}{f} \frac{\partial f}{\partial x} \frac{\delta x}{x} + \frac{D_h}{f} \frac{\partial f}{\partial D_h} \frac{\delta D_h}{D_h} + \frac{A}{f} \frac{\partial f}{\partial A} \frac{\delta A}{A} + \frac{G}{f} \frac{\partial f}{\partial G} \frac{\delta G}{G} \\ u_f &= \frac{P_1}{f} \frac{\partial f}{\partial P_1} u_{P_1} + \frac{P_2}{f} \frac{\partial f}{\partial P_2} u_{P_2} + \frac{x}{f} \frac{\partial f}{\partial x} u_x + \frac{D_h}{f} \frac{\partial f}{\partial D_h} u_{D_h} + \frac{A}{f} \frac{\partial f}{\partial A} u_A + \frac{G}{f} \frac{\partial f}{\partial G} u_G \end{aligned} \quad (3.26)$$

Since all the errors are improbably in the same direction, we use the following technique of taking the square root of the sum of all terms squared.

$$u_f = \pm \left[ \left( \frac{P_1}{f} \frac{\partial f}{\partial P_1} u_{P_1} \right)^2 + \left( \frac{P_2}{f} \frac{\partial f}{\partial P_2} u_{P_2} \right)^2 + \left( \frac{x}{f} \frac{\partial f}{\partial x} u_x \right)^2 + \left( \frac{D_h}{f} \frac{\partial f}{\partial D_h} u_{D_h} \right)^2 + \left( \frac{A}{f} \frac{\partial f}{\partial A} u_A \right)^2 + \left( \frac{G}{f} \frac{\partial f}{\partial G} u_G \right)^2 \right]^{\frac{1}{2}} \quad (3.27)$$

Now the partial derivatives of the friction equation are evaluated to give the following equation. Rather than writing out all six terms included in the brackets, the new form of just the first term is given below.

$$\left(\frac{P_1}{f} \frac{\partial P_1}{\partial P_1} u_{P_1}\right)^2 = \left(\frac{P_1}{f} \left(-\frac{\rho D_h A^2}{2 \times G^2}\right) u_{P_1}\right)^2 \quad (3.28)$$

Next, the values of  $u_{D_h}$  and  $u_A$  must be calculated using the same method, as they depend both on the base and width of the channel. As such, we repeat this calculation for the the area and the hydraulic diameter.

$$A = ab$$

$$u_A = \pm \left[ \left( \frac{a}{A} \frac{\partial A}{\partial a} u_a \right)^2 + \left( \frac{b}{A} \frac{\partial A}{\partial b} u_b \right)^2 \right]^{\frac{1}{2}} \quad (3.29)$$

$$u_A = \pm \left[ \left( \frac{ab}{A} u_a \right)^2 + \left( \frac{ab}{A} u_b \right)^2 \right]^{\frac{1}{2}}$$

$$D_h = \frac{2ab}{a+b}$$

$$u_{D_h} = \pm \left[ \left( \frac{a}{D_h} \frac{\partial D_h}{\partial a} u_a \right)^2 + \left( \frac{b}{D_h} \frac{\partial D_h}{\partial b} u_b \right)^2 \right]^{\frac{1}{2}} \quad (3.30)$$

$$u_{D_h} = \pm \left[ \left( \frac{a}{D_h} \frac{2b(a+b) - 2ab}{(a+b)^2} u_a \right)^2 + \left( \frac{b}{D_h} \frac{2a(a+b) - 2ab}{(a+b)^2} u_b \right)^2 \right]^{\frac{1}{2}}$$

Next, the error in the Reynolds number is found using the same technique. The details of the derivation are the same, so the beginning steps are skipped in the following derivation.

$$Re = \frac{4G}{\mu P} = \frac{4G}{\mu(2a+2b)}$$

$$u_{Re} = \pm \left[ \left( \frac{G}{Re} \frac{\partial Re}{\partial G} u_G \right)^2 + \left( \frac{a}{Re} \frac{\partial Re}{\partial a} u_a \right)^2 + \left( \frac{b}{Re} \frac{\partial Re}{\partial b} u_b \right)^2 \right]^{\frac{1}{2}} \quad (3.31)$$

$$u_{Re} = \pm \left[ \left( \frac{G}{Re} \frac{4}{\mu(2a+2b)} u_G \right)^2 + \left( \frac{a}{Re} \frac{-8G}{\mu(2a+2b)^2} u_a \right)^2 + \left( \frac{b}{Re} \frac{-8G}{\mu(2a+2b)^2} u_b \right)^2 \right]^{\frac{1}{2}}$$

This analysis is based on being able to find the uncertainty of each measurement in the experiment. To do this, the calibration performed on each sensor is used. The points used for the linear calibration are used to find the error between measured and the calibration value. For each sensor, 30 points are checked, and the maximum value of error of the 30 is recorded. The average of these maximum errors is used for the error of the pressure sensors. The same is performed for each of the three flow sensors. This approach yields extremely conservative error values, of 0.998% for pressure sensors and around 2.2% for the flow sensors. These points can be found in Table 3.5. Using this analysis, the maximum errors occur at the smallest value of  $b$  at the lowest flow rates encountered. These uncertainties are 7.58% for friction factor and 2.67% for Reynolds number.

Transducer	Max Error
1	0.65%
2	0.70%
3	1.53%
4	0.77%
5	1.79%
6	0.64%
7	0.60%
8	2.40%
9	0.64%
10	0.52%
11	1.82%
12	0.64%
13	0.59%
14	1.12%
15	0.56%
<b>Average</b>	<b>1.00%</b>

Flow Sensor	Flow Range	Max Error
Low	13-100 mL/min	2.27%
Medium	60-1000 mL/min	2.26%
High	500-5000 mL/min	1.22%

**Table 3.5: Summary of max errors used in uncertainty analysis for the pressure and flow sensors**

## 4 Results

### 4.1 Summary and Major Findings

	Test	Sample	εFP	Constricted Sep.		Hyd. Diameter	Const. Diameter	Relative Roughness,cf	Critical Reynolds Num.	
				Width a	Separation b					
			μm	μm	μm	μm	μm	RR,cf	Re <sub>crit</sub>	
<b>First Experiment</b>	1	Ground Smooth	1.00	12192	172	174	343	339	0.29%	N/A
	2	Ground Smooth	1.00	12192	216	218	428	424	0.24%	2350
	3	Ground Smooth	1.00	12192	289	291	568	565	0.18%	2400
	4	Ground Smooth	1.00	12192	439	441	851	847	0.12%	N/A
	5	Ground Smooth	1.00	12192	912	914	1701	1697	0.06%	N/A
	7	405μm Sawtooth	99.71	12192	216	415.42	803	424	23.49%	410
	8	405μm Sawtooth	99.71	12192	310	509.42	978	605	16.49%	610
	9	405μm Sawtooth	99.71	12192	439	638.42	1213	847	11.77%	790
	10	405μm Sawtooth	99.71	12192	910	1109.42	2034	1694	5.89%	820
	11	815μm Sawtooth	105.55	12192	216	427.1	825	424	24.87%	210
	12	815μm Sawtooth	105.55	12192	289	500.1	961	565	18.69%	350
	13	815μm Sawtooth	105.55	12192	420	631.1	1200	812	13.00%	380
	14	815μm Sawtooth	105.55	12192	850	1061.1	1952	1589	6.64%	960
	<b>Second Experiment</b>	1	Lapped	0.20	12192	100	100.4	199	198	0.10%
2		Lapped	0.20	12192	200	200.4	394	394	0.05%	2613
3		Lapped	0.20	12192	300	300.4	586	586	0.03%	2478
4		Lapped	0.20	12192	400	400.4	775	775	0.03%	2449
5		Lapped	0.20	12192	500	500.4	961	961	0.02%	2509
6		100 Grit	9.17	12192	567	585.34	1117	1084	0.85%	2250
7		100 Grit	9.17	12192	374	392.34	760	726	1.26%	2604
8		100 Grit	9.17	12192	278	296.34	579	544	1.69%	2375
9		100 Grit	9.17	12192	221	239.34	469	434	2.11%	2124
10		100 Grit	9.17	12192	184	202.34	398	363	2.53%	2242
11		60 Grit	23.19	12192	382	428.38	828	741	3.13%	1975
12		60 Grit	23.19	12192	326	372.38	723	635	3.65%	1949
13		60 Grit	23.19	12192	284	330.38	643	555	4.18%	1885
14		60 Grit	23.19	12192	252	298.38	583	494	4.70%	1821
15		60 Grit	23.19	12192	226	272.38	533	444	5.23%	2038
16		60 Grit	23.19	12192	206	252.38	495	405	5.72%	1676
17		60 Grit	23.19	12192	188	234.38	460	370	6.26%	1558
18		60 Grit	23.19	12192	174	220.38	433	343	6.76%	1282
<b>Third Experiment</b>	1	100 Grit	9.17	12192	700	718.34	1357	1324	0.69%	2423
	2	100 Grit	9.17	12192	500	518.34	994	961	0.95%	2051
	3	100 Grit	9.17	12192	314	332.34	647	612	1.50%	2238
	4	100 Grit	9.17	12192	234	252.34	494	459	2.00%	2275
	5	100 Grit	9.17	12192	186	204.34	402	366	2.50%	2409
	6	60 Grit	23.19	12192	500	546.38	1046	961	2.41%	2041
	7	60 Grit	23.19	12192	400	446.38	861	775	2.99%	2028
	8	60 Grit	23.19	12192	350	396.38	768	680	3.41%	2118
	9	60 Grit	23.19	12192	300	346.38	674	586	3.96%	2024
	10	60 Grit	23.19	12192	265	311.38	607	519	4.47%	1862
	11	60 Grit	23.19	12192	235	281.38	550	461	5.03%	1798
	12	405μm Sawtooth	99.71	12192	1100	1299.42	2349	2018	4.94%	1279
	13	405μm Sawtooth	99.71	12192	800	999.42	1847	1501	6.64%	1232
	14	405μm Sawtooth	99.71	12192	700	899.42	1675	1324	7.53%	1092
15	405μm Sawtooth	99.71	12192	600	799.42	1500	1144	8.72%	1003	
16	405μm Sawtooth	99.71	12192	500	699.42	1323	961	10.38%	800	
17	405μm Sawtooth	99.71	12192	400	599.42	1143	775	12.87%	698	
18	405μm Sawtooth	99.71	12192	300	499.42	960	586	17.03%	600	
19	1008μm Sawtooth	52.51	12192	700	805.02	1510	1324	3.97%	1968	
20	1008μm Sawtooth	52.51	12192	600	705.02	1333	1144	4.59%	1925	
21	1008μm Sawtooth	52.51	12192	500	605.02	1153	961	5.47%	1728	
22	1008μm Sawtooth	52.51	12192	400	505.02	970	775	6.78%	1737	
<b>Fourth</b>	1	503μm Sawtooth	46.41	12192	500	592.82	1131	961	4.83%	1847
	2	503μm Sawtooth	46.41	12192	400	492.82	947	775	5.99%	1894
	3	1008μm Sawtooth	52.51	12192	500	605.02	1153	961	5.47%	1992
	4	1008μm Sawtooth	52.51	12192	400	505.02	970	775	6.78%	2044
	5	2015μm Sawtooth	49.11	12192	500	598.22	1140	961	5.11%	2293
	6	2015μm Sawtooth	49.11	12192	400	498.22	957	775	6.34%	2194

**Table 4.1: Summary of all experimental work. Each row represents an individual test**

Even though one test is listed for each of the experimental situations, many other tests were run at various stages throughout construction of the test setup. To address the issue of repeatability, four tests that were run with smooth samples to verify the test section at 300  $\mu\text{m}$  will be examined. The laminar  $f^*\text{Re}$  value was found for each of these four tests.

Test Number	Laminar $f^*\text{Re}$
1	26.0
2	24.8
3	26.1
4	25.1
<b>Average</b>	25.5
<b>St Dev</b>	0.68

**Table 4.2: Repeatability**

Table 4.2 illustrates the laminar  $f^*\text{Re}$  in four separate tests. We can see the average of these tests is 25.5 with a standard deviation of 0.68.

## 4.2 Results of first Experimentation

The pump used in this experimentation limited the possible Reynolds numbers that could be run. Hydraulic diameters ranged from  $D_h = 424 \mu\text{m}$  to  $D_h = 1.697 \mu\text{m}$ . Reynolds numbers from 200 to 3000 were used. First the setup is verified with the smooth channels. The smooth channels were fabricated with a precision grinder. When the smooth channel friction factor was plotted against Reynolds number, the results agreed well with conventional theory. The agreement is to be expected, as continuum mechanics should still hold at the length scales involved.

An example plot from this verification is given in Figure 4.2, for a hydraulic diameter of  $565\mu\text{m}$ .

In this work, the data was plotted first with the root parameters, and then with the constricted parameters. A few examples of this will be given for spacial concerns, however all separations tested ended up yielding similar results. Figure 4.1 shows the results of a single experiment with the  $405\mu\text{m}$  sawtooth elements. The results are plotted using the unconstricted parameters. It can be seen that the experimental data fall far above what is predicted with conventional theory. This method of calculation is what is used currently for pressure drop calculations.

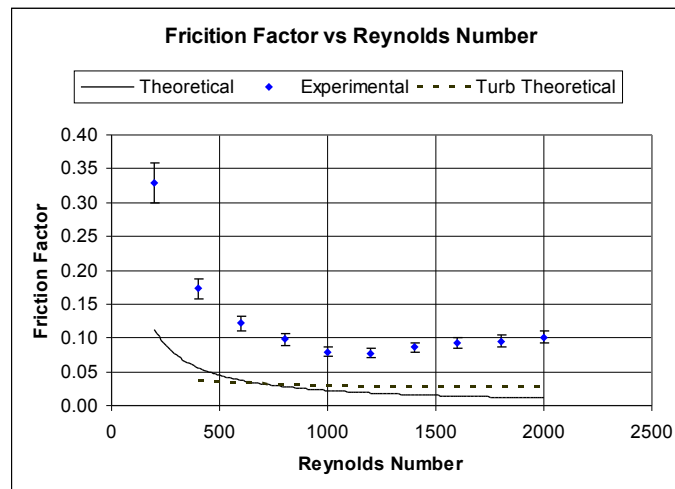


**Figure 4.1: Uncorrected - aligned sawtooth roughness  $p=405\mu\text{m}$ ,  $D_h=1240\mu\text{m}$ ,  $b = 653\mu\text{m}$**

When the data of Figure 4.1 is replotted using the constricted parameters (Figure 4.3), good agreement with theory is obtained. This finding correlates with the findings of Schmidt and Kandlikar [21]. This trend was

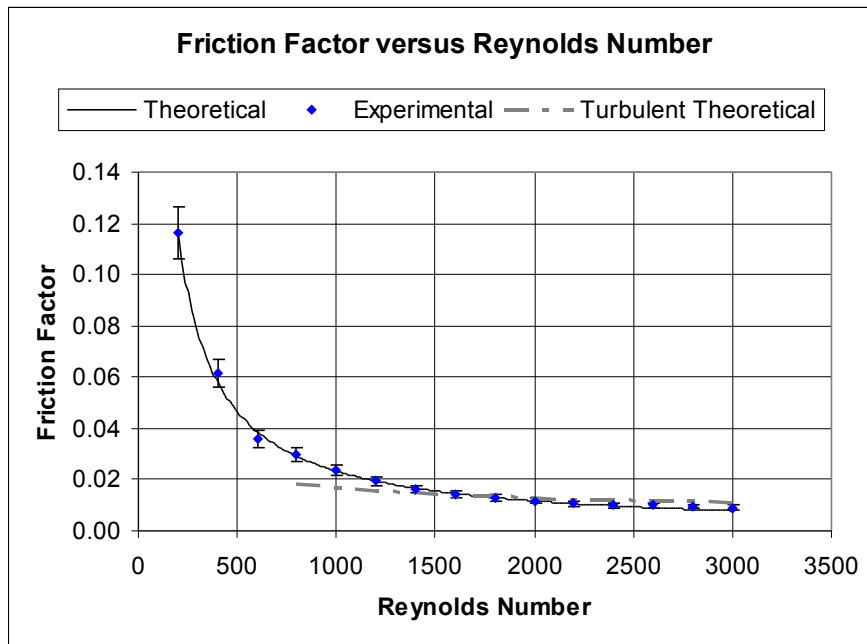


**Figure 4.2: Smooth channel verification with Dh = 565um**

present in all of the tests that were run, and the rest are not provided due to similarity. For this test, you can also note transition around a Reynolds number of 1200. Transition can be assumed when the experimental data begins departing the laminar theory line.

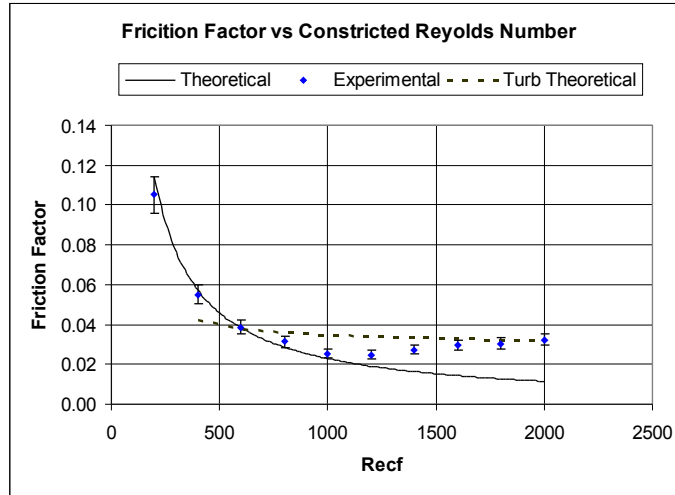


**Figure 4.3: Corrected - aligned sawtooth  
 $p=405\mu\text{m}$ ,  $D_{h,cf}=847\mu\text{m}$**

Differences in behavior were also seen between the two pitches in the transition region. The friction factor for the  $405\mu\text{m}$  pitch transitions to turbulence later than that of the  $815\mu\text{m}$  pitch, which also contributes to a

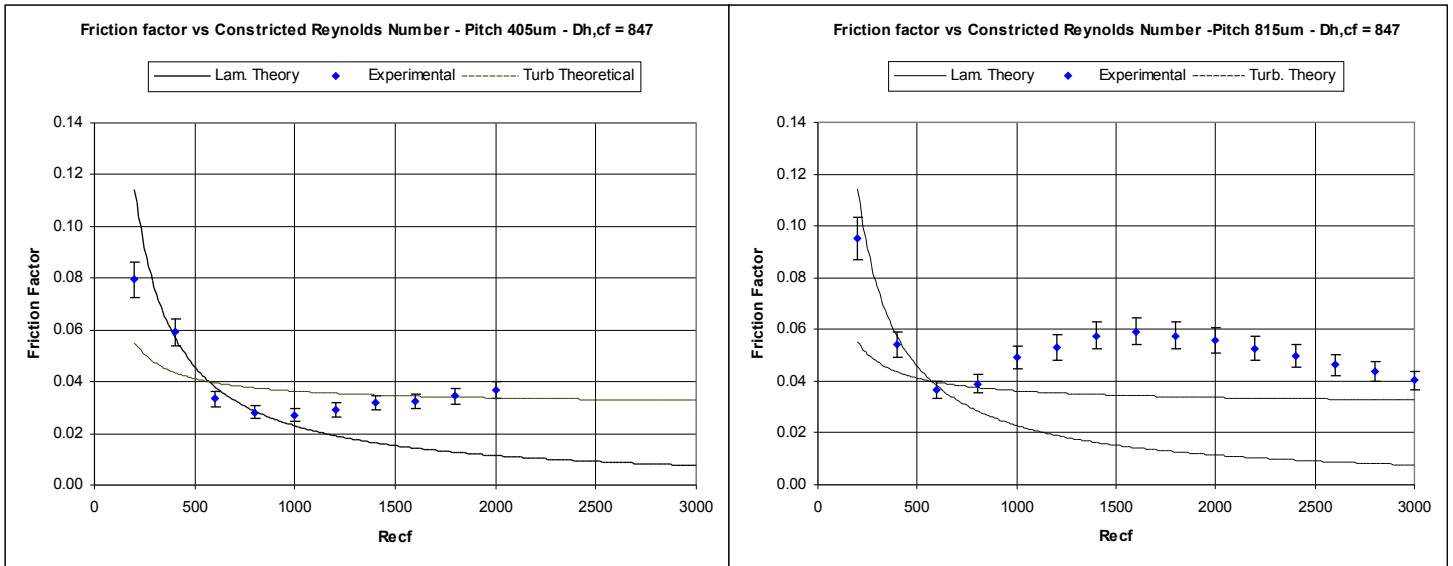


**Figure 4.4: Comparison of the two different pitches with the same constricted hydraulic diameter**  
 difference in the friction factor plot. Both appear to converge to the

turbulent theory value, but the 405 $\mu$ m pitch approaches from below the value and the larger pitch approaches from higher values.

The critical Reynolds numbers for these trials were also recorded. They were compared to a correlation constructed from data obtained by Schmidt [21] in a similar experiment. The entirety of the critical Reynolds number work is contained in a different section.

This experimentation serves as the first of its kind for very high relative roughnesses in laminar and transition flow.

## **4.3 Results of second Experimentation**

### **4.3.1 Experimental Results**

The intent of the samples used in this experimentation was to determine whether the use of the constricted parameters could be extended to non-patterned surfaces. In the two previous studies on this work, the roughness elements had always been repeating sawtooth elements. The roughened samples made with sandpaper differed in that they had no repeating structures, and were mostly random in nature.

It was found that with increasing relative roughness, the error in predicting the hydraulic performance of the roughened channels also increased. When the experimental data was replotted with the constricted parameters, all the sample data is better predicted. This can be compared with some of the representative sample runs in Figure 4.5.

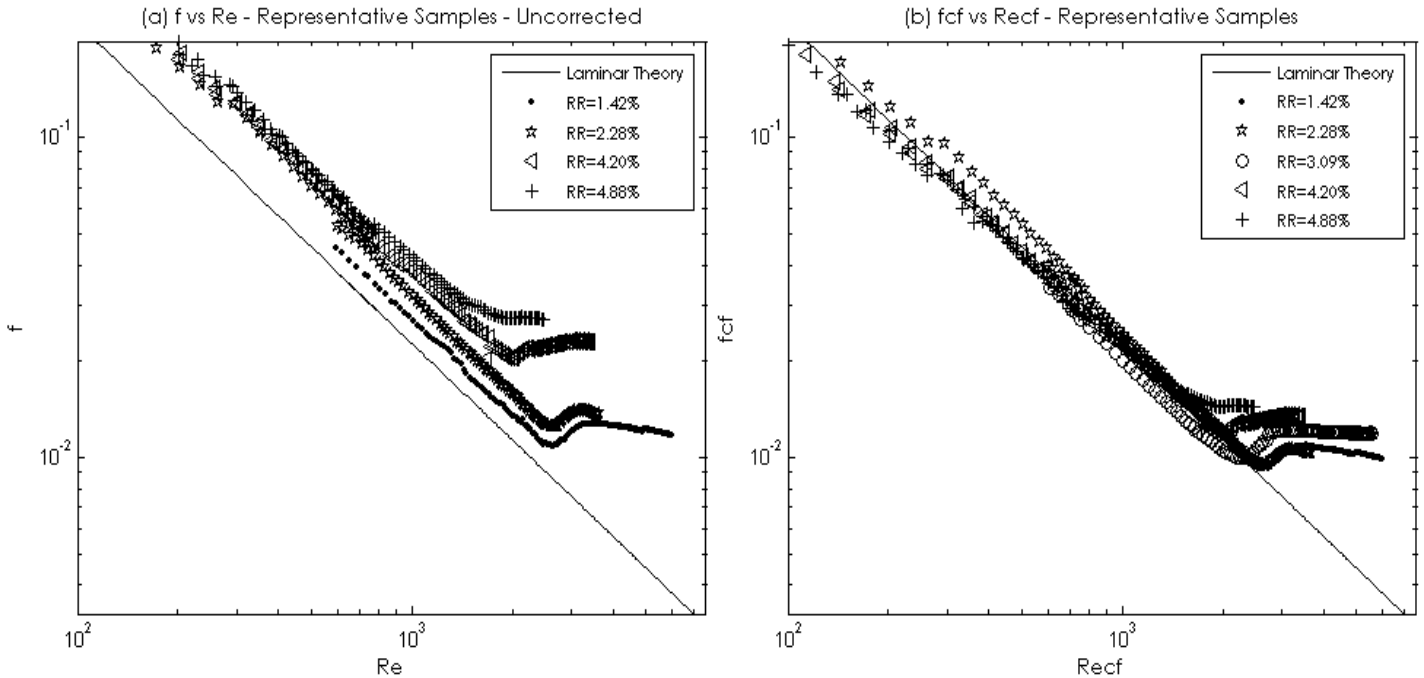


**Figure 4.5: Representative samples from the low uniform roughness testing plotted with (a) root parameters (b) constricted parameters**

Additionally, with increasing relative roughness, the transition to turbulence decreases from its smooth channel transition value of around 2700. The lowest relative roughness in Figure 4.5 is 1.42%, which yielded an experimental critical Reynolds number of  $Re_{cf} = 2604$ . When the relative roughness increases to 4.88%, this transition occurs much lower at  $Re_{cf} = 1821$ . This data serves as one of the first systematic study of channels with the exact same roughness structures and varying hydraulic diameters.

### 4.3.2 Results of applying lubrication theory

The results of applying lubrication theory as outlined earlier were also examined. First, the method for finding  $b_{\text{eff,theory}}$  was applied to the 60 grit surface, and the parameters illustrated. This is shown in Figure 4.6.

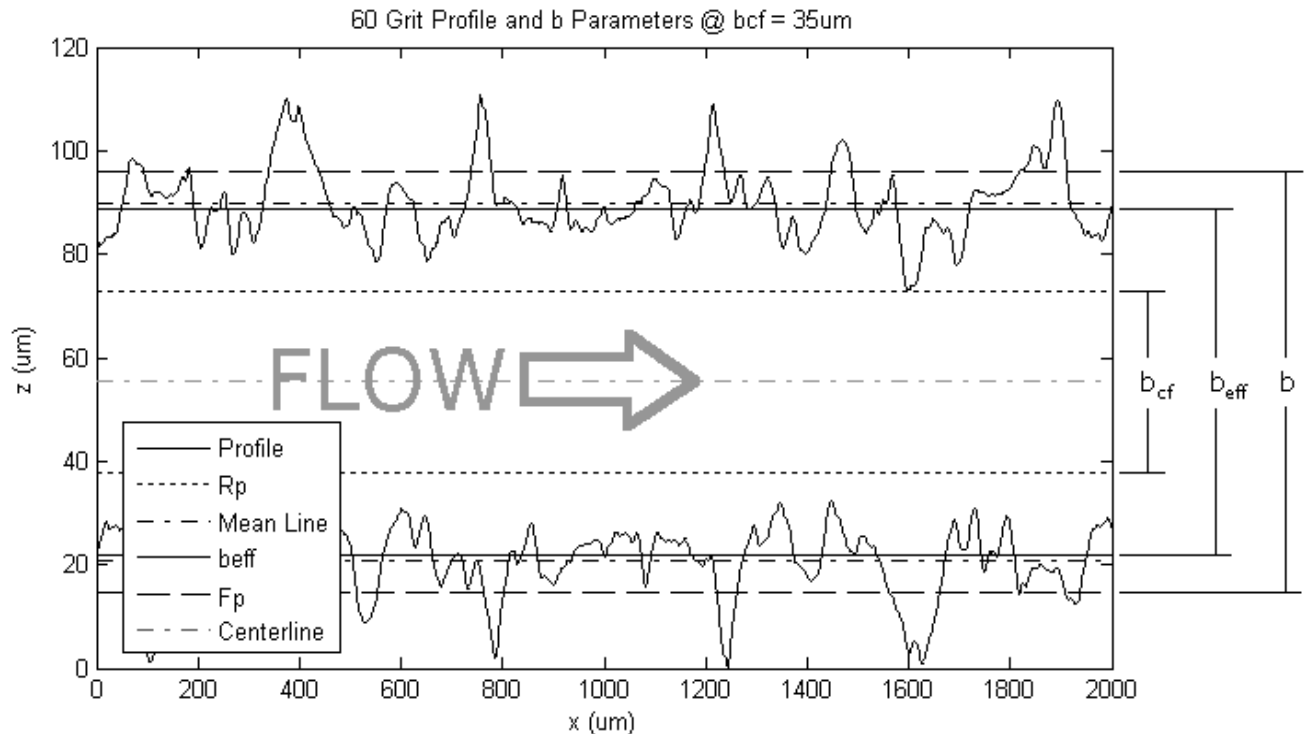


**Figure 4.6: Illustration of all parameters used in experimentation applied to the 60 grit channel profile**

The first finding of this type of analysis is that the value of  $b_{\text{eff,exp}}$  is constant throughout the laminar range. On the plot in Figure 4.7, all of the data points are within the experimental uncertainty of the test section. The following diagram illustrates this phenomena, for the 60 grit sandpaper samples at a relative roughness of 4.53%.

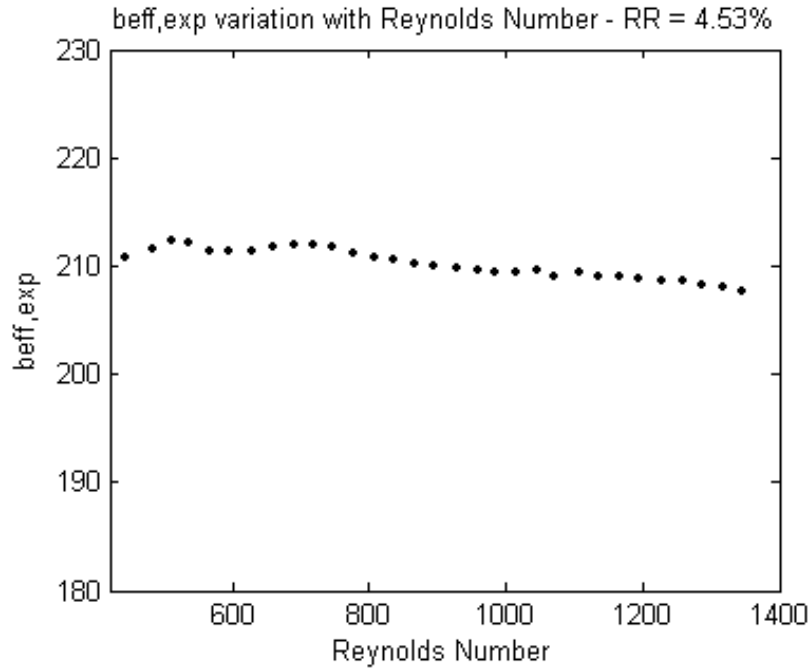


**Figure 4.7: Variation of  $b_{eff,exp}$  with Reynolds Number**

To calculate a single  $b_{eff,exp}$  for each experiment with the illustrated decreasing trend (Figure 4.7), the values are averaged in the laminar regime. This experimentally obtained effective separation can be

	Rel. Roughness	$b$ $\mu\text{m}$	$b_{cf}$ $\mu\text{m}$	$b_{eff,theory}$ $\mu\text{m}$	$b_{avg}$ $\mu\text{m}$	$b_{eff,exp}$ (average) $\mu\text{m}$	$\epsilon_{FP}$ $\mu\text{m}$	Ra $\mu\text{m}$
<b>100 Grit</b>	0.85%	585.3	567.0	580.7	580.7	564.8	9.17	2.13
	1.26%	392.3	374.0	387.7	387.7	371.3	9.17	2.13
	1.69%	296.3	278.0	291.6	291.7	280.0	9.17	2.13
	2.11%	239.3	221.0	234.6	234.7	217.5	9.17	2.13
	2.53%	202.3	184.0	197.6	197.7	187.1	9.17	2.13
<b>60 Grit</b>	3.13%	428.4	382.0	415.8	416.2	388.6	23.19	5.45
	3.65%	372.4	326.0	359.7	360.2	338.6	23.19	5.45
	4.18%	330.4	284.0	317.7	318.2	290.4	23.19	5.45
	4.70%	298.4	252.0	285.6	286.2	257.2	23.19	5.45
	5.23%	272.4	226.0	259.5	260.2	228.5	23.19	5.45
	5.72%	252.4	206.0	239.5	240.2	210.1	23.19	5.45
	6.26%	234.4	188.0	221.4	222.2	191.2	23.19	5.45

**Table 4.3: Summary of experimental results from lubrication theory**

compared with the constricted separation, floor separation, and mean line separation. These results can be found in Table 4.3.

Furthermore the prediction parameters are all normalized by dividing by  $b_{eff,exp}$  to see what trends are apparent. If the parameter is a good fit to experimental data, the data point will be nearest to a value of one. This plot is given in Figure 4.8. At 1% RR, the use of lubrication theory results in 3% error from experimental results. Below 0.5% RR the theory is applicable with minimal error. This follows because this is where the asymptotic method used to model the non-flat wall surfaces is valid, that

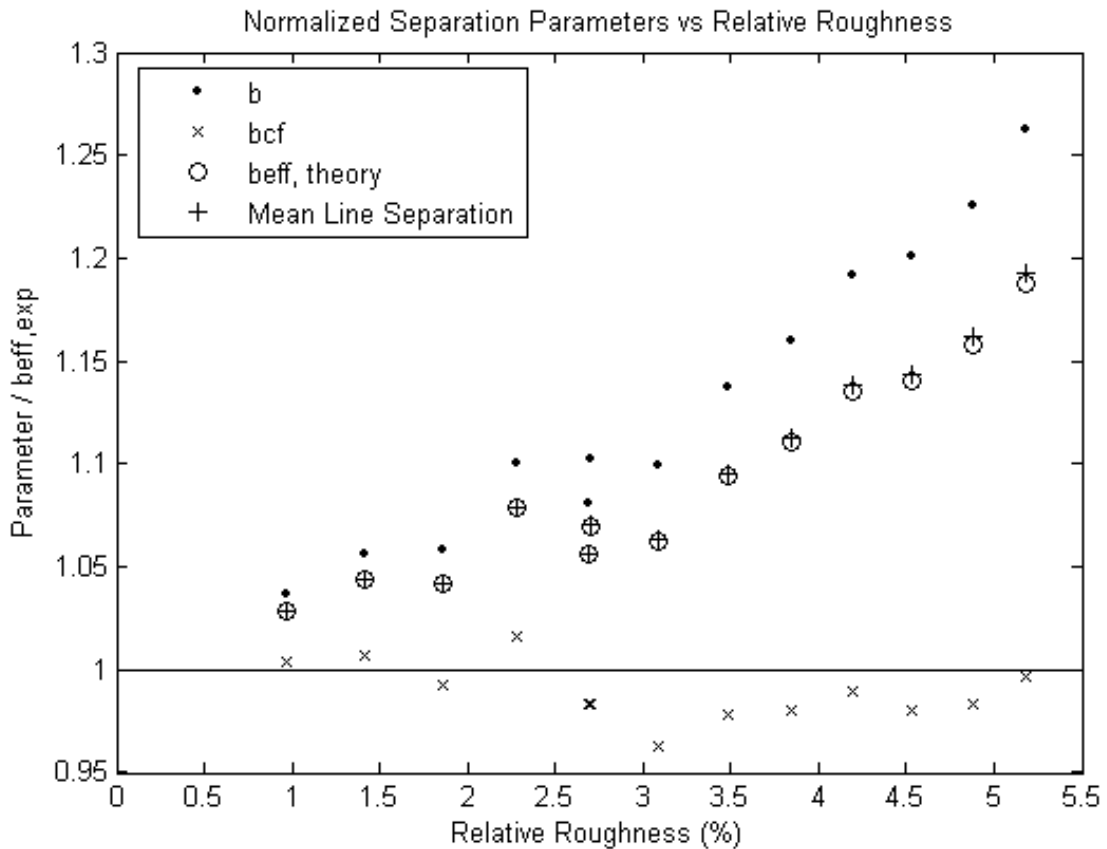


**Figure 4.8: Parameters for separation normalized with experimental results**

is for  $\epsilon_{FP} \ll b$ . It is clear that a better method of incorporating irreversible viscous effects is required for higher relative roughnesses.

## 4.4 Results of Third Experiment - Turbulent experiments

This experiment aimed to look at what happens past the transition region.

According to the constricted parameter definition of Kandlikar [28]

roughened samples past a relative roughness of 5% should plateau to a

single value of friction factor in the turbulent regime. The Moody diagram

replotted with these constricted parameters can be found in Figure 1.1.

For this experiment, the experimental loop was modified to allow for

higher pressure and flow rates. The laminar region agreed with previous

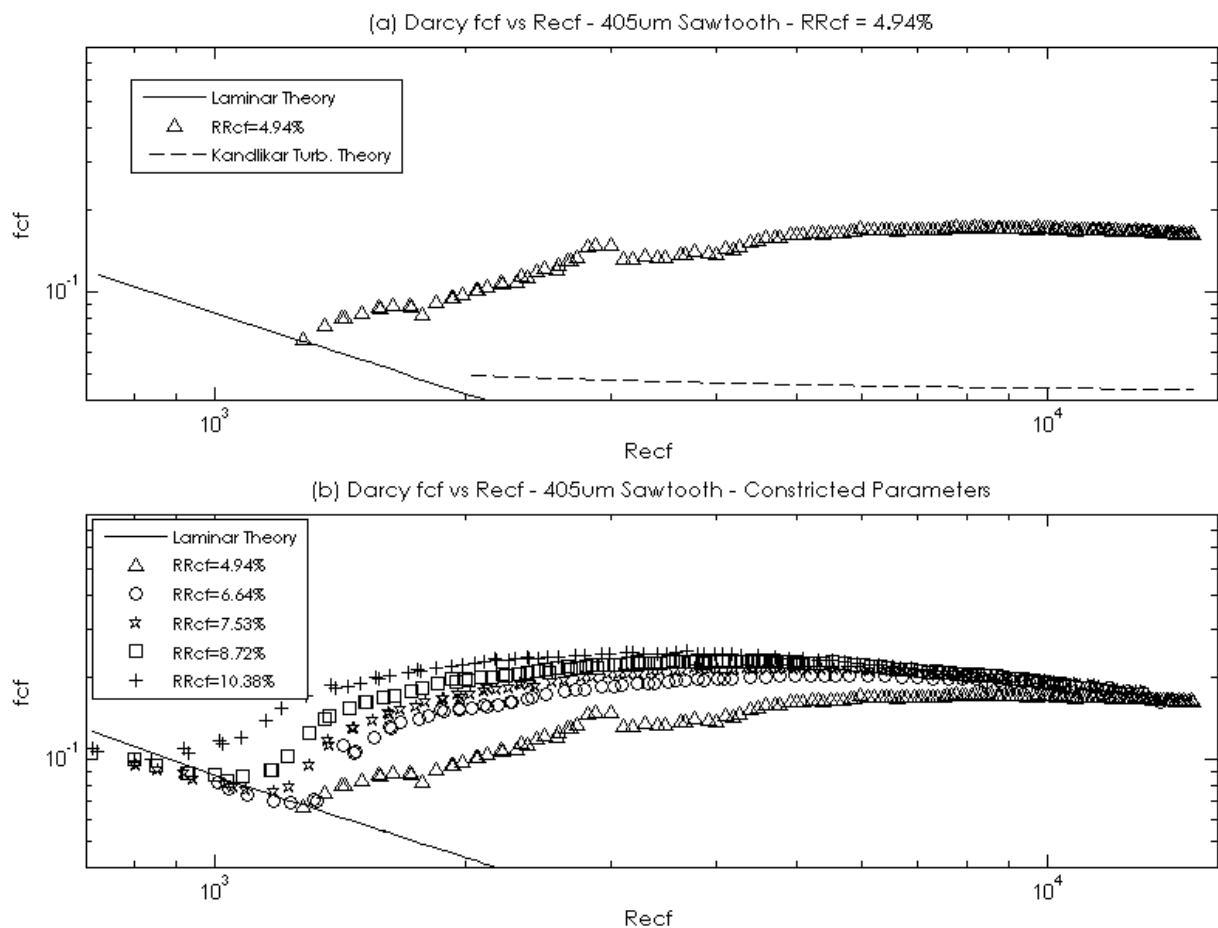


**Figure 4.9: Results of turbulent testing with 405um samples (a) a single test plotted with a prediction of friction factor (b) all the samples**

findings. First, the 405 $\mu\text{m}$  sawtooth results are examined. In Figure 4.9(a), we can see that the results of constricted friction factor versus constricted Reynolds number. Also plotted with the dashed line is the prediction from Kandlikar with the replotted Moody diagram. The theory in this case does not do well when compared with experimental data. For this theory, Kandlikar assumed the correlations for circular tubes, and the high aspect ratio of the rectangular channels may be part of the error. Also, the repeating structure of the elements may also be affecting the results.

All the data is plotted in Figure 4.9(b) where the turbulent regime appears to be converging to a single value for friction factor. To figure out whether this was just incidental to this set of samples, this testing was repeated with the 1008 $\mu\text{m}$  pitch samples. The resulting constricted friction factor versus constricted Reynolds number plot can be found in Figure 4.10. The 1008 $\mu\text{m}$  results (in green) appear to also converge to a single value in the turbulent regime, however this value is different than that of the 405 $\mu\text{m}$  samples. This data is truly the first of its kind, with high relative roughnesses run to high Reynolds numbers. There is much to be understood in terms of flow phenomena, and is difficult to fully analyze here.

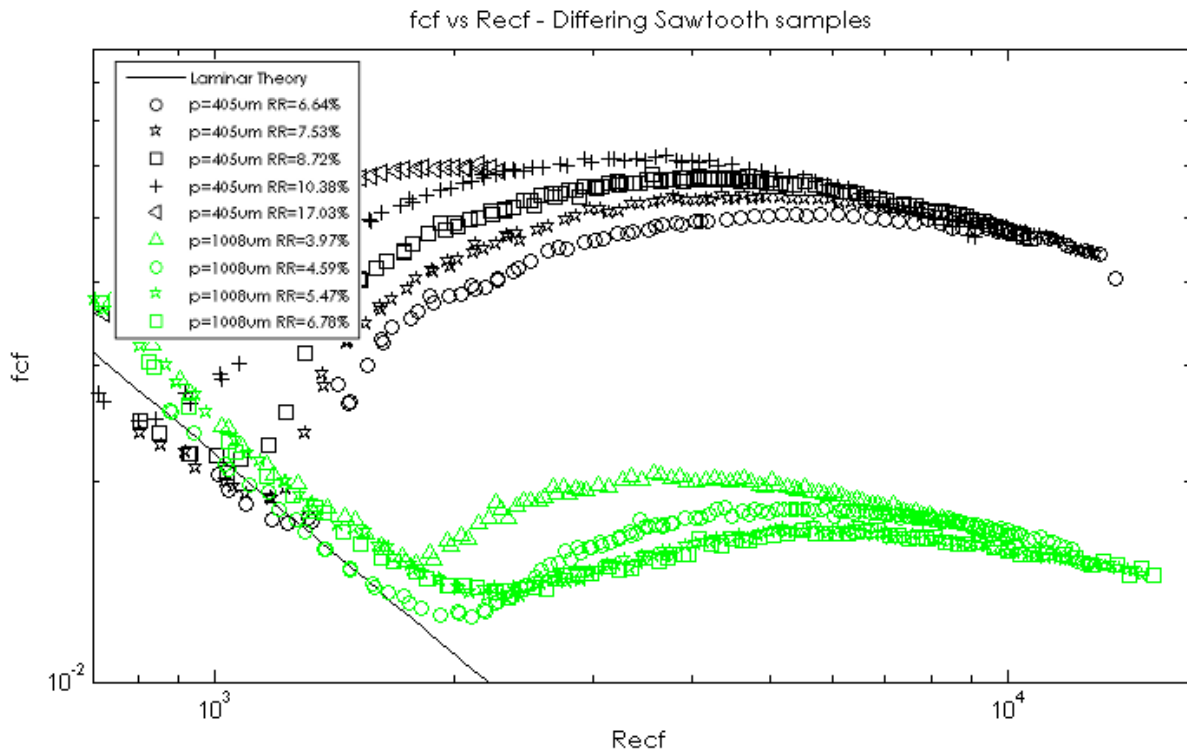


**Figure 4.10: Comparing the two different sawtooth pitches**

#### 4.5 Results of fourth experimentation - varying pitch

In this experiment, samples with varying pitches were tested in the laminar regime. The roughness elements heights were all near 50 $\mu\text{m}$ . The samples were tested at two constricted separations, 400 $\mu\text{m}$  and 500 $\mu\text{m}$ . The plots of friction factor versus Reynolds numbers for both separations can be seen in Figure 4.11.

From these two tests, it can be seen that as the pitch of the elements increases, the experimental data begins departing the theory as predicted using constricted parameters. Also of interest when comparing the two plots, with higher relative roughness the transition to turbulence is much more abrupt, even when changing

the amount from 5.1% to 6.4%. Not only does the friction factor depart more from the theory, but the transition to turbulence increases with increasing pitch. As the elements become further and further spaced the channel more closely resembles a smooth channel, with its higher transition value. Also, the root parameters more closely predict the hydraulic performance for the longest pitch tested. This is shown in Figure 4.13. This itself shows that for roughness with a nature of widely separated elements cannot be predicted with constricted parameters alone.

We can then plot  $f^*Re$  for the laminar regimes of this testing, and compare it to theoretical values. Note  $f^*Re$  is a constant until transition to turbulence. We will use a parameter, defined in Equation 4.1, to represent different repeating roughness structures.

$$\beta = \frac{pitch}{\epsilon_{FP}} \quad (4.1)$$

This parameter,  $\beta$ , is the ratio of pitch of the roughness structures to their height,  $\epsilon_{FP}$ . At  $\beta$  approaching 0, the maximum effect of having closely spaced, high roughness structures is evident. As  $\beta$  approaches infinity, the surfaces approaches a smooth channel, and thus one would expect the corresponding smooth channel results. When the  $f^*Re$  of each of the experiments are plotted with unconstricted parameters against  $\beta$ , we obtain the plot showing what we would expect. The data shows a downward trend with increasing  $\beta$ .

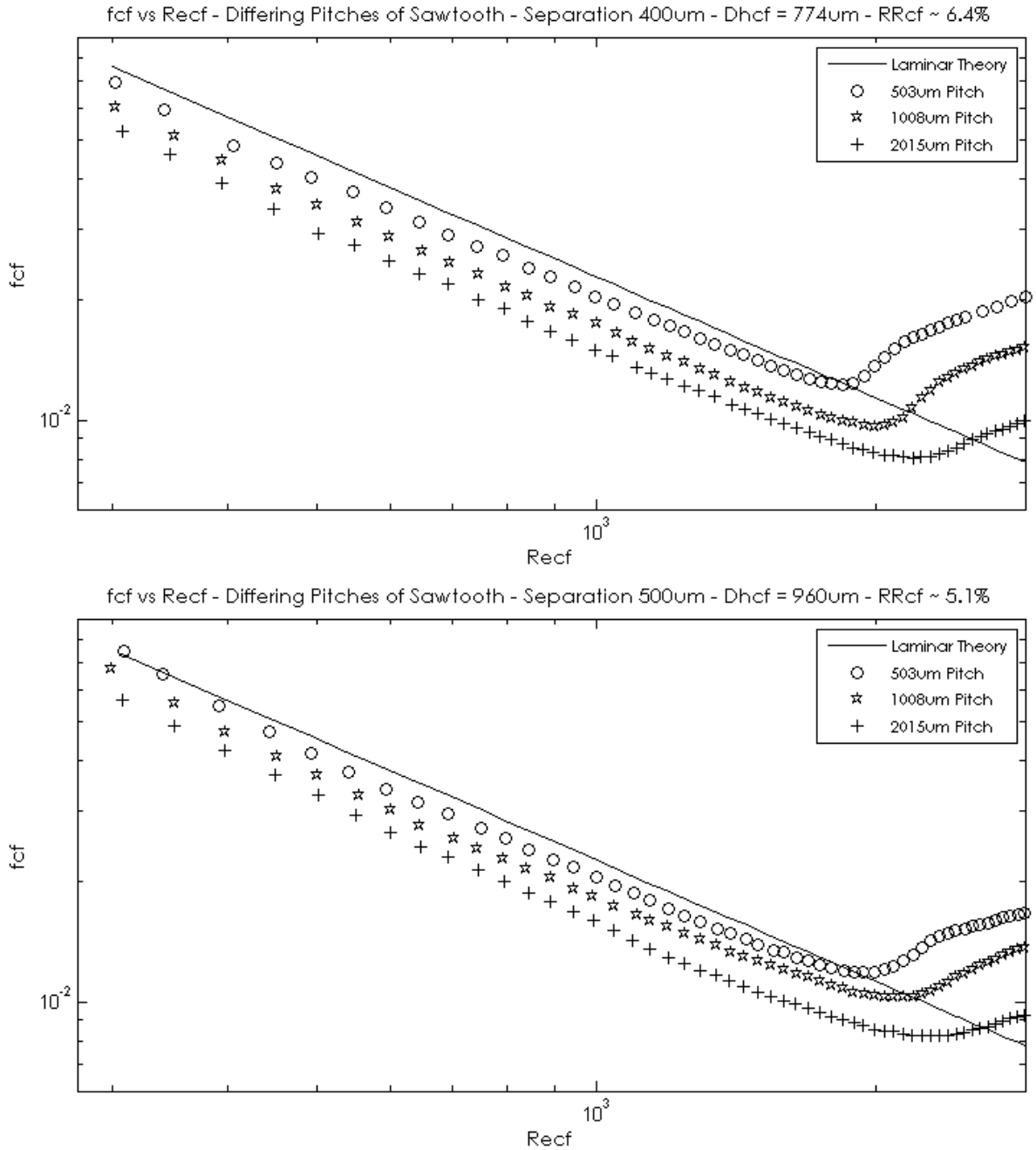


**Figure 4.12: Constricted friction factor vs Reynolds number for 3 varying pitches**

## 4.6 Transition to turbulence

A result of the roughness on the sides of the channels is that the transition to turbulence occurs sooner than it would in a smooth channel.

It was also This transition is recorded for all the tests that have been

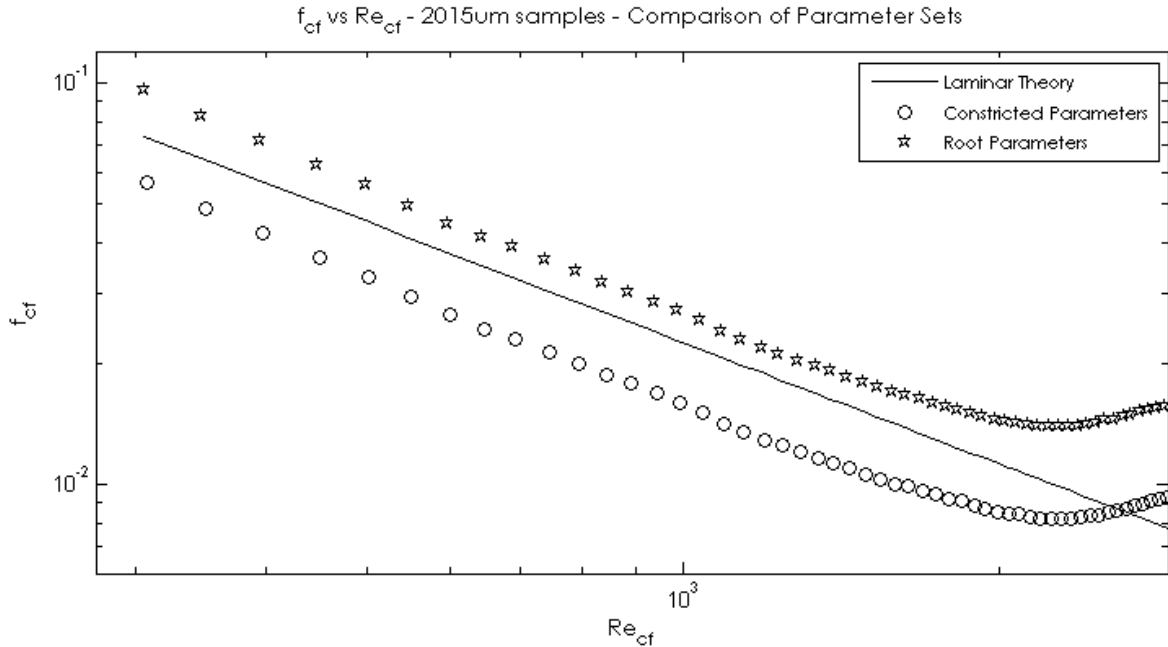


**Figure 4.13: Constricted friction factor vs Reynolds number for the largest pitch, plotted with both root and constricted parameters**

performed in this work. Kandlikar and Schmitt [28] characterized the results of their testing with the following correlation.

$$\begin{aligned}
 0 < \frac{\epsilon}{D_{h,cf}} \leq 0.08 & \quad Re_{t,cf} = 2300 - 18,750 \left( \frac{\epsilon}{D_{h,cf}} \right) \\
 0.08 < \frac{\epsilon}{D_{h,cf}} \leq 0.15 & \quad Re_{t,cf} = 800 - 3,270 \left( \frac{\epsilon}{D_{h,cf}} - 0.08 \right)
 \end{aligned}
 \tag{4.2}$$

Based on more experimental evidence, Brackbill and Kandlikar [37] further modified this correlation to include the smooth channel transition,  $Re_0$ . With this introduced, the correlation to determine transition is given in Equation 4.3.

$$\begin{aligned}
 0 < \frac{\epsilon}{D_{h,cf}} \leq 0.08 & \quad Re_{t,cf} = Re_0 - \frac{Re_0 - 800}{0.08} \left( \frac{\epsilon}{D_{h,cf}} \right) \\
 0.08 < \frac{\epsilon}{D_{h,cf}} \leq 0.25 & \quad Re_{t,cf} = 800 - 3,270 \left( \frac{\epsilon}{D_{h,cf}} - 0.08 \right)
 \end{aligned}
 \tag{4.3}$$

Where  $Re_0$  is the transition for a smooth channel of the sort tested  
 $Re_0$  is a parameter to account for the varying smooth channel transition value with differing channel geometry. This is a function of aspect ratio, and channel geometry.

The transition point for each of the tests run is plotted in Figure 4.14.

Note that the samples where the pitch was large enough to cause discrepancies in the use of constricted parameters are plotted in red. This data falls further from the rest as a result of the distance between roughness elements.

Of further interest with increasing relative roughness, more abrupt Transition Reynolds number vs constricted relative roughness

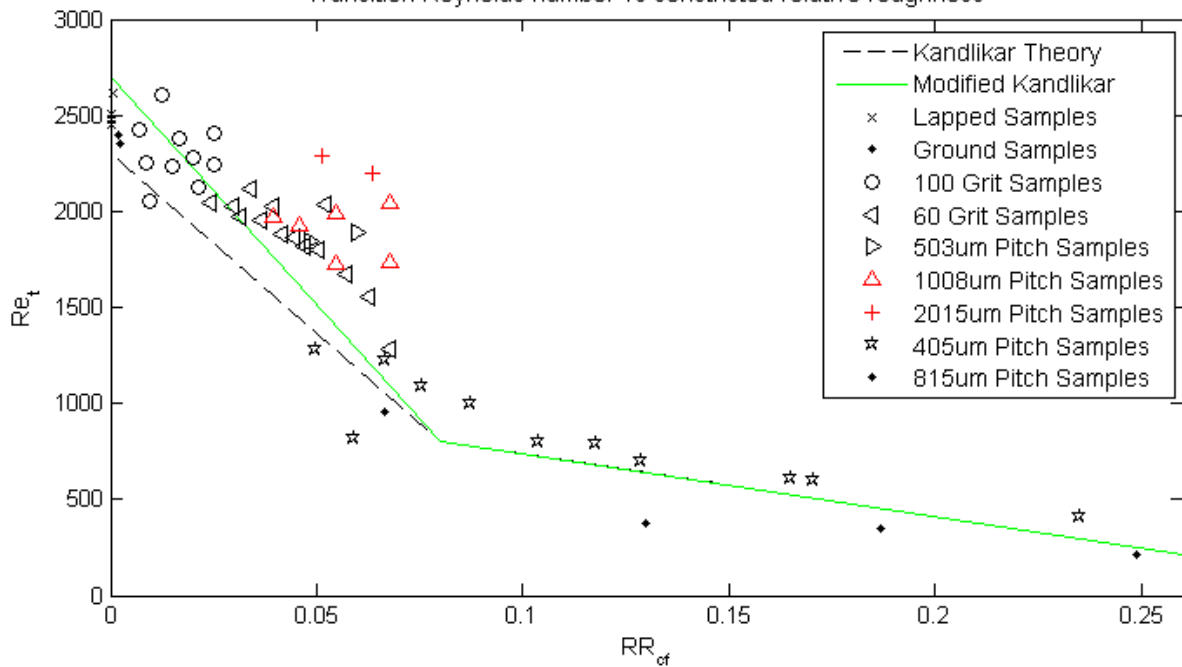


**Figure 4.14: Transition Reynolds number vs Relative Roughness**



## 5 Conclusions

1. By comparing an idealized version of Nikuradse's roughness elements,  $\varepsilon_{FP}$  was shown to better predict the height of roughness elements, as compared to the commonly used Ra.
2. Contrary to other studies, and the seminal paper on roughness by Nikuradse, roughness structures of less than 5% RR were shown to have appreciable effects on laminar flow.
3. Uniform roughness less than 5% RR also led to earlier transition to turbulence from the smooth channel values.
4. The use of constricted parameters was shown to work well for roughness of two different structures, as long as the pitch of roughness elements was not excessively large. Both uniform roughness and sawtooth roughness elements were tested.
5. Lubrication theory is able to predict roughness with RR less than 0.5% well. Past this point, the irreversible effects and 2D nature of the flow around the roughness elements limits this theories applicability.
6. As pitch of roughness elements increases, the friction factor and transition data approaches that of a channel without roughness

elements.  $\beta$ , defined as roughness pitch over roughness height, is shown to be a good parameter to compare these effects.

7. To further predict hydraulic performance with higher relative roughness, theories would have to incorporate a method of dealing with more irreversible effects.
8. With increasing relative roughness, more abrupt transitions to turbulence were observed.

## 6 References

1. F.C. Colebrook, "Turbulent flow in pipes, with particular reference to the transition region between the smooth and rough pipe laws," J. Inst. Civ. Eng., Vol. 11, pp. 133-156. 1939.
2. J. Nikuradse, "Forschung auf dem Gebiete des Ingenieurwesens," Verein Deutsche Ingenieure, Vol. 4, pp. 361. 1933.
3. P. Wu, and W.A. Little, "Measurement of Friction Factors for the Flow of Gases in Very Fine Channels used for Microminiature Joule-Thomson Refrigerators," Cryogenics, Vol. 23, pp. 273-277. 1983.
4. P. Wu and W.A. Little, "Measurement of Heat Transfer Characteristics in the Fine Channel Heat Exchangers used for Microminiature Refrigerators," Cryogenics, Vol. 24, pp. 415-420. 1984.
5. X.F. Peng, G.P. Peterson, and B.X. Wang "Frictional Flow Characteristics of Water Flowing Through Rectangular Microchannels," Experimental Heat Transfer, Vol. 7, pp. 249-264. 1994.
6. D. Pfund, "Pressure Drop Measurements in a Microchannel," AIChE Journal, Vol. 46. 8 August 2000.
7. X. Tu, and P. Hrnjak, "Experimental Investigation of Single-Phase Flow Pressure Drop Through Rectangular Microchannels," International Conference on Microchannels and Minichannels. ICNMM2003-1028. 2003.
8. H.Y. Wu and P. Cheng, "An experimental study of convective heat transfer in silicon microchannels with different surface conditions," International Journal of Heat and Mass Transfer, Vol. 46, pp. 2547-2556. 2003.
9. G.P. Celata, M. Cumo, S. McPhail, and G. Zummo, "Hydrodynamic Behaviour and Influence of Channel Wall Roughness and Hydrophobicity in Microchannels," International Conference on Microchannels and Minichannels. ICNMM2004. 2004.
10. G.M. Mala and D. Li, "Flow characteristics of water in microtubes," International Journal of Heat and Fluid Flow, Vol. 20, pp. 142-148. 1999.
11. C.L. Merkle, T. Kubota, and D.R.S. Ko, "An analytical study of the effects of surface roughness on boundary-layer transition," AF Office of Scien. Res. Space and Missile Sys. Org. AD/A004786. 1974.
12. I. Tani, "Boundary-Layer Transition," Annual Review of Fluid Mechanics, Vol. 1. 1969.

- 13.S.G. Kandlikar, S. Joshi, and S. Tian, "Effect of Channel Roughness on Heat Transfer and Fluid Flow Characteristics at Low Reynolds Numbers in Small Diameter Tubes," National Heat Transfer Conference. NHTC01-12134. 2001.
- 14.R. Baviere, F. Ayela, S. LePerson, and M. Favre-Marinet, "An Experimental Study of Water Flow in Smooth and Rough Rectangular Micro-channels," International Conference on Microchannels and Minichannels. ICNMM2004. 2004.
- 15.P. Hao, Z. Yao, F. He, and K. Zhu, "Experimental investigation of water flow in smooth and rough silicon microchannels," Journal of Micromechanics and Microengineering, Vol. 16, pp. 1397-1402. 2006.
- 16.Q. Weilin, G.M. Mala, and L. Dongqing, "Pressure-driven water flows in trapezoidal silicon microchannels," Int. J. of Heat Mass Transfer, Vol. 43, pp. 353-364. 2000.
- 17.S. Shen, J.L. Xu, J.J. Zhou, and Y. Chen "Flow and heat transfer in microchannels with rough wall surface," Energy Conversion and Management, Vol. 47, pp. 1311-1325. 2006.
- 18.G.P. Celata, M. Cumo, M. Guglielmi, G. Zummo. "Experimental Investigation of Hydraulic and Single Phase Heat Transfer in 0.130mm Capillary Tube," International Conference on Microchannels and Minichannels. ICNMM2004. 2004.
- 19.Z. Li, D. Du, and Z. Guo, "Experimental Study on Flow Characteristics of Liquid in Circular Microtubes," Intl. Conference on Heat Transfer and Transport Phenomena in Microscale. pp. 162-167. 2000.
- 20.A. Bucci, G.P. Celata, M. Cumo, E. Serra, and G. Zummo, "Water Single-Phase Fluid Flow and Heat Transfer in Capillary Tubes," International Conference on Microchannels and Minichannels. ICNMM2003-1037. 2003.
- 21.D.J. Schmitt, and S.G. Kandlikar, "Effects of Repeating Microstructures on Pressure Drop in Rectangular Minichannels," International Conference on Microchannels and Minichannels. ICNMM2005-75111. 2005.
- 22.W. Wibel, and P. Ehrhard, "Experiments on Liquid Pressure-Drop in Rectangular Microchannels, Subject to Non-Unity Aspect Ratio and Finite Roughness," International Conference on Nanochannels, Microchannels, and Minichannels. ICNMM2006-96116. 2006.

- 23.L.A. Campbell, and S.G. Kandlikar, "Effect of Entrance Condition on Frictional Losses and Transition to Turbulence in Minichannel Flows," International Conference on Microchannels and Minichannels. ICNMM2004-2339. 2004.
- 24.G.P. Celata, M. Cumo, M. Guglielmi, G. Zummo. "Experimental Investigation of Hydraulic and Single Phase Heat Transfer in 0.130mm Capillary Tube." Proceedings of the International Conference on Heat
- 25.A. Bucci, G.P. Celata, M. Cumo, E. Serra, G. Zummo Water Single-Phase Fluid Flow and Heat Transfer in Capillary Tubes International Conference on Microchannels and Minichannels. ICNMM2003-1037, 2003.
- 26.X. Tu and P. Hrnjak. "Experimental Investigation of Single-Phase Flow Pressure Drop Through Rectangular Microchannels,"
- 27.R. Bavier, F. Ayela, S. Le Person, and M. Favre-Marinet. "An Experimental Study of Water Flow in Smooth and Rough Rectangular Micro-Channels." International Conference on Microchannels and Minichannels. ICMM2004. 2004.
- 28.S. G. Kandlikar, D. Schmitt, A. L. Carrano and J. B. Taylor, "Characterization of surface roughness effects on pressure drop in single-phase flow in minichannels," Physics of Fluids 10, Vol. 17. October 2005.
- 29.S.G. Kandlikar, S. Garimella, and D. Li, "Heat Transfer and Fluid Flow in Minichannels and Microchannels." 1st Edition. s.l. : Elsevier, 2006.
- 30.A.S. Rawool, S.K. Mitra, and S.G. Kandlikar, "Numerical simulation of flow through microchannels with designed roughness," Springer-Verlag, 2005, Microfluidics and Nanofluidics. DOI 10.1007/S10404-005-0064-5. 2005.
- 31.Y. Chen, and P. Cheng, "Fractal Characterization of Wall Roughness on Pressure Drop in Microchannels," Intl. Comm. Heat Transfer 1, Vol. 30, pp. 1-11. 2003.
- 32.M. Bahrami, M.M. Yovanovich, and J.R. Cullham, "Pressure Drop of Fully-Developed, Laminar Flow in Rough Microtubes,"
- 33.X.N. Jiang, X.Y. Huang and C.Y. Liu, "Laminar flow through microchannels used for microscale cooling systems," IEEE CPMT Electronic Packaging Technology Conference. pp 119-122. 1997.
- 34.J. Zou, and X. Peng, "Effects of Roughness on Liquid Flow Behavior in Ducts," ASME - European Fluids Engineering Summer Meeting. FEDSM2006-98143. pp. 49-56. 2006.

- 35.S. Kakac, R.K. Shah and W. Aung, Handbook of Single-Phase Convective Heat Transfer. John Wiley and Sons, pp 3-122, 1987.
- 36.P.L. Young, T.P. Brackbill, and S.G. Kandlikar, "Estimating Roughness Parameters Resulting from Various Machining Techniques for Fluid Flow Applications," Proceedings of the International Conference on Nanochannels, Microchannels, and Minichannels ICNMM2007-30033, 2007.
- 37.T. P. Brackbill and S. G. Kandlikar, "Effects of Low Uniform Relative Roughness on Single-Phase Friction Factors in Microchannels and Minichannels," Proceedings of the International Conference on Nanochannels, Microchannels, and Minichannels. ICNMM2007-30031. 2007.

## 7 Appendices

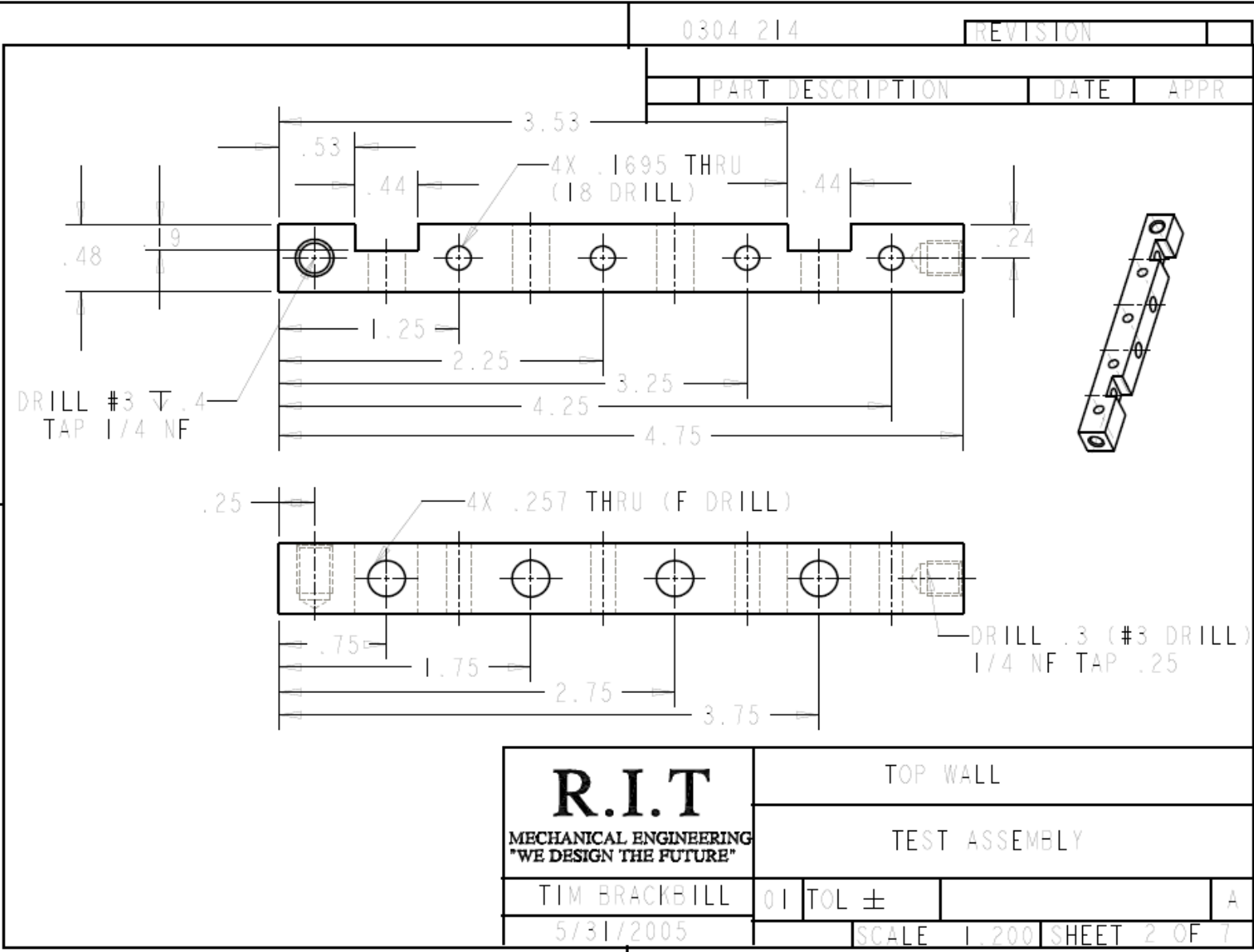
### 7.1 Appendix A - First setup drawings

0304 214		REVISION	
PART DESCRIPTION	DATE	APPR	

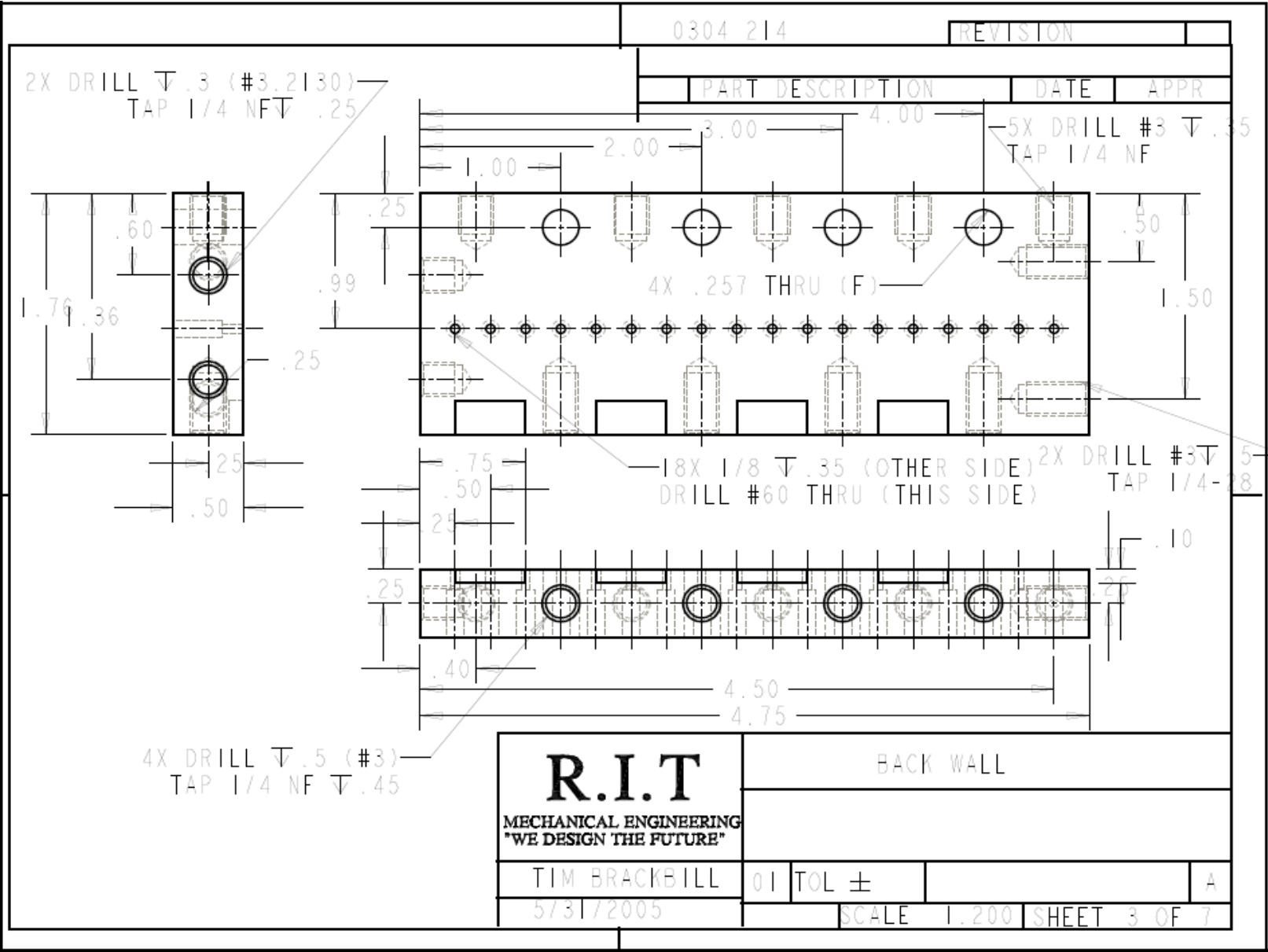
6	1	OUT MANIFOLD
5	1	IN MANIFOLD
4	1	FRONT WALL
3	1	BOTTOM WALL
2	1	BACK WALL
1	1	TOP WALL
IDX	QTY	PART

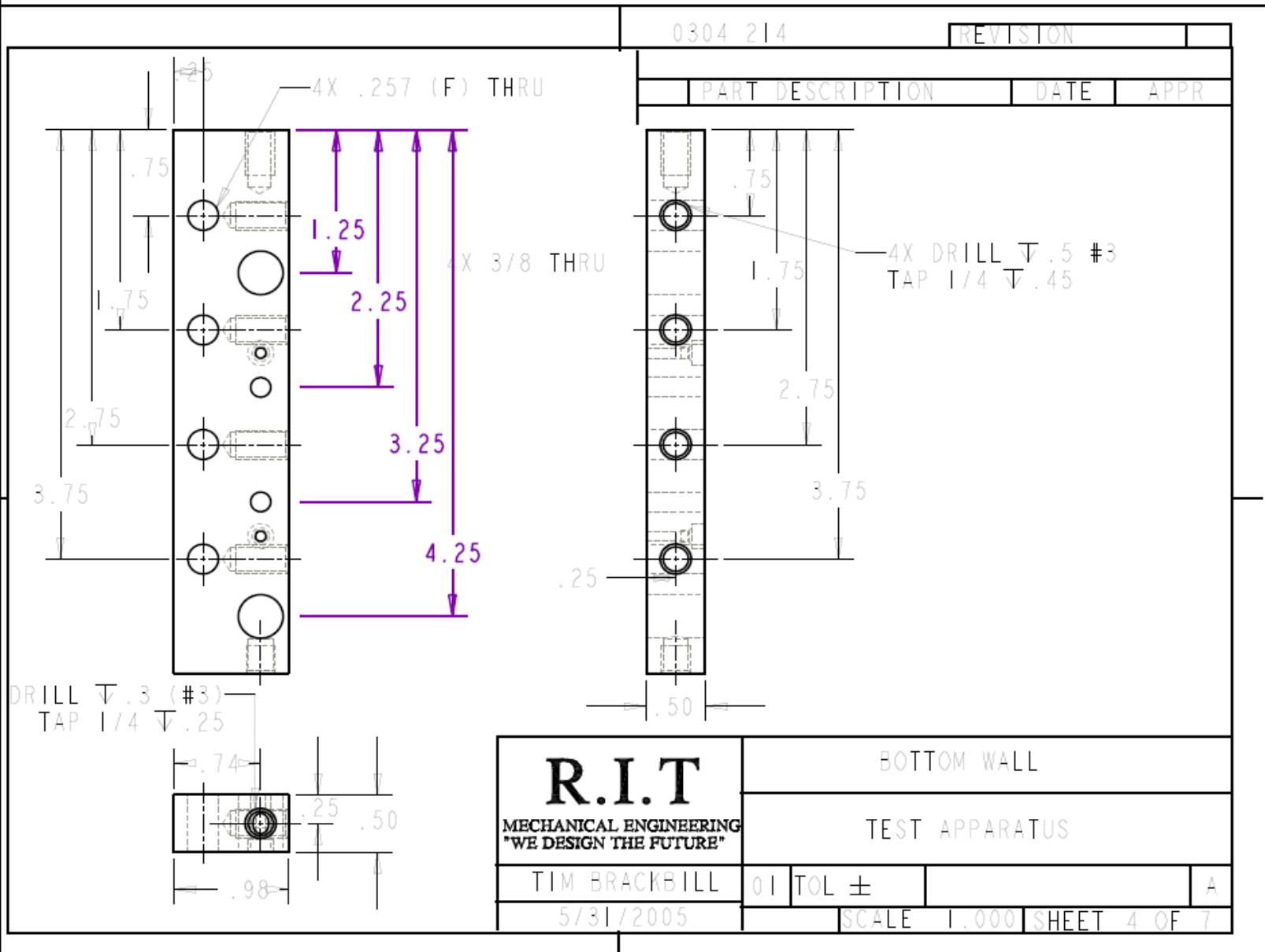
<b>R.I.T</b> MECHANICAL ENGINEERING "WE DESIGN THE FUTURE"	TEST APPARATUS		
	PART INDEX		
TIM BRACKBILL	01	TOL ±	A
5/31/2005			SHEET 1 OF 7

SCALE: 1:1



<b>R.I.T</b> MECHANICAL ENGINEERING "WE DESIGN THE FUTURE"	TOP WALL		
	TEST ASSEMBLY		
TIM BRACKBILL	01	TOL $\pm$	A
5/31/2005	SCALE 1:200 SHEET 2 OF 7		





0304 214

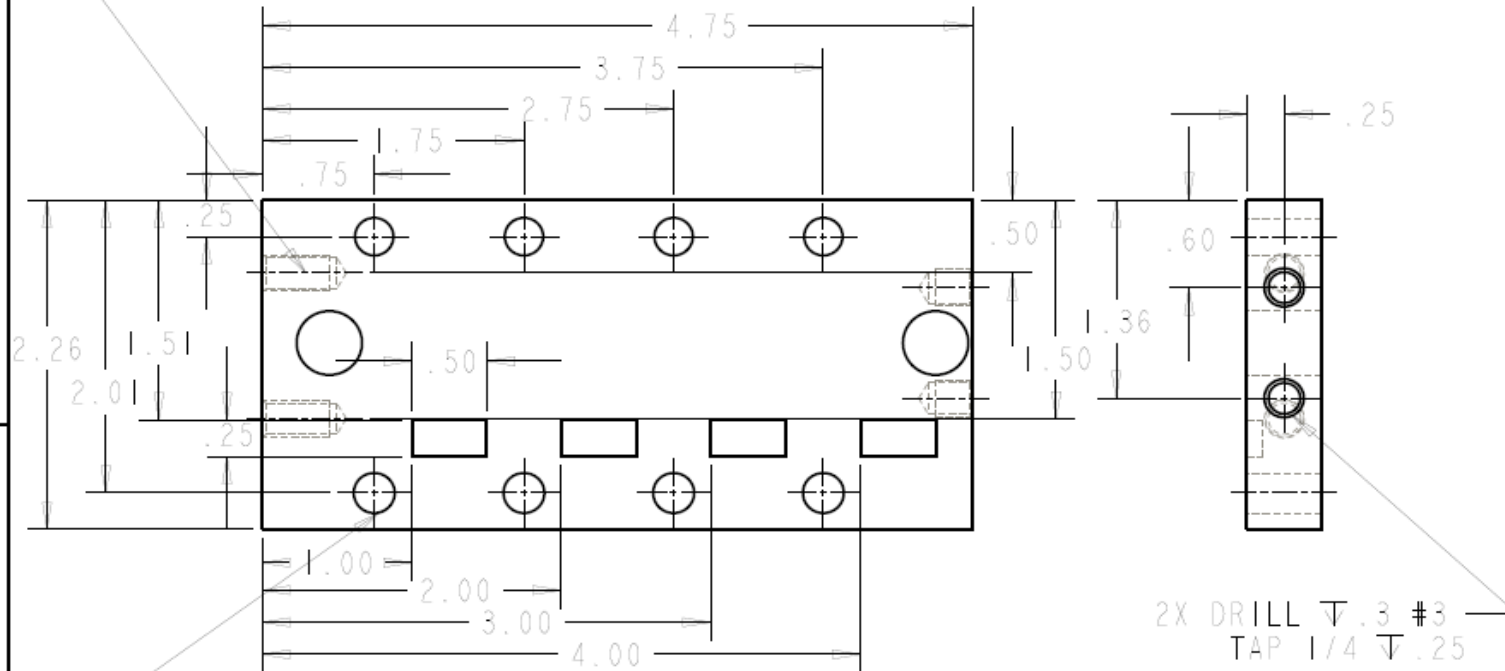
REVISION

PART DESCRIPTION

DATE

APPR

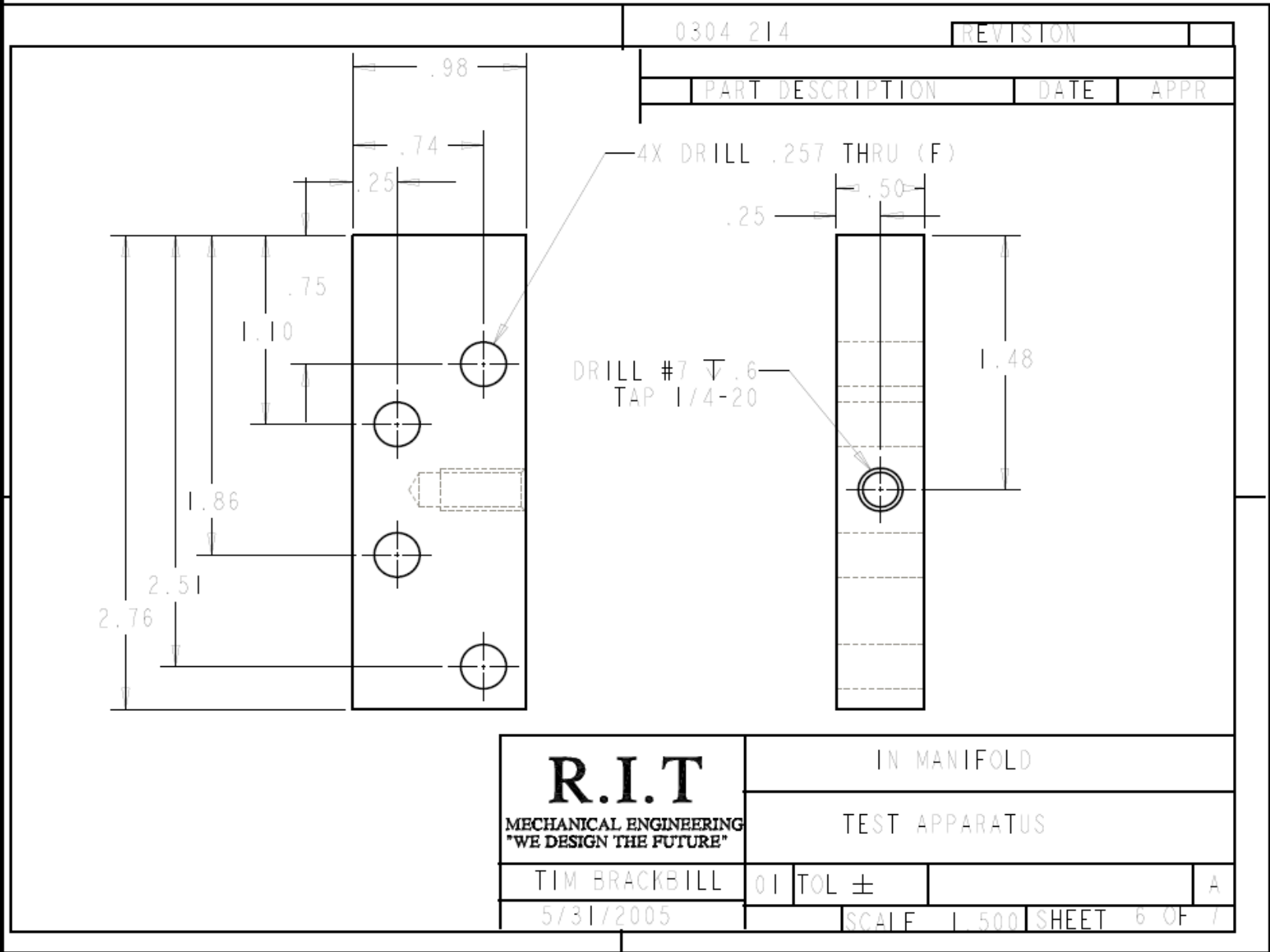
2X DRILL #3  $\nabla$ .5  
TAP 1/4-28



2X DRILL  $\nabla$ .3 #3  
TAP 1/4  $\nabla$ .25

8X DRILL THRU F (.2570)

<b>R.I.T</b> MECHANICAL ENGINEERING "WE DESIGN THE FUTURE"	FRONT WALL		
	TEST APPARATUS		
TIM BRACKBILL	01	TOL $\pm$	A
5/31/2005	SCALE 1.000 SHEET 5 OF 7		



<b>R.I.T</b> MECHANICAL ENGINEERING "WE DESIGN THE FUTURE"	IN MANIFOLD		
	TEST APPARATUS		
TIM BRACKBILL	01	TOL $\pm$	A
5/31/2005	SCALE 1 500 SHEET 6 OF 7		

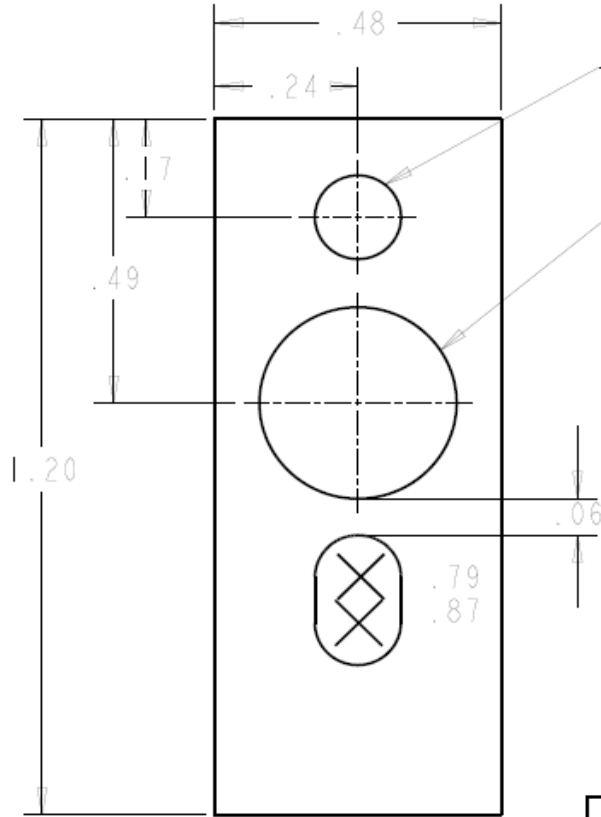
0304 214

REVISION

PART DESCRIPTION

DATE

APPR



DRILL .1440 THRU

9/16 THRU  
1/8 NPT TAP

<b>R.I.T</b> MECHANICAL ENGINEERING "WE DESIGN THE FUTURE"	OUT MANIFOLD		
	TEST APPARATUS		
TIM BRACKBILL	01	TOL ±	A
5/31/2005	SCALE 4.000 SHEET 7 OF 7		

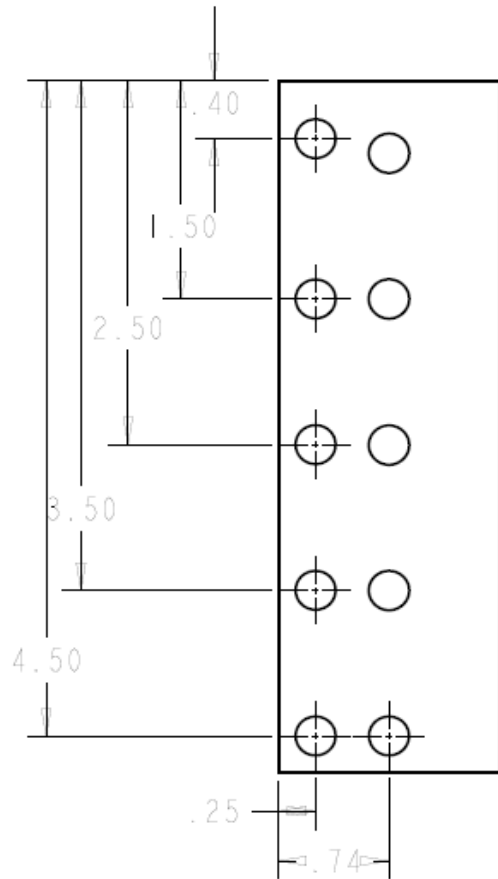
0304 214

REVISION

PART DESCRIPTION

DATE

APPR



ALL HOLES 17/64 THRU

<b>R.I.T</b> MECHANICAL ENGINEERING "WE DESIGN THE FUTURE"	TOP COVER		
	TEST APPARATUS		
TIM BRACKBILL	01	TOL ±	A
6/7/2005	SCALE 1.000 SHEET 8 OF 8		

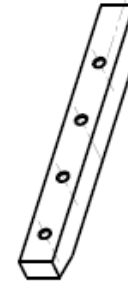
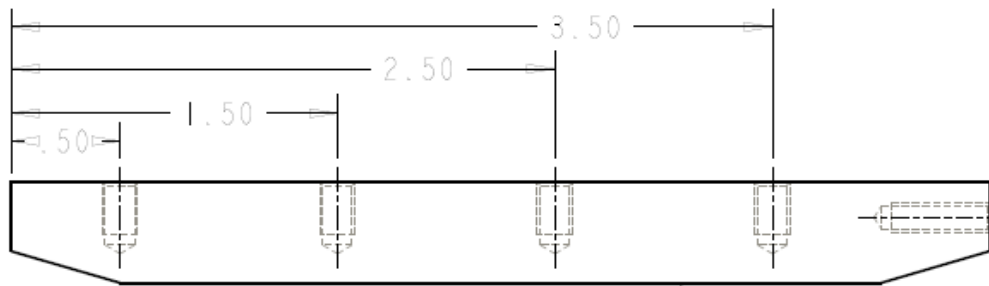
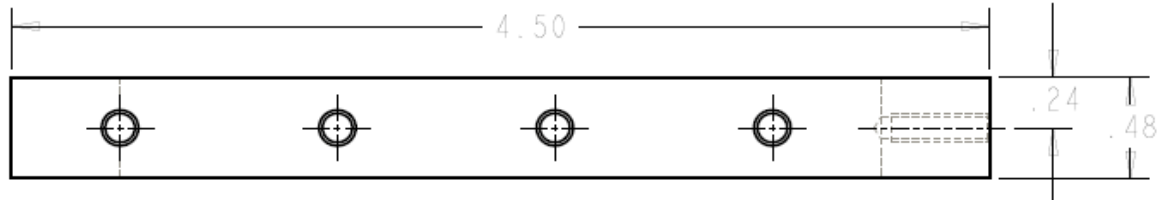
0304 214

REVISION

PART DESCRIPTION

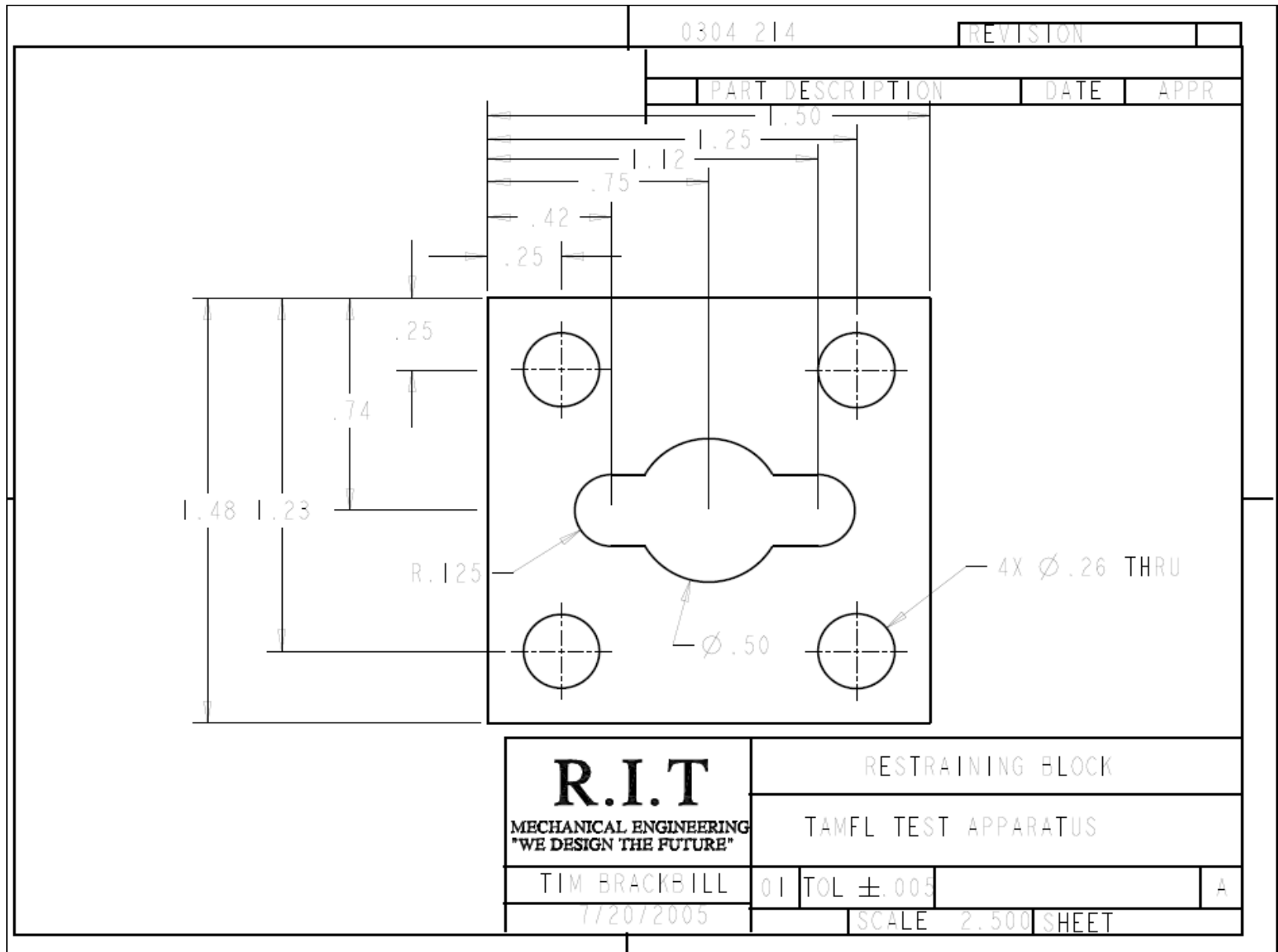
DATE

APPR



PATTERNED SURFACE

<b>R.I.T</b> MECHANICAL ENGINEERING "WE DESIGN THE FUTURE"	TOP SAMPLE		
	TEST APPARATUS		
TIM BRACKBILL	01	TOL ±	A
6/07/2005	INCHES	SCALE 1.450	SHEET 9 OF 10



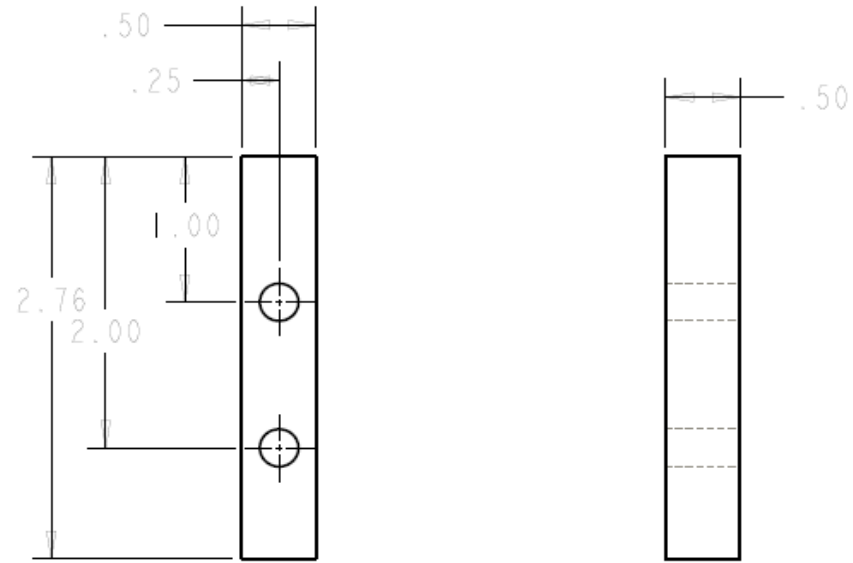
0304 214

REVISION

PART DESCRIPTION

DATE

APPR



ALL HOLES  $\phi$ .2570 (F) THRU

<b>R.I.T</b> MECHANICAL ENGINEERING "WE DESIGN THE FUTURE"	COVER EXTENSION OUT		
TIM BRACKBILL	01	TOL $\pm$	A
8/02/2005	SCALE 1.000 SHEET		

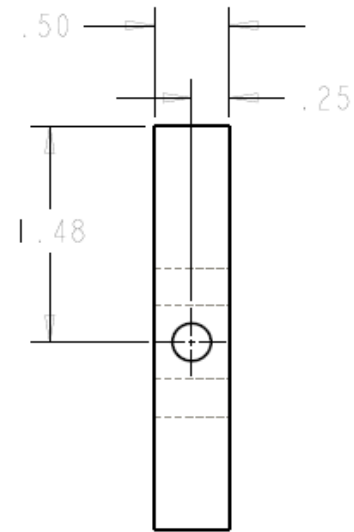
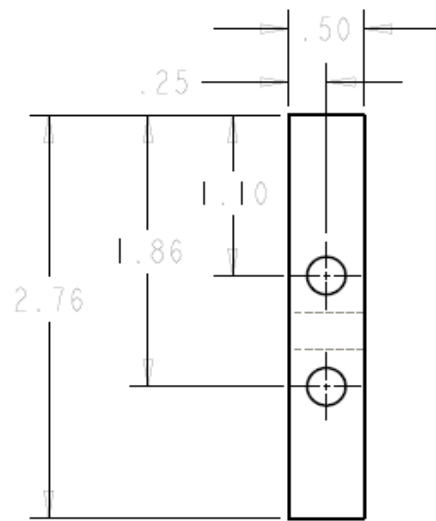
0304 214

REVISION

PART DESCRIPTION

DATE

APPR



ALL HOLES  $\varnothing$ .2570 (F) THRU

**R.I.T**

MECHANICAL ENGINEERING  
"WE DESIGN THE FUTURE"

COVER EXTENSION IN

TIM BRACKBILL

01 TOL  $\pm$

A

8/02/2005

SCALE 1.000 SHEET

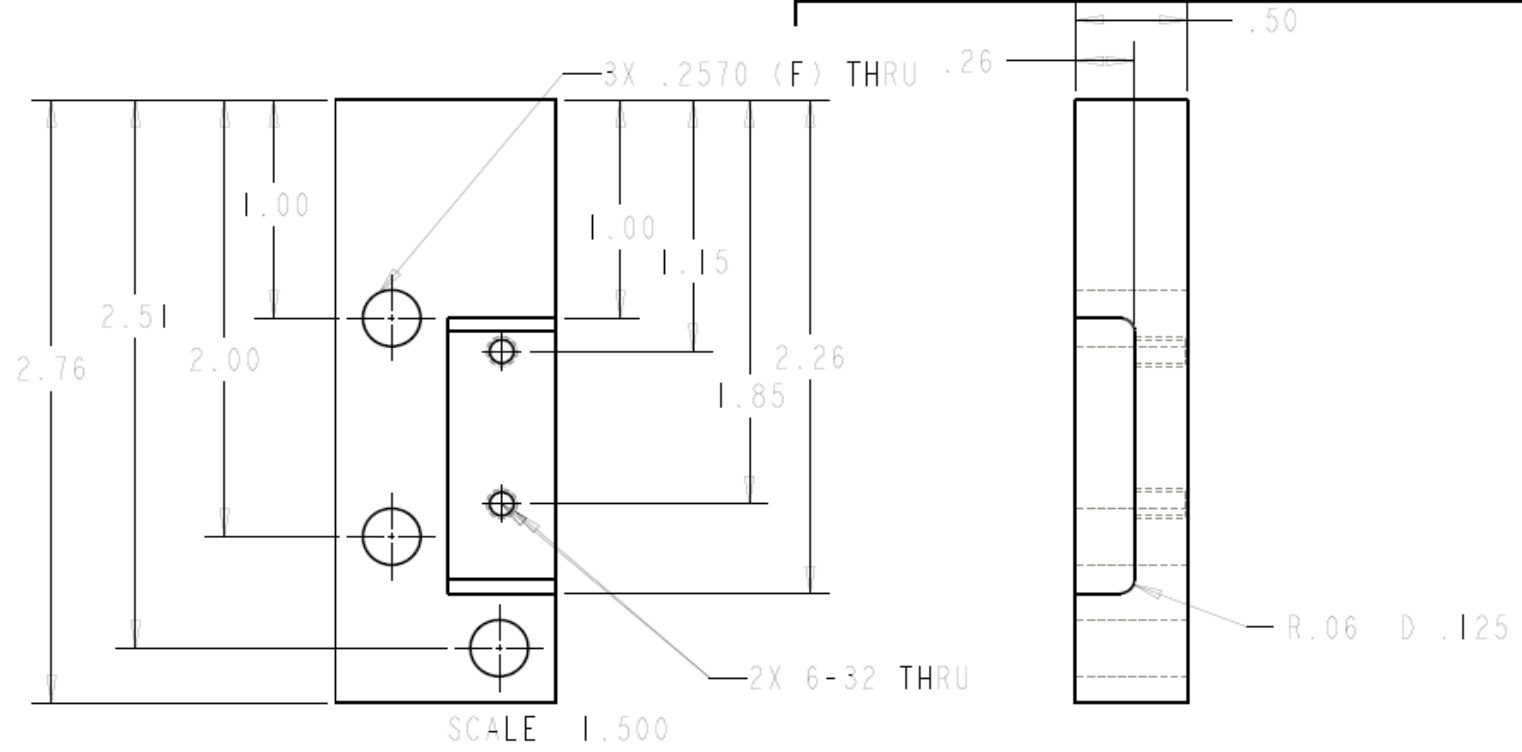
0304 214

REVISION

PART DESCRIPTION

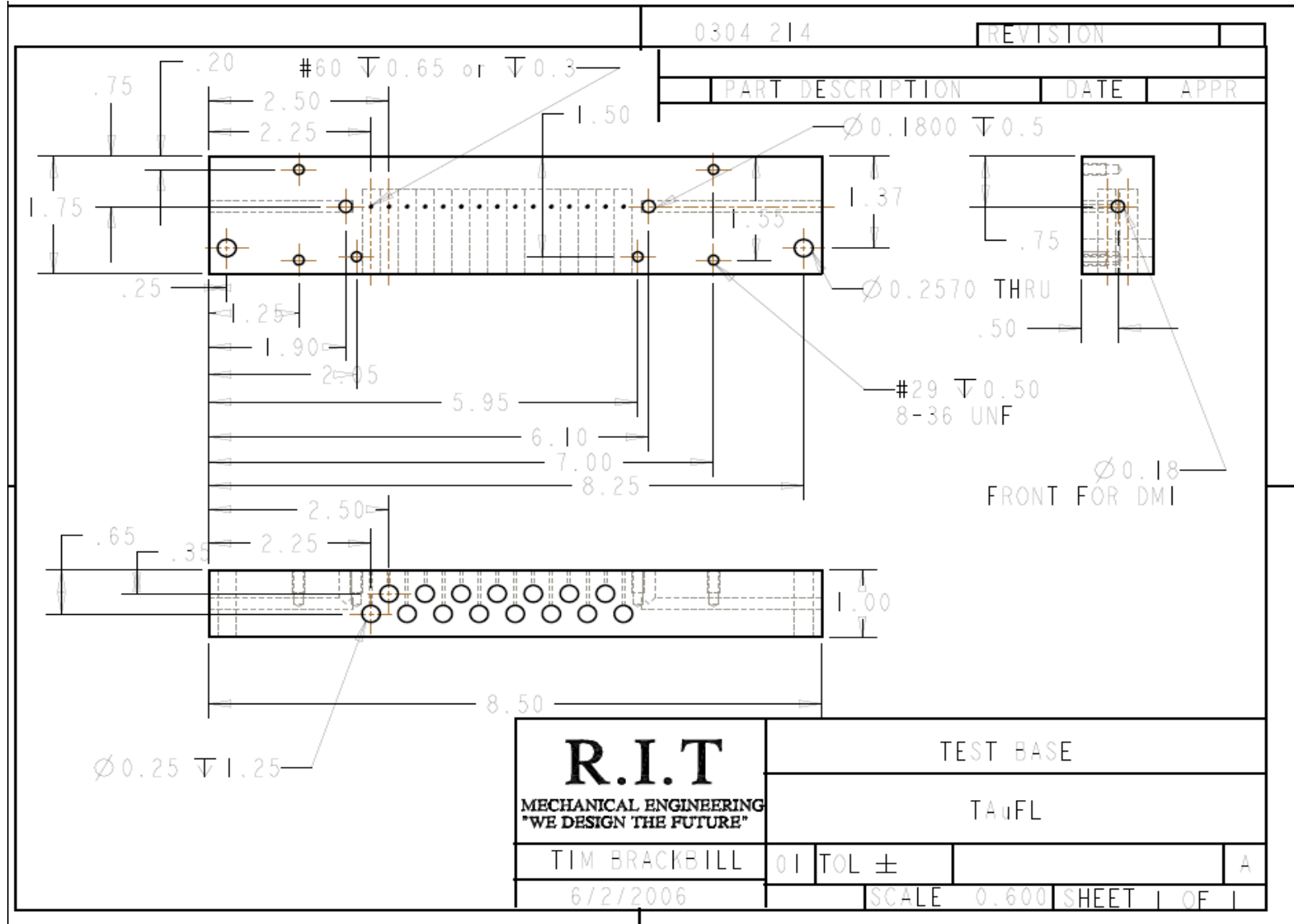
DATE

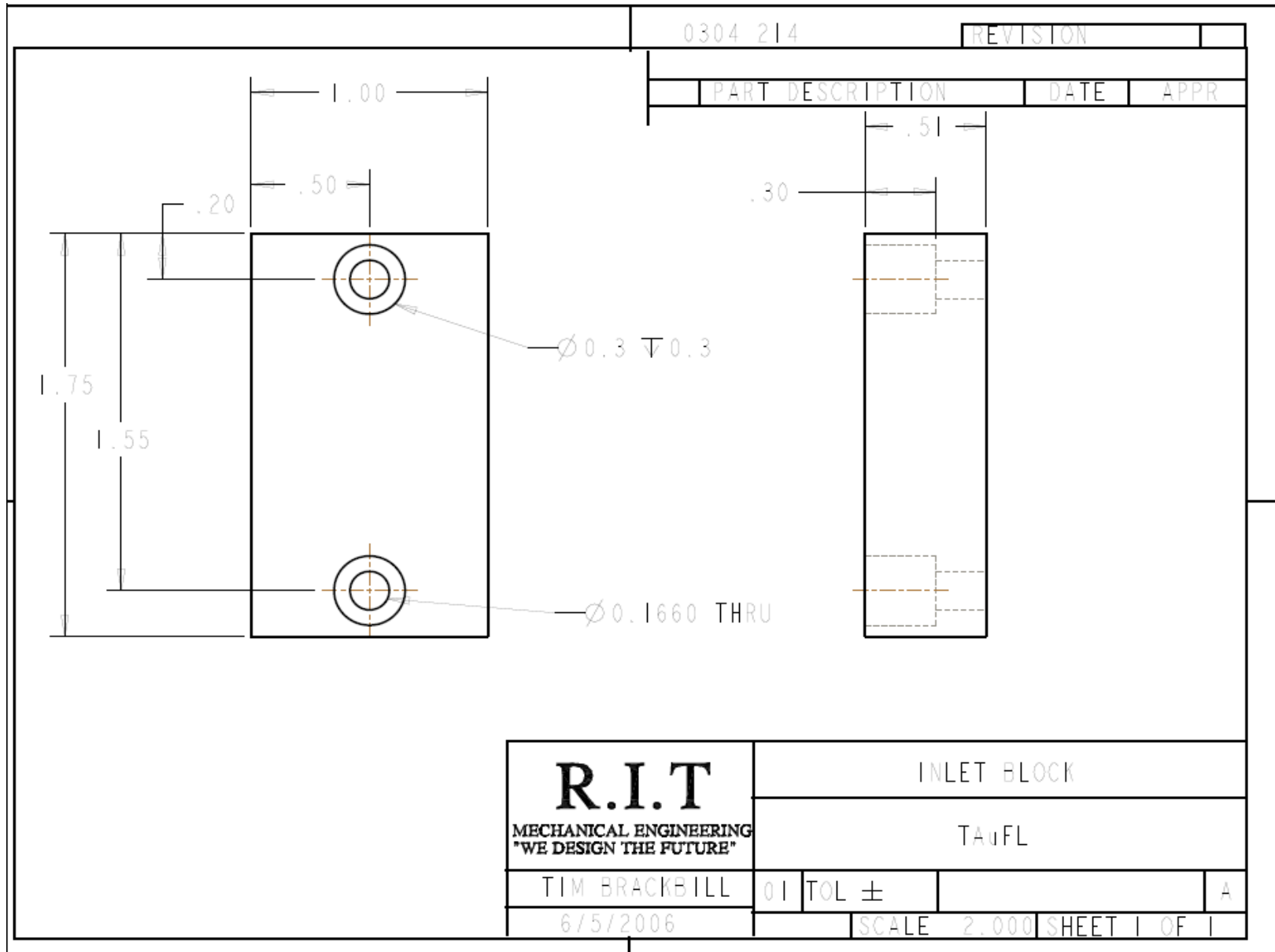
APPR

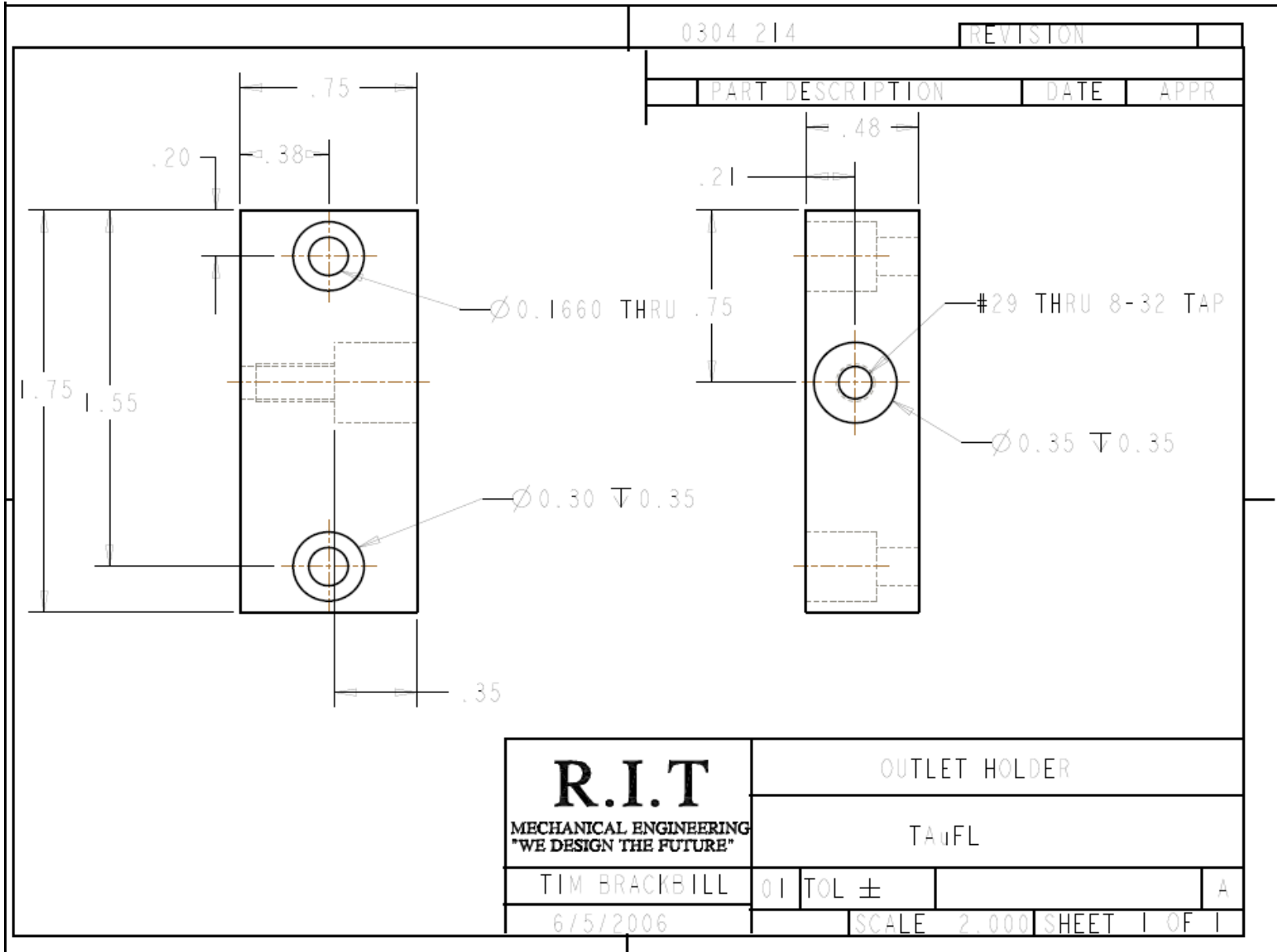


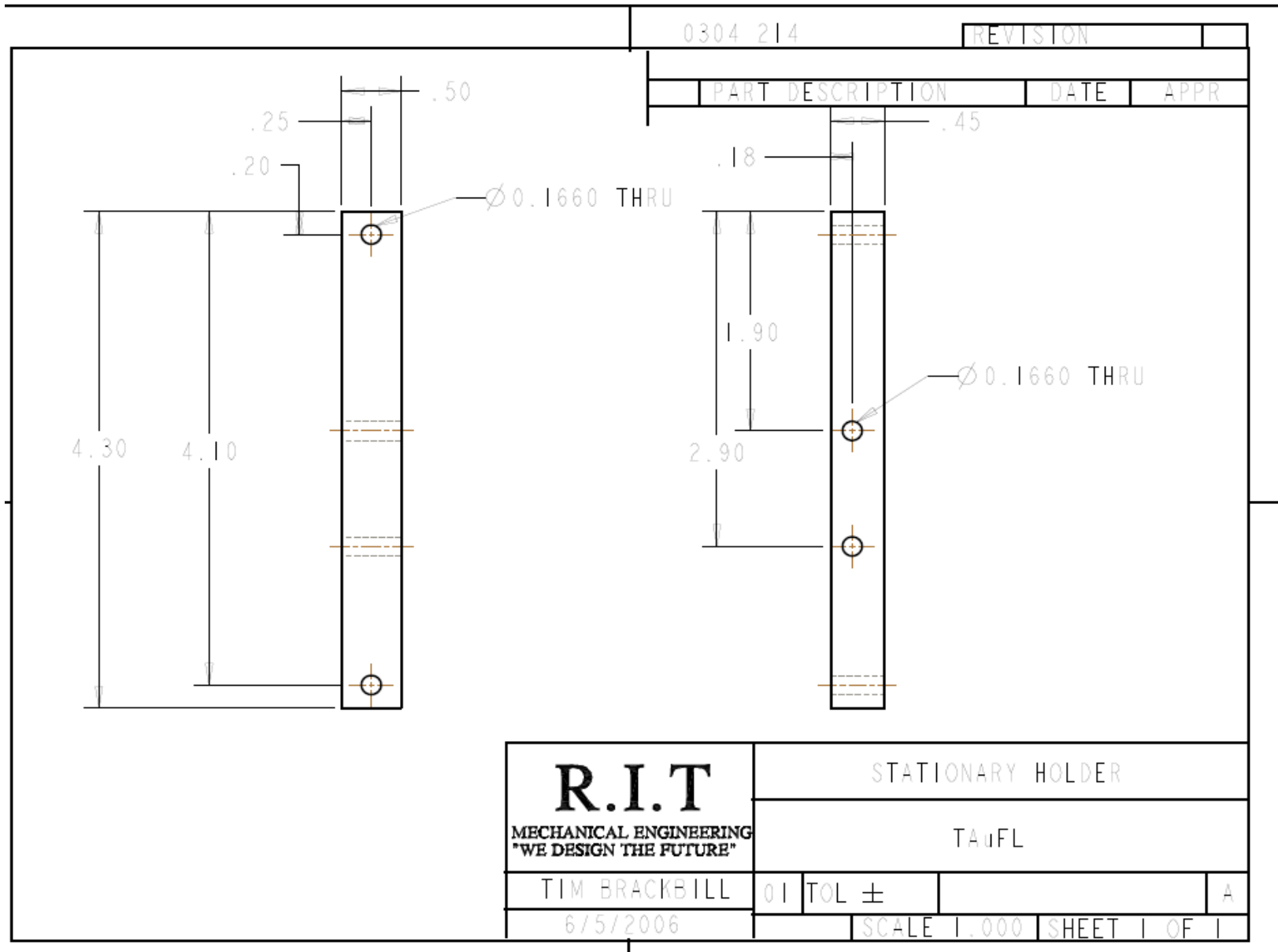
<b>R.I.T</b> MECHANICAL ENGINEERING "WE DESIGN THE FUTURE"			
TIM BRACKBILL	01	TOL ±	A
		SHEET	

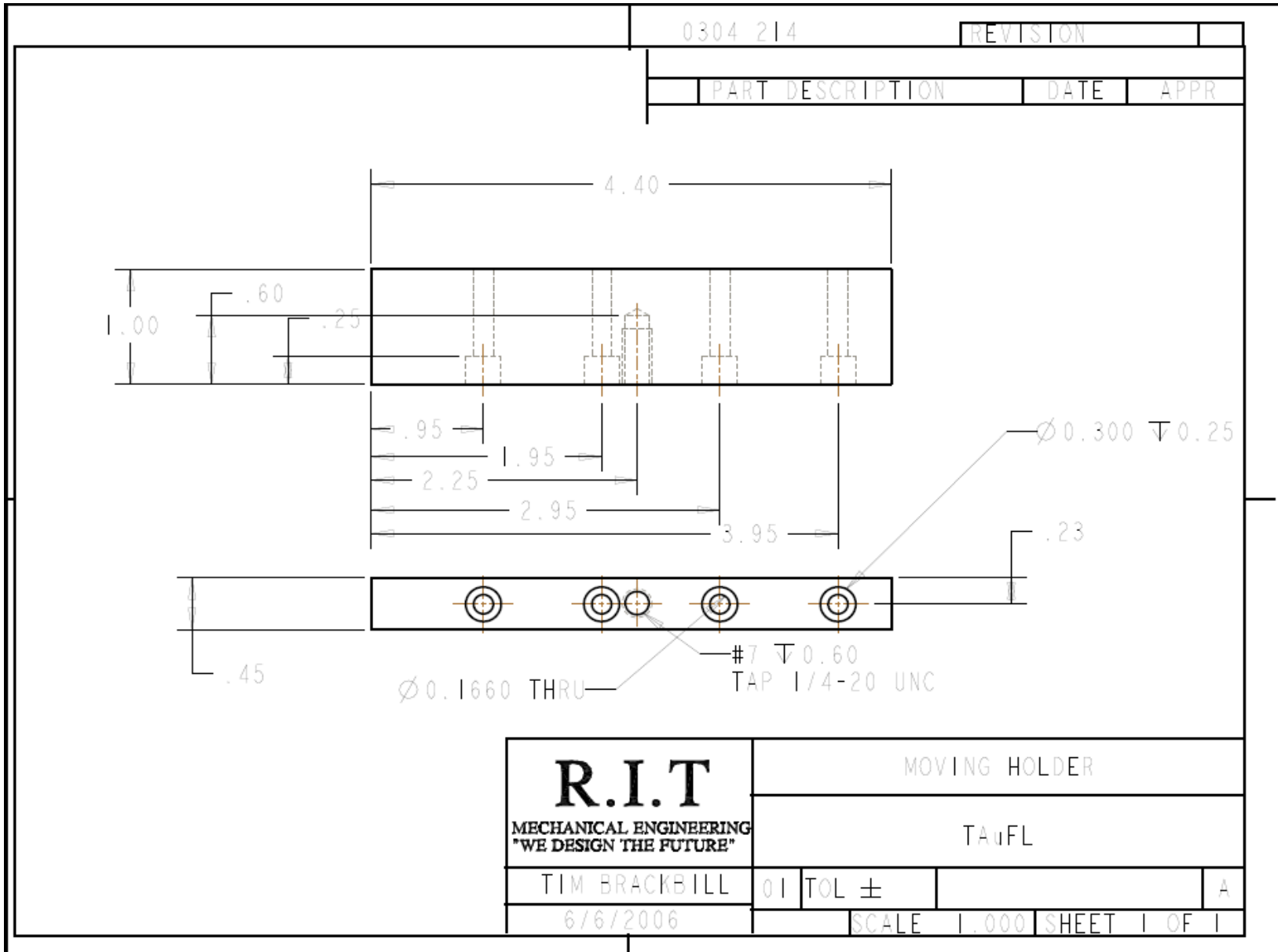
## 7.2 Second Experimental Setup



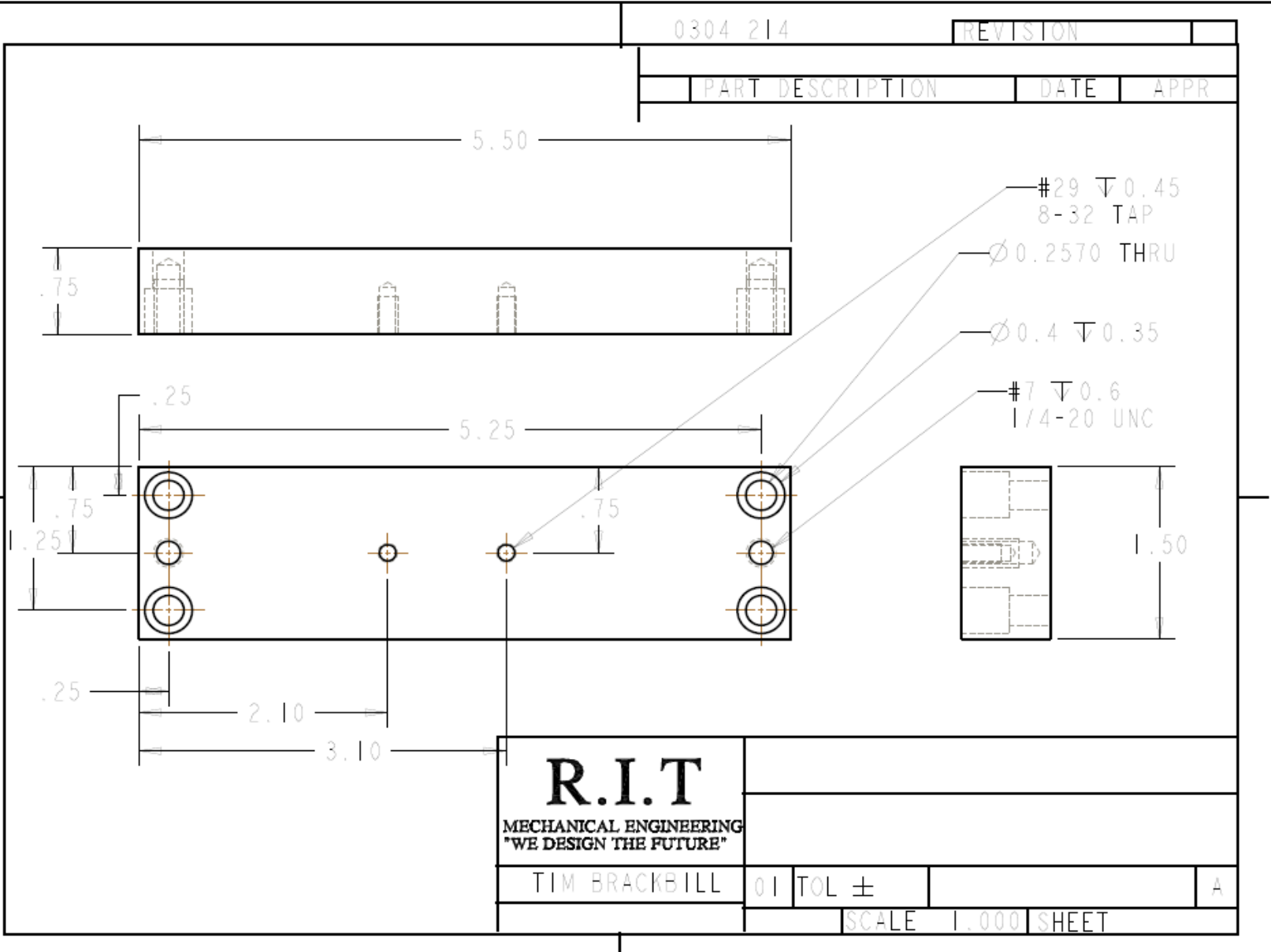








<b>R.I.T</b> MECHANICAL ENGINEERING "WE DESIGN THE FUTURE"	MOVING HOLDER		
	TAUFL		
TIM BRACKBILL	01	TOL $\pm$	A
6/6/2006	SCALE 1.000 SHEET 1 OF 1		



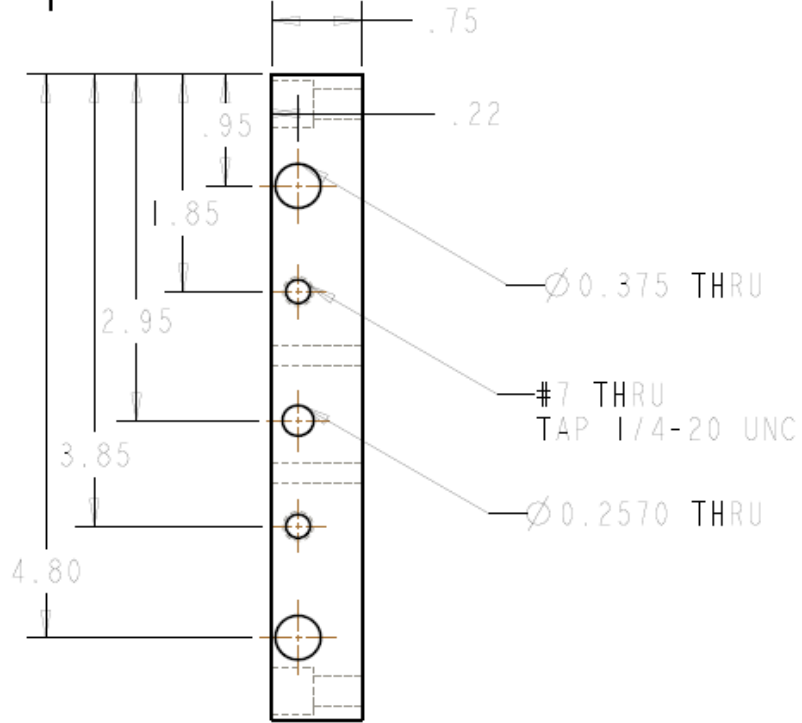
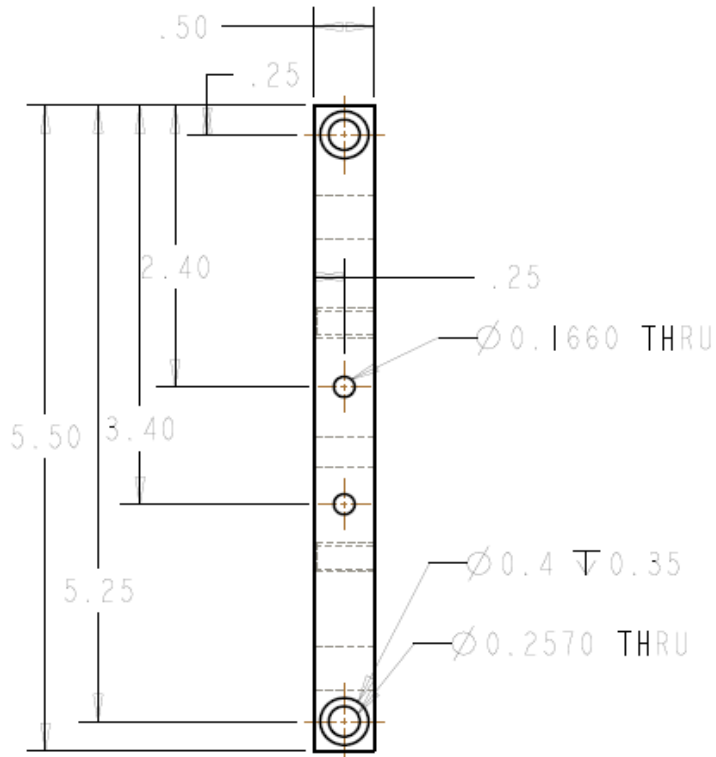
0304 214

REVISION

PART DESCRIPTION

DATE

APPR



<b>R.I.T</b> MECHANICAL ENGINEERING "WE DESIGN THE FUTURE"	MEASURER		
	TAMFL		
TIM BRACKBILL	01	TOL ±	A
6/6/06	SCALE 0.800		SHEET 1 OF 1

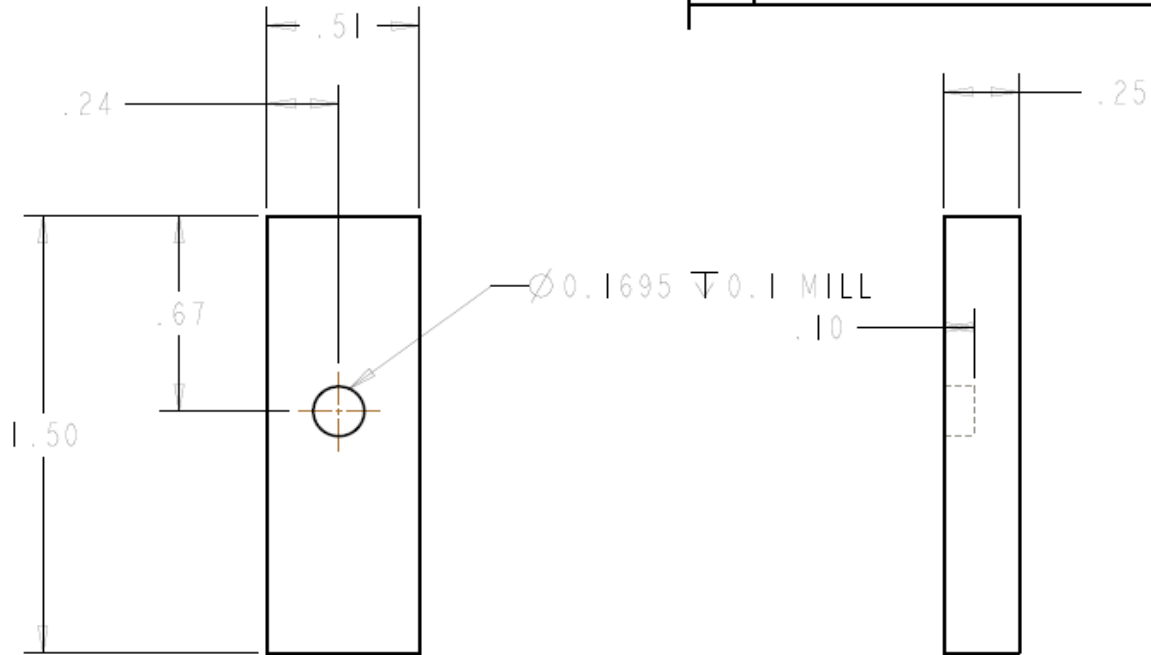
0304 214

REVISION

PART DESCRIPTION

DATE

APPR



<b>R.I.T</b> MECHANICAL ENGINEERING "WE DESIGN THE FUTURE"	OUTLET		
	TAUFL		
TIM BRACKBILL	01	TOL $\pm$	A
6/8/2006	SCALE 2.000 SHEET 1 OF 1		

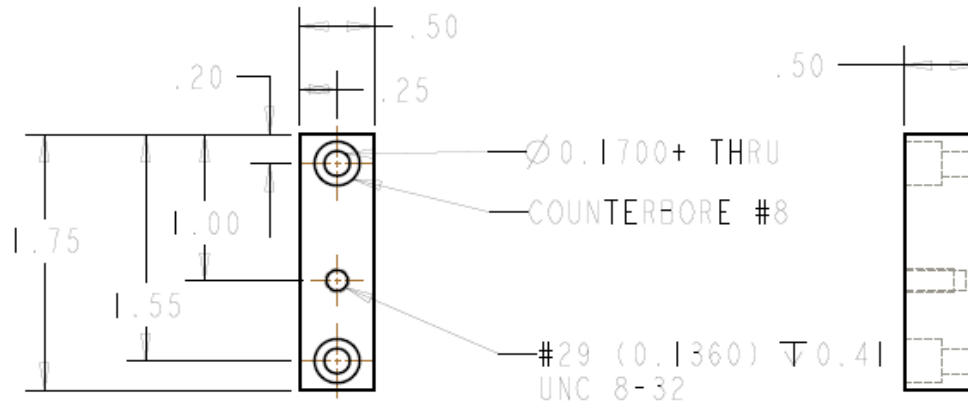
0304 214

REVISION

PART DESCRIPTION

DATE

APPR



**R.I.T**

MECHANICAL ENGINEERING  
"WE DESIGN THE FUTURE"

ELEVATOR BLOCK (QUAN 2)

TAUFL

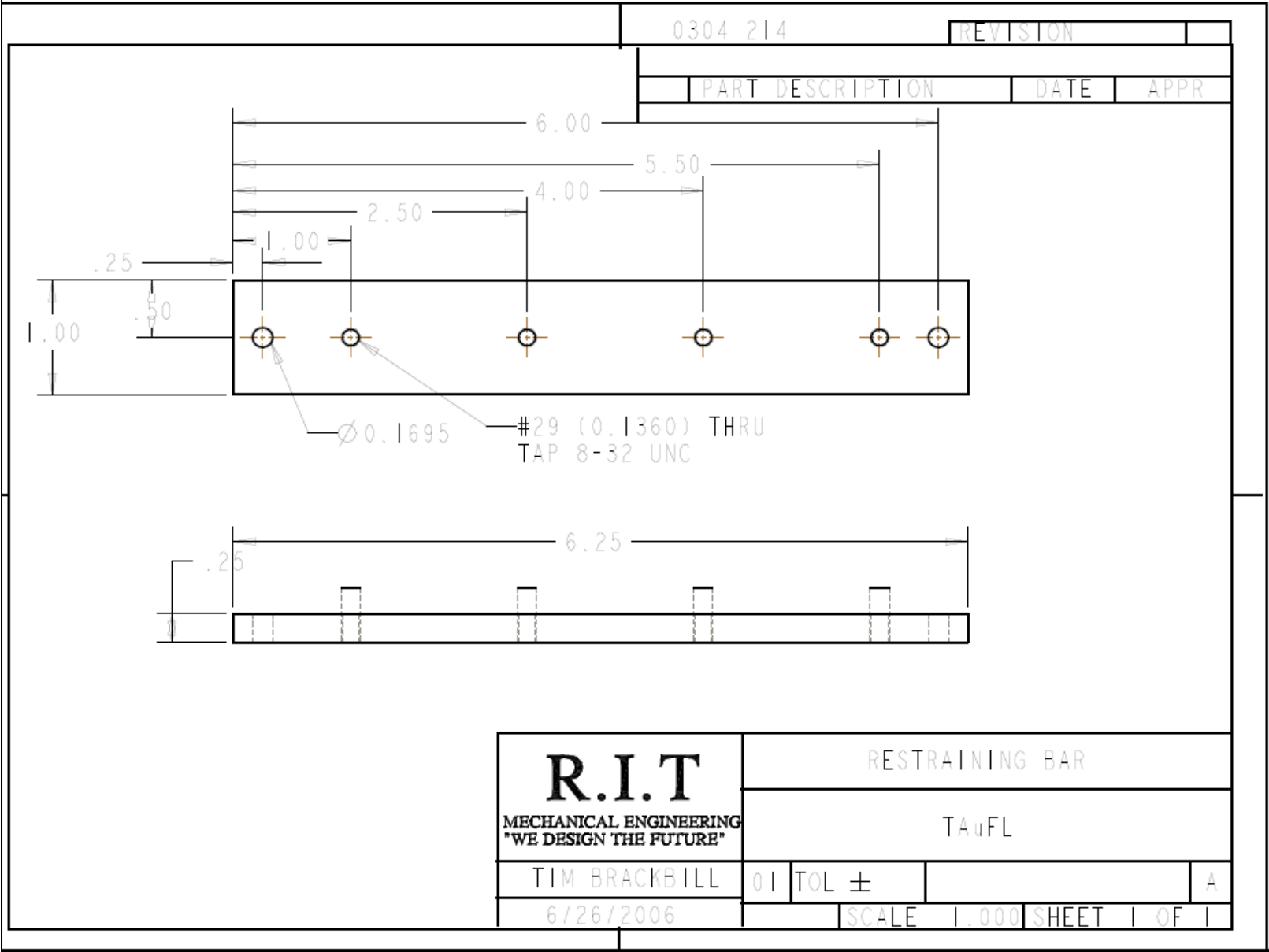
TIM BRACKBILL

01 TOL ±

A

6/26/2006

SCALE 1.000 SHEET 1 OF 1



<b>R.I.T</b> MECHANICAL ENGINEERING "WE DESIGN THE FUTURE"	RESTRAINING BAR		
	TAUFL		
TIM BRACKBILL	01	TOL ±	A
6/26/2006	SCALE 1.000 SHEET 1 OF 1		